LEAKAGE POTENTIAL OF SEQUESTERED CO2:

NUMERICAL MODELING ANALYSIS

by

Richard James Franz

A thesis submitted to the faculty of
The University of Utah
in partial fulfillment of the requirements for the degree of

Master of Science

Department of Civil and Environmental Engineering

The University of Utah

August 2013

The University of Utah Graduate School

STATEMENT OF THESIS APPROVAL

The thesis of **Richard James Franz**

has been approved by the following supervisory committee members:

Brian McPherson	, Chair	**April 24, 2013** Date Approved
Steven Burian	, Member	**April 24, 2013** Date Approved
Christine Pomeroy	, Member	**April 24, 2013** Date Approved

and by **Chris Pantelides** , Chair of

the Department of **Civil and Environmental Engineering**

and by Donna M. White, Interim Dean of The Graduate School.

ABSTRACT

The purpose of this research is to present an analysis of the leakage potential of sequestering CO2 in a reservoir that exhibits faulting, but may or may not have a fault penetrating the reservoir seal. A hypothesis is that CO2 injected into the reservoir will leak through a fault system. The questions addressed by this thesis are: (1) Under what conditions will CO2 leak through a fault and how much will leak under different conditions? (2) How much time is required for CO2 to migrate through an unbroken seal formation? (3) Under what conditions will permeable reservoirs above the target reservoir intercept or "catch" CO2 leaking through a fault? (4) Is injecting into two reservoirs preferable to injection into one? Questions (1) and (4) were addressed with site-specific models, whereas questions (2) and (3) were addressed with generic hydrogeologic models.

Simulations using multi- and single-continuum models were used to analyze the leakage potential from a geological storage reservoir. Fault conduits and geologic formation porosities and permeabilities were used as constraining parameters in a sensitivity analysis.

Model results highlighted that a fault above (but not penetrating) the injection reservoir increases the seepage velocity through a seal, causing a greater risk of CO2 leakage due to the increase of pressure during injection (question (1) above). Simple 1-D seal models illustrate that un-fractured, low-permeability formations are very effective at trapping CO2 for decades and longer, depending on permeability (question (2) above). Additional simulation results illustrated that with a penetrating fault through a seal facilitating direct CO2 leakage, a ratio of fault to medium permeability of two orders of magnitude difference or greater will, in many if not most cases, recapture the CO2 in shallower formations, reducing or eliminating leakage to the surface (question (3) above). Finally, this analysis suggests that a single-reservoir injection (question (4)

above) is best since a stacked reservoir would decrease the overall risk of CO2 leakage during and after injection, highlighted by results of the question (3) analysis.

TABLE OF CONTENTS

APPENDIX

LIST OF FIGURES

LIST OF TABLES

NOMENCLATURE

CCS	Carbon capture and storage
CO2	Carbon dioxide
MINC	Multiple interacting continua
PDF	Probability density function
SCO2	Supercritical carbon dioxide
SG	Supercritical gas
SS	Steady-state condition
TOUGH2	Transport of unsaturated groundwater and heat version 2
USDW	Underground source of drinking water
XCO2	Dissolved carbon dioxide

INTRODUCTION

Background

The increase of CO2 concentration in the atmosphere has prompted many to develop ways to mitigate CO2 emissions from energy power plants. One idea is to sequester the emissions in deep underground aquifer reservoirs (Birkholzer, et al., 2009; Birkholzer, et al., 2011; Gale, 2004; Han, et al., 2010a; Holloway, 2005; IEA, 2001; IPCC, 2005; Meckel, et al., 2009; Orr, 2004; Thomas, et al., 2005). For long term storage of CO2, several mechanisms are traditionally known: residual trapping, dissolved trapping, stratigraphic trapping and mineral trapping (McPherson, et al., 2009). In the injection period, a large amount of CO2 remains in the supercritical phase. Some of this CO2 is held in place by capillary tension (residual trapping), and the amount dissolved in the formation water (dissolved trapping) gradually increases. After injection stops, residual trapping increases and dissolved trapping increases significantly. This is due to migration and diffusion of the CO2 plume and mixing between CO2-saturated and unsaturated water. The amount trapped by mineral precipitation of carbonate minerals increases with time (Audigane, et al., 2007; Doughty, et al., 2004; Flett, et al., 2007; Han, et al., 2010b; Ide, et al., 2007; Knauss, et al., 2005; Suekane, et al., 2008; White, et al., 2005; Xu, et al., 2004; Zhang, et al., 2009). These trapping mechanisms can occur in different sequestration options such as enhanced oil recovery fields, unmineable coal beds, depleted oil or gas reservoirs, and deep saline formations (Figure 1). The focus of this study will be on deep saline reservoirs.

Aquifer reservoirs that have the potential to be long term storage facilities are common in the Colorado Plateau and Southern Rocky Mountain region (Allis, et al., 2001). Studies of these regions have shown that the Navajo sandstone has a good potential for long term storage (Allis, et al., 2003). The depth of 800m or greater is needed for these reservoirs to maintain CO2 in a

supercritical state, thus maximizing its density (Figure 2 and Figure 3) with Figure 3 showing the variability of CO2 density.

It is important to understand all aspects in the geologic structure of a CO2 injection site, especially the formation of faults. Faults have the potential of leaking the CO2 that is injected into reservoirs and, therefore, need to be considered when selecting a site (Dockrill, et al., 2010; Price, et al., 2009).

CO2 interactions with the aquifer reservoir could induce fault slip, leading to seismic activity and/or changing fault permeability. The characteristics of a fault (permeability, porosity and damage zones) affect the storage of CO2 (Caine, et al., 1996; Evans, et al., 1997; Geraud, et al., 2006; Orlic, et al., 2011; Shipton, et al., 2001; Sibson, 2000; Streit, et al., 2004).

Critical Questions to Address

If mitigation of CO2 emissions from power plants and other point sources is to become practical, then many questions need to be investigated. For example, studies must be done to determine what geologic formations would be best for storage, how much can be stored, and potential impacts of CO2 leaks. These questions are currently being researched by different organizations to evaluate the potential outcomes and risks associated with carbon capture and sequestration (CCS).

This research is focused on the potential of CO2 leakage. More specifically I investigated the role of known (or unknown) faults in the target area of CO2 storage. For a "typical" fault in a CCS area, several critical questions addressed include:

(1) Under what conditions CO2 will leak through a fault and how much will leak under different conditions?

(2) How much time is required for CO2 to migrate through an un-broken seal formation?

(3) Under what conditions will permeable reservoirs above the target reservoir intercept or "catch" CO2 leaking through a fault?

(4) Is injecting into two reservoirs preferable to injection in one?

These questions are the primary focus of this thesis under the auspices of the hypothesis that CO2 will leak through a faulted system.

Conceptual Models of a Faulted CCS Site

Figure 4 illustrates four schematics of conceptual models, each expressing a generalized model to address the four critical research questions listed in the preceding section. Figure 4(a) represents a cross-section of a geologic storage site with alternating sandstone reservoirs (stippled or dotted pattern) layers and shale sealing layers (dashed patterns). The entire section is faulted (diagonal line), but in Figure 4(a), the fault does not penetrate the seal layer above the target formation. A model like Figure 4(a) is used to address critical question (1), under what conditions CO2 will leak through a fault and how much will leak under different conditions? This generalized schematic is similar to an actual CCS site in western Texas, the SACROC field (Han, et al., 2010b).

Figure 4(b) is the same schematic, but with the fault penetrating the seal of the target reservoir. In most CCS scenarios, such a fault would not be known about a priori, and thus evaluating the potential ramifications of such an unforeseen fault is important. Such a model scenario will be used to address a second important permutation of critical question (1).

Figure 4(c) is schematic of a simple, 1-D model of a seal, used to address critical question (2), how much time is required for CO2 to migrate through an unbroken seal formation?

Finally, Figure 4(d) is the same generalized geologic section as Figure 4(a) and 4(b), but represents the more general case of a vertical fault (or, alternatively, the vertical leak path may represent an abandoned wellbore). This general model is used to address critical question (3), under what conditions will permeable reservoirs above the target reservoir intercept or “catch” CO2 leaking through a fault? A slightly-modified form of this model (Figure 4(d)) was used to address critical question (4), is injecting into two reservoirs preferable to injection in one? In this case, the specific layers were tailored to represent those of an actual candidate CCS site in central Utah, the Gordon Creek field (Morgan, et al., 1991).

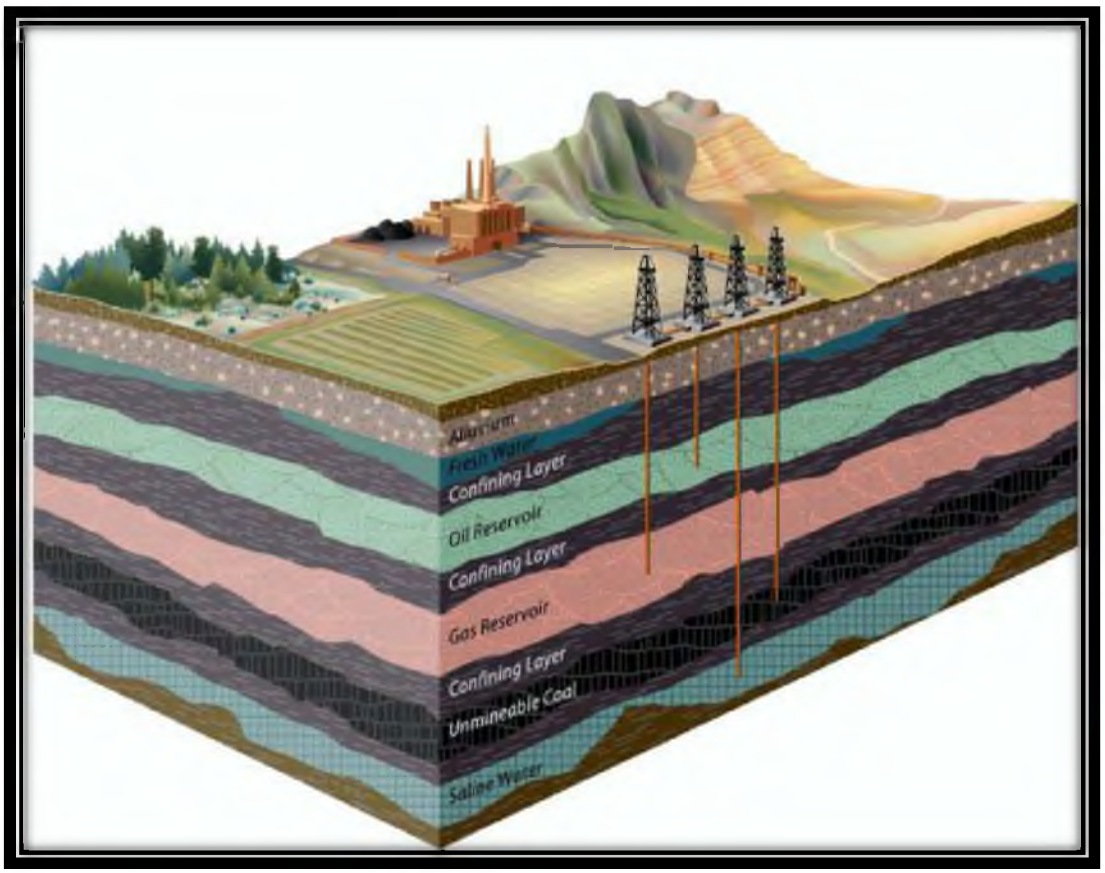

Figure 1. Carbon sequestration options.

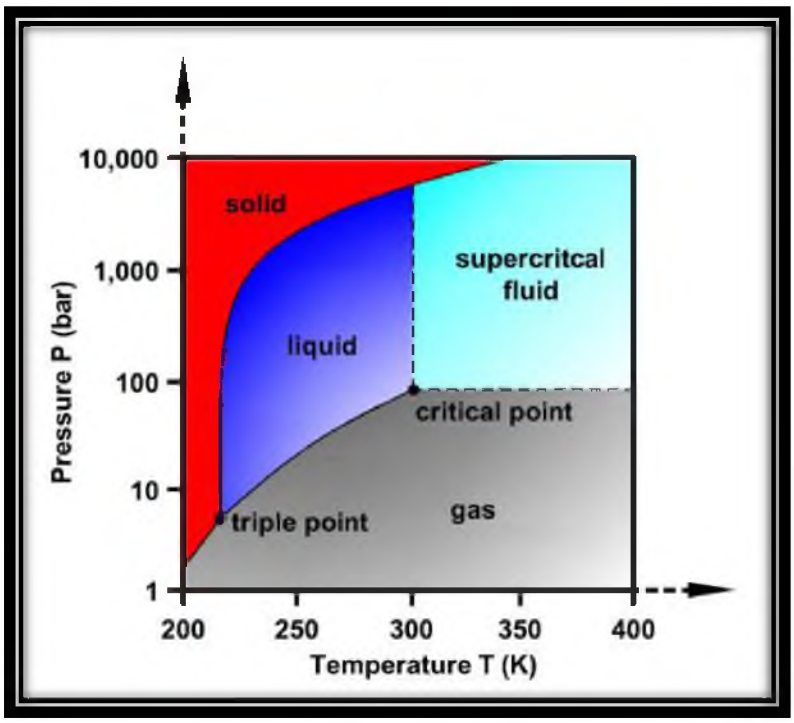

Figure 2. CO2 Pressure-Temperature phase diagram.

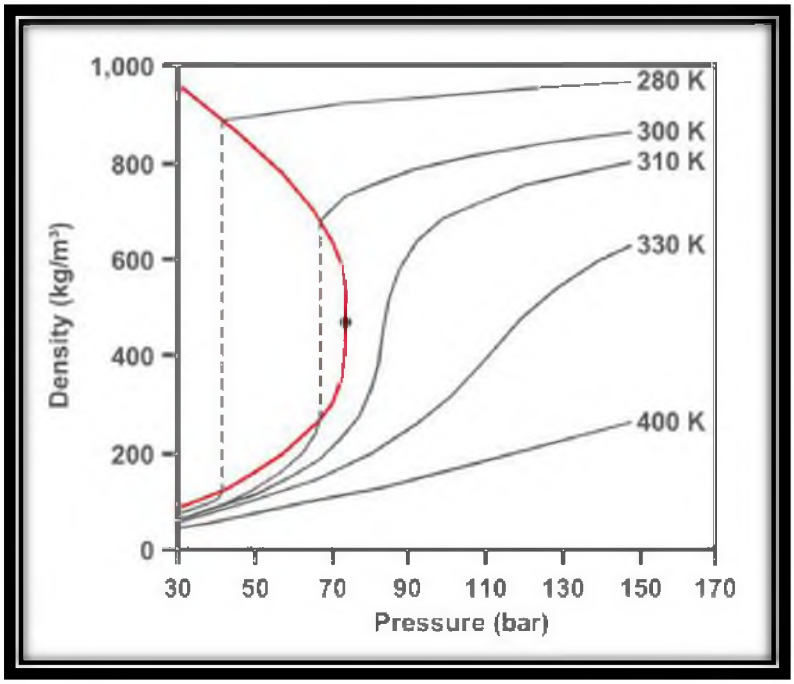

Figure 3. CO2 Density-Pressure phase diagram.

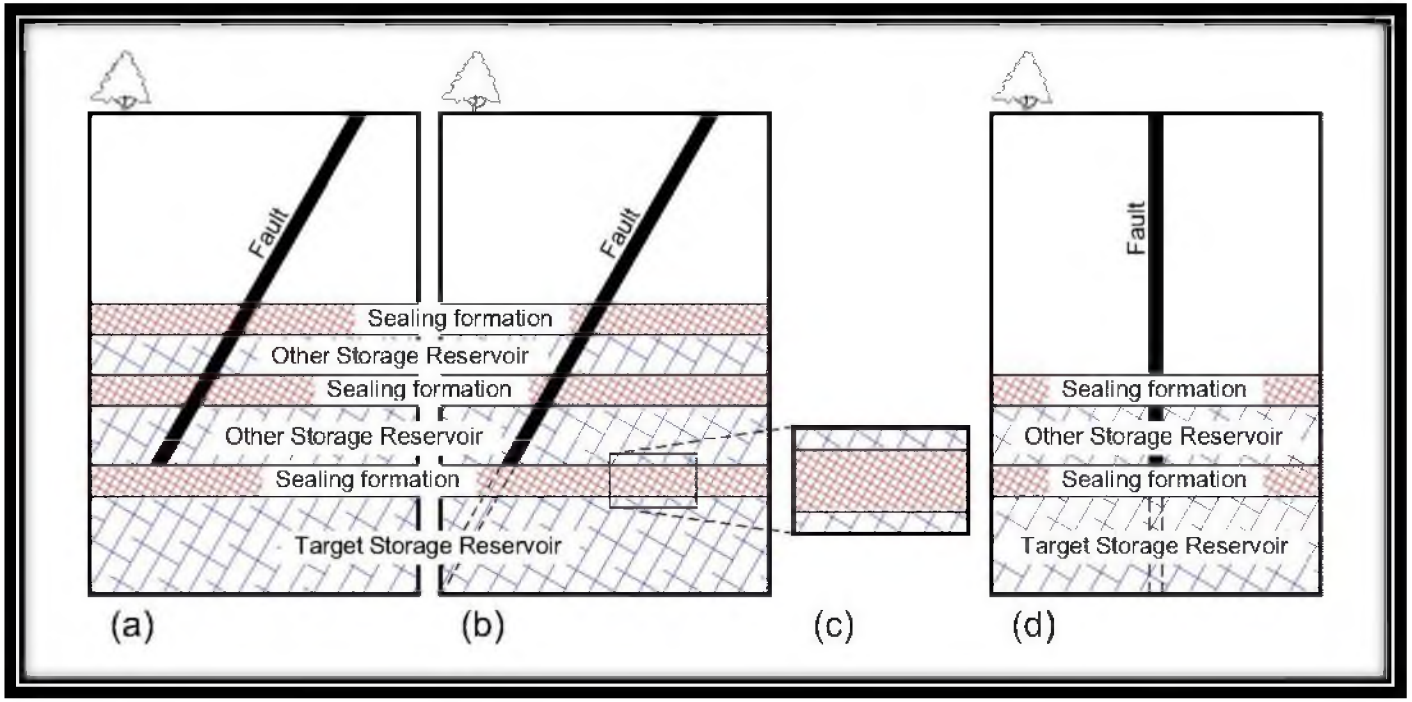

Figure 4. Generalized schematics of different models used in this study. Scale is general, with total depth approximately 1 to 2 kilometers and surface extent less than 1 kilometer. See text for discussion of details.

METHODS

General Approach: Numerical Modeling

To evaluate CO2 sequestration in subsurface reservoirs with faults, computer models are often used to simulate injection, migration, storage and associated effects in the subsurface (Soltanzadeh, et al., 2008). These simulations are done to evaluate potential outcomes and are not necessarily what will happen (Cappa, et al., 2010; Pasala, et al., 2003; Zhou, et al., 2010).

Conceptual models and simulations are also applied to forecast risks of CO2 injection, since effects of injection do not stop once injection stops. These models and simulations require a defined area (length, width, depth), media or medium (permeability, porosity for each media), existing/proposed thermodynamic conditions, location and flow rate (injection, production). Trapping and surface movement continues for years after injection, and the risks associated with them continue (Nghiem, et al., 2009; Rohmer, et al., 2010; Schmit, et al., 2003). I used TOUGH2 (Transport of Unsaturated Groundwater and Heat version 2) (Pruess, et al., 1999) to simulate the potential outcomes of the models for this analysis.

Fractures

Models developed for this study designate fractures and fracture networks as key conduits for migration of fluids in a subsurface medium and reservoir. These fractures are the pathways through which fluids may escape impermeable or low permeable media that seal reservoirs for long term storage. Characterizations of fractures, water flow, transport, and two-phase flow have to be considered (Berkowitz, 2002). Fluid flow through a fracture bounded by rough surfaces can be predicted with general governing equations. Transport though fractured

rock in a multiphase system can be addressed with dual-continua methods (Ge, 1997; Wu, et al., 2000), and TOUGH2 includes such continua.

For fractured media, heterogeneity is generally characterized by the length and aperture distribution (Dreuzy, et al., 2001). The interactions in the geometry, or structure, of the phases between the immiscible fluids are a critical control. Under conditions of two phases, immiscible fluid flow and phase structure (i.e., the geometry that is filled by each phase) in fractures control the fluid pressure of phase, including solute dispersion and mass transfer (Glass, et al., 2001).

With the use of laboratory and numerical simulations to evaluate mass transfer between the fracture and matrix, experimental results can be compared to results of numerical simulations (Trivedi, et al., 2009). Analysis of dissolution and how it may be significant as a long term trapping mechanism in a fractured reservoir allows for two-phase flow of CO2 and water (Iding, et al., 2011).

Porosity

The porosity (ϕ) of a medium is defined as the ratio of the void space divided by the total volume of material, represented as a fraction between 0 and 1, where the void may contain fluids or gases. However, not all voids are connected and so the fraction of the total volume in which the fluid can flow through is the effective void space or

$$\phi = \frac{V_V}{V_T} = n_e \tag{1}$$

with the values

V_V = volume of void space (m^3); V_T = volume of total material (m^3);

n_e = effective porosity (unitless).

The effective void space is more important for groundwater flow and solute transport.

Dual porosity refers to the concept of two overlapping reservoirs which interact. The matrix (or rock) and fracture system are simulated as overlapped but distinct bodies in one model.

Dual porosity of the model is estimated by means of first order rate equations. The water flow in the matrix and fracture can be described by Richard's equation, and solute transport is described with the convection dispersion equation (Gerke, et al., 1993; Hattingh, et al., 2009; Haws, et al., 2005; Samardzioska, et al., 2005; Tseng, et al., 1995; Xia, et al., 2012; Zhang, et al., 2000).

In a dual porosity model with a fractured reservoir, it is assumed that fractures are storage areas and a means of fluid transport, therefore, having accurate values of porosity can effect predictions of water and solute flux. Since porosity values of subsurface media typically decrease as particle size increases and not knowing how the gain size varies across the models boundaries, having accurate values point out the limitations do to the fact that models are constructed with limited known values. This introduction of uncertainty into initial estimates for calibration propagates uncertainty into the final outcome (Presho, et al., 2011).

Permeability

Another factor that has to be considered in geological modeling of water flow and solute transport is how important accurate estimates of hydraulic conductivity are. The permeability (k) of a medium is a measure of a material to allow fluids to pass through. It is also part of the constant in Darcy's law which relates discharge (q) and fluid properties (μ) to a pressure gradient, summarized as

$$K = \frac{k \rho_w g}{\mu} \quad \text{and} \quad q = -K \frac{dh}{dL} \tag{2}$$

with the values

K = hydraulic conductivity (m/s); k = intrinsic permeability (m^2);

p_w = fluid density (kg/m^3); g = gravity (m/s^2); μ = viscosity of fluid (kg/(m*s));

q = discharge (m^3/s); dh/dL = hydraulic gradient (unitless).

For dual permeability models, different techniques have been utilized as follows;

- A Forchheimer flow equation through the fractures and the Darcian flow through the matrix. Indicating nonlinear model predictions of high flow rates in most cases compared to the Darcian model (Choi, et al., 1997).
- A new Laplace-domain solution for fluid flow in dual permeability media with a horizontal well (Wang, et al., 2010).
- In coupling effects for effective stress and swelling/shrinkage on methane production, from which the effective stress and micropore shrinkage have a significant contribution to fluid flow (Thararoop, et al., 2012; Wei, et al., 2010).
- A double diffusion phenomenon in porous media layers affected the governing equations for heat, mass transport and a fracture within a matrix that can influence the plume geometry (Saghir, et al., 1999).

For single and dual permeability, fracture geometry is important in the characterization and subsequent remediation in fractured porous media (Stafford, et al., 1998). Modeling saturated flow and transport in a heterogeneous system may require a 2D dual permeability approach (Uleberg, et al., 1996; Vogel, et al., 2000).

Relative Permeability

Relative permeability and capillarity pressure (surface tension) must also be accounted for in geological models. The determination of these two parameters is important for CO2/brine systems. These factors influence plume migration, residual trapping, and dissolution in storage reservoirs (Busch, et al., 2011). CO2/brine relative permeabilities for extensive rock types are rare in literature and usually are based on experiment data and associated mathematical relations (Al-Quraishi, et al., 2005; Dana, et al., 2002a; Dana, et al., 2002b).

Modeling reservoirs in the subsurface relies on a small number of core samples to characterize large scale multiphase flow properties that affect the production and recovery from these fields (Angeles, et al., 2010). A question is whether laboratory measurements are a true representation of in-situ rock. Nonlinear regression methods are proposed to estimate relative

permeabilities to improve the models and account for variations in rock properties (Al-Otaibi, et al., 1998; Burton, et al., 2009; Nguyen, et al., 2006).

In petroleum production, simulations are done involving simultaneous flow of three immiscible fluids through subsurface formations. These experiments with flow rates of brine and gas increasing gradually while oil rates decreasing are compared, outlining how the impacts of history dependent saturation functions affect modeling simulations relative permeabilities (Masihi, et al., 2011). Some of the results indicated that oil or gas recovery was a function of composition, injection rate and pore pressure and that the calculated relative permeability data of these fluids and gases were limited (Sidiq, et al., 2011; Spiteri, et al., 2006).

Also, in most cases the relative permeability functions need to be upscaled for coarse grid simulations or analytical models (Gasda, et al., 2005). For upscaled grids a different numerical simulation outlined an approach that relative permeability functions were not directly specified in the simulation. Allowing for this technique to show that the performance calculated from simulation without application of relative permeabilities was about the same as experimental data (Li, et al., 2008; Wang, et al., 2011). In either case relative permeabilities need to be adjusted for simulating because of their significant importance in fluid flow.

Uncertainty

Numerical models are efficient tools for groundwater management. However, modeling requires a huge amount of data and gathering those data is not an easy endeavor. For reliable results, accurate values of the study area need to be collected (Baalousha, 2008). Most groundwater models handle input parameters in a deterministic way, without considering any variation, uncertainty, or randomness in the parameters. Because of heterogeneity of reservoirs, it is difficult to determine the hydrological properties of reservoir rock. To account for uncertainty, many approaches have been used, including special sampling reliability methods, and Monte Carlo simulations (Frey, et al., 2002; Nilsen, et al., 2003; Oberkampf, et al., 2004; Pate-Cornell, 1996; Winkler, 1996; Yang, 2011).

Of these techniques, the Monte Carlo method is the most widely used in risk assessment. This method is known as a universal numerical technique and became practical with the advent of computers. A Monte Carlo simulation is suited for analysis that requires the quantification of uncertainties (Kunstmann, et al., 2002). Traditional risk assessment requires uncertainty estimation to be accounted for outside of the model results due to predicted values used, while others are looking at incorporating the uncertainty in the model which will directly propagate into the results (Helton, 1993; Kunstmann, et al., 2006a).

Monte Carlo Example

The general procedure is illustrated in Figure 5. The first step is generation of multiple realizations of each random variable. The second step is to run a simulation of each realization for each input parameter. After all simulations, the third step is construction of a histogram of the results for the quantity of interest. From the histogram the mean, variance, confidence limit and other parameters can be determined. A fourth step needed is to ensure convergence. This is done by carrying out another set of simulations with an increased number of realizations. The histogram and the statistical parameters from the second set are compared with the first set. If there are any significant differences then the Monte Carlo simulation has not converged.

Another technique is evaluation of probability density functions (PDF) for risk management. This approach of uncertainty in hydrological equations is developed that propagates the uncertainty of model input parameters into the corresponding model output (Kunstmann, et al., 2006b). A framework of error and uncertainty in simulations that deal with the numerical solution of PDF's and incorporate them into the final results (Oberkampf, et al., 2002). Direct PDF propagation has the advantage of yielding an exact solution rather than approximating discontinuous frequency distributions.

A PDF or probability density function of a continuous random variable is a function that describes the likelihood of the random variable to define a given value. Figure 6 illustrates the probability for the random variable to fall within a particular region is defined by the integral of this variable's density over the region. The PDF is non-negative and its integral is equal to one. So

the random variable X has density *f*, where *f* is a non-negative function computed with equation (3), or

$$P[a \le X \le b] = \int_a^b f(x)\,dx \tag{3}$$

Numerical Modeling Methods Used in this Study

This study is focused on post injection of CO2 in an over pressurized reservoir, including the amount of CO2 injected and stored over a 3-year period, and the potential distance the CO2 will migrate through the reservoir under different conditions. Mineralization due to CO2 traveling through the reservoirs and fault conduits was neglected, to simplify the analysis.

Figure 7 depicts the concept for modeling flow in fractured multicontinuum media using the multiple interacting continua (MINC) approach (Pruess, et al., 1999). Fractures are interconnected in a network surrounding a matrix block of low permeability. Flow through the reservoir occurs in the fractures, and fluids propagate rapidly through the fracture system, while the rock matrix can exchange fluid (or heat), while invading the tight matrix slowly by means of interporosity flow. The term “interporosity flow” was developed by Warren, et al., (1963) and approximated the flow as being quasi-steady, with a matrix-fracture interflow proportional to the pressure difference.

Figure 8 depicts a schematic of a mesh of a single continuum medium. Single continuum media are simpler in that the reservoir is not broken into multiple matrix blocks. The interconnection of the matrix is continuous, unlike fractured media. Flow through the reservoir is only in the rock matrix, defined in part by the porosity of the grid cells.

Governing Equations

With these two different modeling options, multiple continua and single continuum, each model is defined by specific governing equations, and expressed below in simplified forms (2D for flow in the X (horizontal) and Z (vertical) directions of the matrix). For a simple single phase

(which can be expanded to multiphase) single continuum 2D problem the governing equation (4) is used for heterogeneous and isotropic conditions, or

$$\frac{\partial}{\partial x}\left(K_x \frac{\partial h}{\partial x}\right)+\frac{\partial}{\partial z}\left(K_z \frac{\partial h}{\partial z}\right)=S_s \frac{\partial h}{\partial t}$$
$$K=\frac{k\rho_w g}{\mu} \text{ and } S_s=\rho_w g\left(\beta_p+n\beta_w\right) \quad (4)$$

with the values

K = hydraulic conductivity (m/s); t = time (s); S_s = specific storage (1/m);

k = intrinsic permeability (m^2); p_w = fluid density (kg/m^3); g = gravity (m/s^2);

μ = viscosity of fluid (kg/(m*s)); n = porosity (unitless);

β_p = compressibility of medium ($m^2/(kg(m/s^2))$);

β_w = compressibility of water ($m^2/(kg(m/s^2))$).

For a multicontinuum model, the simplified single phase (which can be expanded to multiphase) 2D governing equation for the fracture is equation (5) and for the matrix is equation (6), for heterogeneous and isotropic conditions, or

$$\frac{\partial}{\partial x}\left(K_f \frac{\partial h_f}{\partial x}-K_f\right)+\frac{\partial}{\partial z}\left(K_f \frac{\partial h_f}{\partial z}-K_f\right)-\frac{\Gamma_w}{w_f}=C_f \frac{\partial h_f}{\partial t} \quad (5)$$

$$\frac{\partial}{\partial x}\left(K_m \frac{\partial h_m}{\partial x}-K_m\right)+\frac{\partial}{\partial z}\left(K_m \frac{\partial h_m}{\partial z}-K_m\right)+\frac{\Gamma_w}{1-w_f}=C_m \frac{\partial h_m}{\partial t} \quad (6)$$

$$C=S_w S_s+\varepsilon \frac{\partial S_w}{\partial h} \text{ and } \Gamma_w=\alpha_w\left(h_f-h_m\right)$$
$$\alpha_w=\alpha_w^* K_a \text{ and } \alpha_w^*=\frac{\beta}{a^2}\gamma_w \quad (7)$$

with the values

K_f = fracture hydraulic conductivity (m/s); K_m = matrix hydraulic conductivity (m/s);

h_f = fracture pressure head (m); h_m = matrix pressure head (m);

C_f = fracture specific soil water capacity (1/m);

C_m = matrix specific soil water capacity (1/m);

Γ_w = space and time dependent exchange (1/s);

w_f = volumetric weighting factor (unitless);

S_w = degree of fluid saturation (unitless); S_s = specific storage (1/m);

ε = porosity (unitless); α_w = first order transfer coefficient for water (1/(m*s));

β = factor depending on the geometry of the aggregate;

a = distance for the center of the matrix block to the fracture boundary (m);

γ_w= empirical coefficient (unitless).

To analyze CO2 migration for a single continuum (expand for multicontinuum with equations (5) and (6)), heterogeneous, isotropic conditions with relative permeability, governing equation (8) applies, or

$$\frac{\partial}{\partial x}\left(\frac{\rho_s k_{rs} k}{\mu_s}\frac{\partial p}{\partial x}\right)+\frac{\partial}{\partial z}\left(\frac{\rho_s k_{rs} k}{\mu_s}\frac{\partial p}{\partial z}\left(p+\rho_s g z\right)\right)+ \frac{\partial}{\partial x}\left(\frac{\rho_w k_{rw} k}{\mu_w}\frac{\partial p}{\partial x}\right)+\frac{\partial}{\partial z}\left(\frac{\rho_w k_{rw} k}{\mu_w}\frac{\partial p}{\partial z}\left(p+\rho_w g z\right)\right)=\frac{\partial\left(n\rho_f\right)}{\partial t} \tag{8}$$

with the values

k_r = permeability relative to the flux of one phase to the other (m^2);

k = permeability of the fluid (m^2); μ = viscosity of fluid (kg/(m*s));

p = fluid density (kg/m^3); p = pressure (Pa);g = gravity (m/s^2);

n = porosity (unitless); t = time (s).

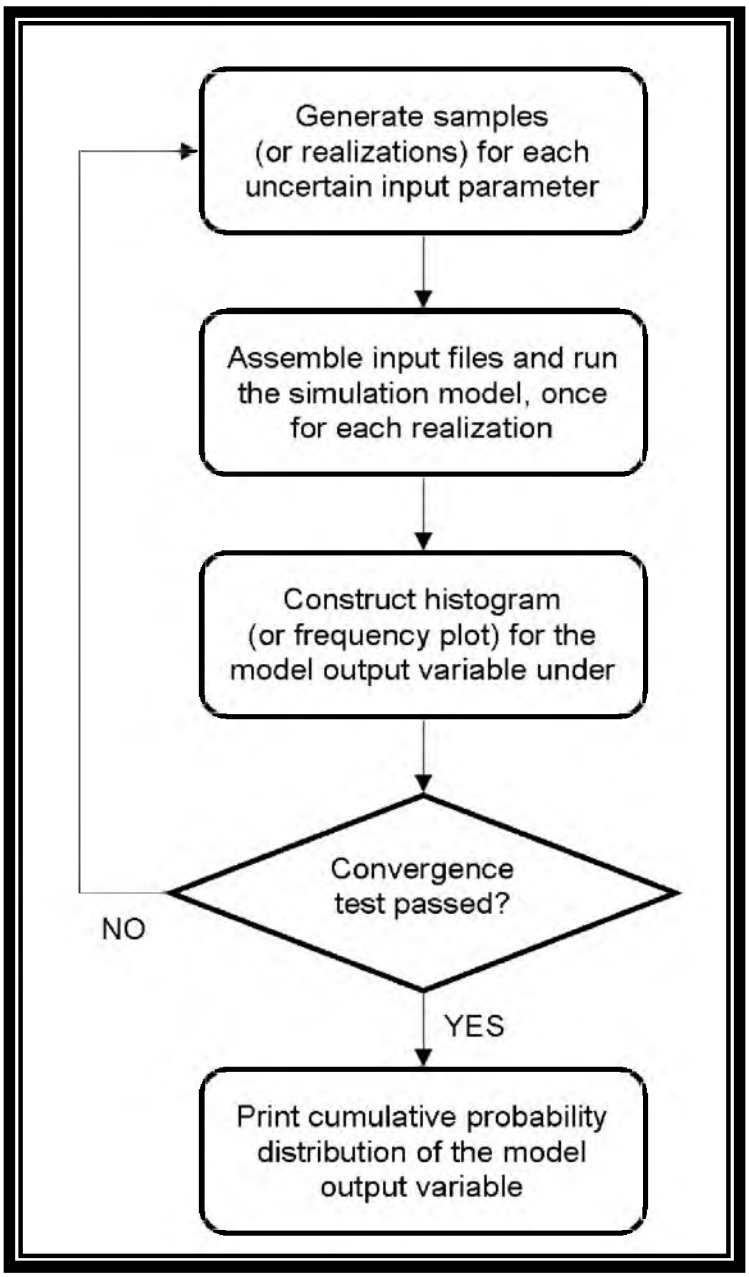

Figure 5. Flowchart of Monte Carlo analysis.
(Modified from Zheng, et al., 2002)

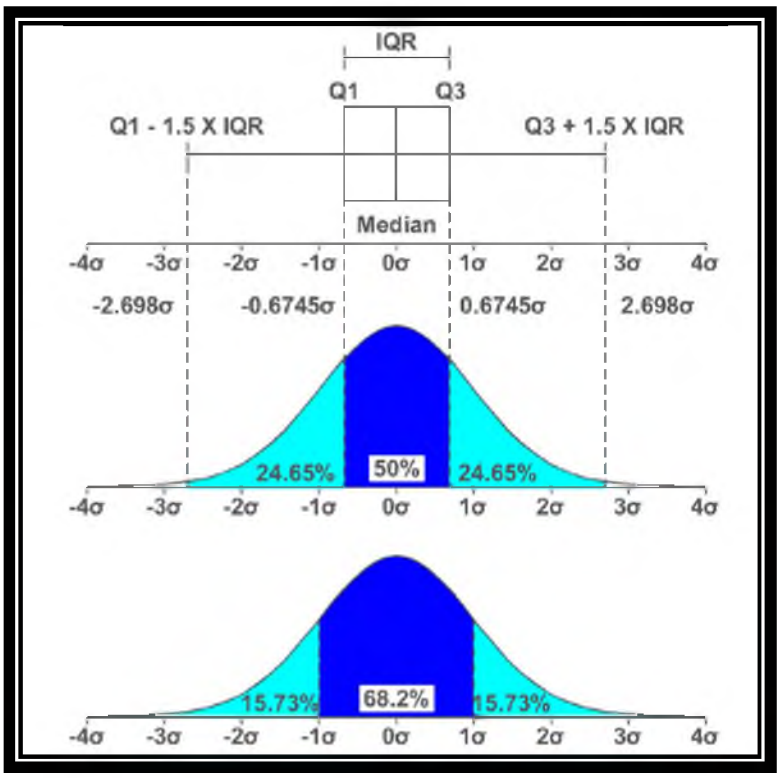

Figure 6. Probability density functions of a normal distribution.

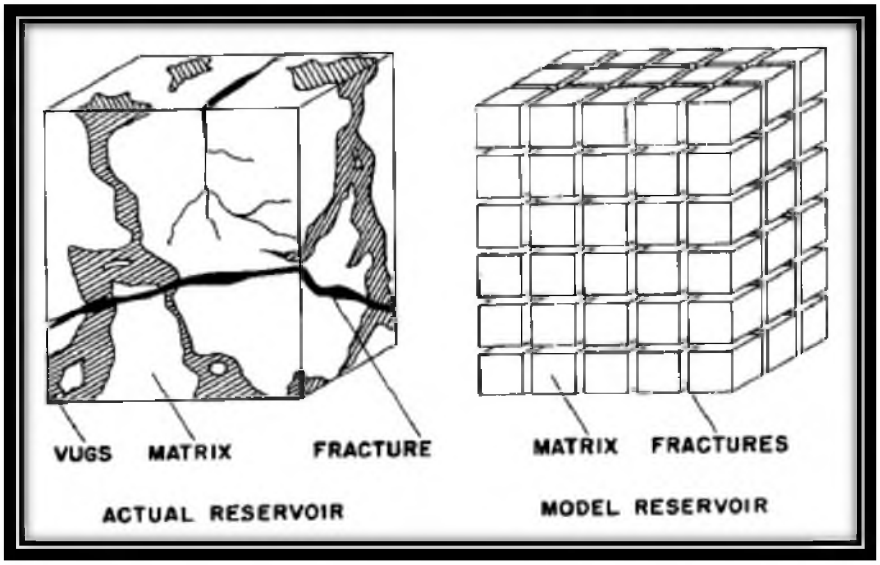

Figure 7. Model of a fractured multicontinuum medium.
(Modified from Warren, et al., 1963)

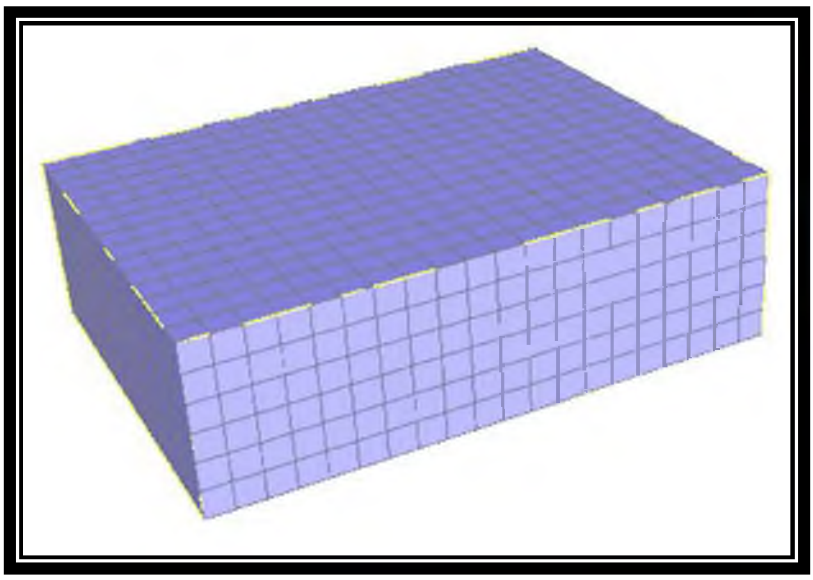

Figure 8. Model of a single continuum medium.

FAULT AND SEAL LEAKAGE ANALYSIS AND RESULTS

(CRITICAL QUESTIONS 1 AND 2)

The conceptual model considered is that of a fault that penetrates the formations terminating above the seal (Figure 4(a), Introduction). An assumption is that the increase in pressure during injection will propagate through the reservoir seal and follow the high permeability of the fault. For the rest of the study, multicontinua grids are referred to as "dual porosity models" since all such models were implemented as dual porosity. The models used in this section are intended to represent an actual CCS site in western Texas, the SACROC field (Han et al., 2010a), and thus the rock layers and associated properties are drawn from data for that field. A Base Model was compiled with all known parameters, and unknown information was estimated using typical values for a western United States sedimentary basin (summarized in Table 1). Based on actual field data, the model's dimensions are 1200m in the horizontal direction and 1550m in the vertical direction (Figure 9). The medium consisted of 6 different formations in the vertical direction with appropriate permeability and porosity values. In model simulations to represent the top surface or atmosphere, a layer was simulated with values as closely representative to those of the atmosphere including 101,500 Pa pressure and ~15 degrees C. The fault medium was assigned its own permeability and porosity values. The boundaries on either side in the horizontal direction and along the bottom in the vertical direction were all assigned to be "no-flow." A no-flow boundary condition implies that there is no flow of any type in or out of a model at these boundaries. From the surface, pressure increases with depth in the vertical direction of the model; the initial condition of the entire model was hydrostatic pressure.

The modeled bottom three formations; Res, WcSh, and WcSS (Table 1), were selected as the basis for a set of permeability and porosity ranges in a sensitivity analysis. Initial simulations included only single phase flow of water to evaluate pressure behavior within the reservoir, but subsequent simulations included multiphase CO2 and brine flow to evaluate the impacts of CO2 in the reservoir. The time required for CO2 to penetrate the seal was among the primary goals.

To address critical questions 1 and 2, a logical progression was designed. The model progression design involved starting with a simple model to simulate to completion, then adding an additional degree of complication to the model upon each simulation completion. The first stage of the analysis for this section involved running a Base Case Model of single phase waterflow under isothermal conditions for the Unpenetrated-Seal (Figure 4(a), Introduction) and Fault-Penetrating-Seal model (Figure 4(b), Introduction) and then evaluating steady-state conditions for a range of different scenarios. Results of this analysis were plotted over time for both the Unpenetrated-Seal and Fault-Penetrating-Seal model. The porosity scenarios were simulated after all permeability model permutations were completed.

The second stage of my analysis for this section was to execute the Base Case Model for multiphase CO2 flow under isothermal conditions. The purpose of this part of the analysis was to evaluate whether the seal at this site could hold CO2 in the reservoir under a range of conditions, specifically, for both the Unpenetrated-Seal (Figure 4(a), Introduction) and Fault-Penetrating-Seal (Figure 4(b), Introduction) models.

The final stage of analysis for this section was to develop and run a simple 1-D model of the seal (Figure 4(c), Introduction) with multiphase CO2 and isothermal for the highest and lowest values of permeability considered in the sensitivity analyses. The time required to flow through a typical seal were evaluated with numerical simulations and compared to analytical calculations of the same.

Simulation Results

To simulate a dual porosity medium, specific and usually different values of porosity value are assigned to the rock matrix and fractures. (see Numerical Modeling Methods used in the Study for discussion of multiple interacting continua, including dual porosity). Assigned parameter values for the Unpenetrated-Seal model (Figure 4(a), Introduction) are summarized in Table 2. The seal layer (WcSh) is assigned a matrix porosity value of 2%, and the fracture is assigned an effective porosity of 0.8%. Effective porosity is the interconnected pore volume (it excludes isolated, nonconnected pore spaces). These porosity values are representative of a low porosity medium that is ideally suited to serve as a seal layer.

The assigned parameters of the Fault-Penetrating-Seal model (Figure 4(b), Introduction) are summarized in Table 3. The seal layer (WcSh) is assigned a matrix porosity value of 2% and the fracture is assigned an effective porosity of 1.6%. These values are representative of fractured shale (Schwartz, et al., 2003).

Details of Base Case Model, referred to as R1H1S1, are summarized in Table 4. Table 4 lists the permeability values assigned within each model permutation, and each model permutation is defined by a key-code. The definition of each key-code is based on the permeability values assigned to the lower-most three formations in the model, which are the only formations that are varied in the sensitivity analysis. For example, R1H2S1 which is defined as Res (R) permeability 1, WcSh (H) permeability 2, and WcSS (S) permeability 1. Much like Table 4 details the permeability variations assigned to the reservoir and the two Wolfcamp units above it, Table 5 summarizes the matrix porosity values assigned to these formations for the sake of the sensitivity analysis. In all models, the fracture effective porosity of 1.6% is maintained constant and uniform (Table 2 and Table 3).

Pressure Dissipation Analysis

Pressure Decline Analysis of a Reservoir with an Unpenetrated Seal

The purpose of the Unpenetrated-Seal model (depicted generally in Figure 4(a), Introduction) was to evaluate the time required for pressure to decline (dissipate) from injection-induced high fluid pressure down to steady-state. Results of this analysis are compared to a reservoir with a fractured/faulted seal, to establish how such penetrations affect reservoir pressures over time, at least in general. All simulations in this and the following section were parameterized as single-phase (water only), for the sake of simplification; relative permeability and capillary tension can impact pressure behaviour significantly, and such effects are evaluated in subsequent sections of this thesis. The initial conditions correspond to an injection-induced reservoir pressure of 25.5MPa. The simulation time was 1 million years. The steady-state pressure distribution was reached at 1317.1 year, shown in Figure 10, corresponding to case 1 (R1H1S1). The total change in pressure (ΔP), also at steady-state, is plotted in Figure 11.

The rest of the permeability/porosity permutation simulations have approximately the same results as shown in Figure 10. The only difference is in the simulation time length to steady-state (Table 6 and Table 7; Appendices A and B).

These simulation results suggest that many reservoirs will require thousands of years for the injection-induced pressure to disperse, even when the seal layer (WsSh) exhibits relatively higher values of permeability. Lower reservoir permeabilities translate to longer times necessary for pressure dissipation; likewise, thicker reservoirs will require more time for injection-induced pressures to dissipate.

In contrast, higher reservoir porosity translate to longer periods of time required for pressure dissipation, inasmuch as fluid occupies more volume in higher-porosity formations, in general.

Evaluation of Pressure Dissipation in a Reservoir with a Breached Seal

To evaluate pressure dissipation in a reservoir with a breached seal, the Fault-Penetrating-Seal model (Figure 4(b), Introduction) was simulated. Specifically, would the

reservoir permeability dictate the amount of time required for pressure dissipation from high (injection-induced) pressure to steady-state? The initial conditions correspond to a reservoir pressure of 25.5MPa, as induced by injection, and the simulation period was 1 million years. The steady-state pressure distribution was reached at 1153.1 year (Figure 12), corresponding to case 1 (R1H1S1), and the total change in pressure at steady-state is plotted in Figure 13.

Simulation results corresponding to the rest of the permeability sensitivity analysis were similar to those depicted by Figure 12. Simulated periods of time necessary to reach steady-state for variations in reservoir and Wolfcamp Shale/Sandstone permeabilities are summarized in Table 8 (see also Appendix C). Similarly, simulated periods of time necessary to reach steady-state for variations in reservoir and Wolfcamp Shale/Sandstone porosities are summarized in Table 9 (see also Appendix D).

Consistent with results of previous studies, these simulation results confirm that time of pressure dissipation is dictated by the lowest permeabilities and highest porosities in the system.

Analysis of CO2 Migration Distance – In and Above Seals

Analysis of CO2 Migration Distance from a Reservoir with an Unbreached Seal

Additional models were assembled to evaluate the distance that CO2 might penetrate a seal and migrate above that seal and specifically in a reservoir with an unbreached seal (depicted generally in Figure 4(b), Introduction). For this particular analysis, the initial conditions include a reservoir pressure of 25.5MPa and 96% CO2 saturation. The total duration of simulated time is 5000 years, inasmuch as this was sufficient time to reach a steady-state CO2 distribution. The final simulated pressure distribution is contoured in Figure 14, the corresponding supercritical CO2 distribution is plotted in Figure 15, and the corresponding dissolved CO2 distribution is contoured Figure 16.

Simulation results corresponding to other permeability permutations (Table 10) are effectively identical to those of Figure 14, Figure 15 and Figure 16, except for the time required to reach steady-state (see also Appendices G, H and I). Table 10 details the times required to

reach steady-state for the different permeability values considered, and Table 11 details the times required to reach steady-state for the different porosity values assigned in the sensitivity analysis.

As these figures (Figure 14, Figure 15, Figure 16) indicate, a decrease in pressure is exhibited as proximity to the fault increases. More importantly, collocated with the fault is an increase in hydraulic head gradient, indicating that local fluid flow rates are higher right at the fault, despite the seal being unbreached. Table 12 summarizes calculated specific discharge values ("Darcy flow velocity" values) next to and directly located at the fault location.

The most critical result of this analysis is that local flow velocities are increased despite the unbreached or unbroken seal. Thus, risk assessment efforts should probably include analysis of faults whether or not they are known to penetrate a CO2 target reservoir's primary seal.

Analysis of Time Required for Multiphase Flow Across/Through an Unbroken Seal and Fault Above

Further flow analysis using simulation models was conducted to evaluate time required for CO2 to migrate across a seal or through a fault. For the sake of simplicity, these travel times are referred to as seal time lengths and fault time lengths, respectively. Based on three locations in the model grid (Table 13), breakthrough plots of pressure and CO2 at these points were constructed for a reservoir model with an unbreached seal (Figure 17, Figure 18 and Figure 19), corresponding to typical values of permeability (R1H1S1 in Table 4) and to more-extreme values of permeability (R2H2S2 in Table 4).

Table 14 and Figure 18 summarize results of this breakthrough analysis for case R1H1S1, corresponding to typical permeability contrasts between a reservoir and seal (see Table 4 for details of this and other permeability permutations considered). Specifically, the values indicated in Table 14 and plotted in Figure 18 express the time required to migrate across the unbreached seal and the pressure contrast across that seal for these permeability values (Table 4). See Figure 17 for relative locations of points on each side of the seal.

Table 15 and Figure 19 summarize results of this breakthrough analysis for case R2H2S2, corresponding to more-extreme permeability contrasts between a reservoir and seal. Specifically, the values indicated in Table 15 and the plot in Figure 19 illustrate the time required

to migrate across the unbreached seal and the pressure contrast across that seal for these permeability permutations. See Table 4 for details about permeability values assigned for case R2H2S2 and see Figure 17 for relative locations of points on each side of the seal.

The main goal of this analysis was to quantify time required for CO2 to migrate across a typical seal and through a fault for different, realistic cases of permeability amongst a reservoir, seal and a fault above the unbreached seal (Figure 17 and Table 4). Naturally, a lower-permeability seal would slow down CO2 "leakage" across the fault (Figure 17). Leakage across such a seal is uniform until it reaches the other side of the seal, and then CO2 tends to flow towards the fault (Figure 18 and Figure 19). As expected by Darcy's Law, a linear correlation between permeability and leakage (specific discharge) is evident when comparing results of the different permeability permutations (Figure 18 and Figure 19).

Analysis of CO2 Migration Distance from a Reservoir with a Breached Seal

Another critical issue to address is the extent of migration or "leakage" that will occur if a fault breaches the seal and CO2 migrates through that single location along the seal (depicted generally in Figure 4(b), Introduction). In particular, does the specific magnitude of reservoir permeability dictate the amount of time required for CO2 to migrate to the surface, or is the permeability of the fault more important in this context? For this modelling analysis, the initial conditions include a reservoir pressure of 25.5MPa and 96% CO2 saturation. The duration or time of simulation was 5000 years (the model reached steady state before 5000 years). The simulation reached steady-state after 147.5 years, and the final pressure distribution is plotted in Figure 20. The final supercritical CO2 distribution is plotted in Figure 21, and dissolved CO2 is plotted in Figure 22, also at the simulation end.

Remaining permutations of the sensitivity analysis are similar to those illustrated in Figure 20, Figure 21 and Figure 22. See also Table 16, Table 17, and Appendices J, K and L.

Figure 20 illustrates a decrease in pressure closer to the fault due to its higher permeability. Simple analysis using Darcy's law implies that flow is higher through the seal and

draws the surrounding pressure through the fault as well (see also Table 12, section Analysis of CO2 Migration Distance from a Reservoir with an Unbreached Seal).

These results suggest that high permeabilities in an unfractured seal will allow for the CO2 to escape within a few years. However, a higher-permeability fault will increase leakage rates. Higher porosity media slows leakage, of course, inasmuch as CO2 must fill a greater volume before it can migrate.

Analysis of Time Required for Leakage Across a Breached Seal

Additional analysis of flow through a faulted seal was conducted with additional simulations. Based on three locations in the model grid (Table 18), breakthrough plots of pressure and CO2 at these points were constructed for a reservoir model with a breached seal (Figure 23, Figure 24 and Figure 25), corresponding to typical values of permeability (R1H1S1 in Table 4) and to more-extreme values of permeability (R2H2S2 in Table 4).

Table 19 and Figure 24 summarize results of this breakthrough analysis for case R1H1S1, corresponding to typical permeability contrasts between a reservoir and seal (see Table 4 for details of this and other permeability permutations considered). Specifically, the values indicated in Table 19 and plotted in Figure 24 express the time required to migrate across the faulted seal and the pressure contrast across that seal for these permeability values (Table 4). See Figure 23 for relative locations of points on each side of the seal.

Table 20 and Figure 25 summarize results of this breakthrough analysis for case R2H2S2, corresponding to more-extreme permeability contrasts between a reservoir and seal. Specifically, the values indicated in Table 20 and the plot in Figure 25 illustrate the time required to migrate across the faulted seal and the pressure contrast across that seal for these permeability permutations. See Table 4 for details about permeability values assigned for case R2H2S2 and see Figure 23 for relative locations of points on each side of the seal.

The main focus of this section was to quantify the primary controls on rates that CO2 will migrate through a seal and associated fault under different conditions. Such leakage across a seal is uniform except in the proximity of such a fault, as illustrated in Figure 20 and Figure 21.

The strong linear correlation between permeability and leakage (specific discharge) observed for an unbreached seal is not as apparent when comparing results of the different permeability permutations (Figure 24 and Figure 25).

Time Required for CO2 to Traverse a Seal (only)

In this section, results for a model simulation analysis of a simplified (1-D) seal are presented. See Figure 4(c), Introduction for a generalized schematic of this simplified model. The model dimensions and initial are conditions were taken from the larger-scale model presented at the beginning of the Section (Figure 9) to create a small-scale model analysis. One specific issue addressed was whether grid cell size influences the migration rates of CO2. The simulated width in the horizontal direction was 20m, which is the length of the cells of the large-scale model. The depth in the vertical direction was 27m, which is the thickness of that original seal in the larger-scale model grid, and on the top and bottom (highlighted) are 1m cells representing the medium on either side of the seal (Figure 26). The bottom layer was assigned a constant pressure of 25.5MPa and 96% CO2 saturation, which represents the original reservoir (Res) conditions. The top cell was assigned a pressure of 12.6MPa and zero CO2 saturation, which represents the WcSS formation above the seal. The permeability of WsSh formation from case 1 (1.0E-18) and case 8 (1.0E-16) were used and a porosity of 2% for both cases.

The simulation results of this analysis are detailed in Table 21. These simulated calculated results were compared to simple analytical calculations of travel time required to pass through the seal, a so-called "Pressure Length Equation," equation (9). The values used for these calculations are listed in Table 22. Table 23 summarizes the estimated travel times for the "typical" permeability case 1 (R1H1S1), 19.9 days and for the more extreme permeability case 8 (R2H2S2), 0.2 days.

$$l = \sqrt{4\frac{K}{S_s}t} \qquad (9)$$

with the values

l = length (m), K = hydraulic conductivity (m/s), S_s = specific storage (1/m),

t = time (s).

These results indicate a linear relationship between permeability and simulated/calculated migration times for CO2 to transverse a seal. When comparing small-scale with large-scale seal migration times, the grid cell size appears to be a significant effect. For the case 1 (R1H1S1; see Table 4) with higher permeabilities, the large-scale model migration time was 21 years while the small-scale model (with smaller grid blocks) time was 27 years. Thus, a finer grid cell size appears to increase migration times. However, analytical values of migration time are less than all numerical results. It is not clear which approach – analytical versus coarse grid versus fine grid – is most accurate, and comparison to laboratory or field results would be necessary to elucidate such.

Table 1. Base case model formation parameter values.

Material	Porosity (%)	Permeability in Horizontal & Vertical direction (m^2)	Density (kg/m^3)	Thermal conductivity @ 20°C (W/(m °K))	Specific heat (J/(kg °K))
Air	100	1.0E-10	2650	0.02	1000
Surface	10	1.0E-14	2323	2.3	920
Dockum	20	1.0E-15	2650	2.3	1000
WcLS	10	1.0E-15	2500	2.5	909
WcSS	15	1.0E-17	2650	2.3	1480
WcSh	2	1.0E-18	2675	1.7	1480
Res	10	1.0E-13	2500	2.5	909
Fault	60	1.0E-12	1954	3.0	840

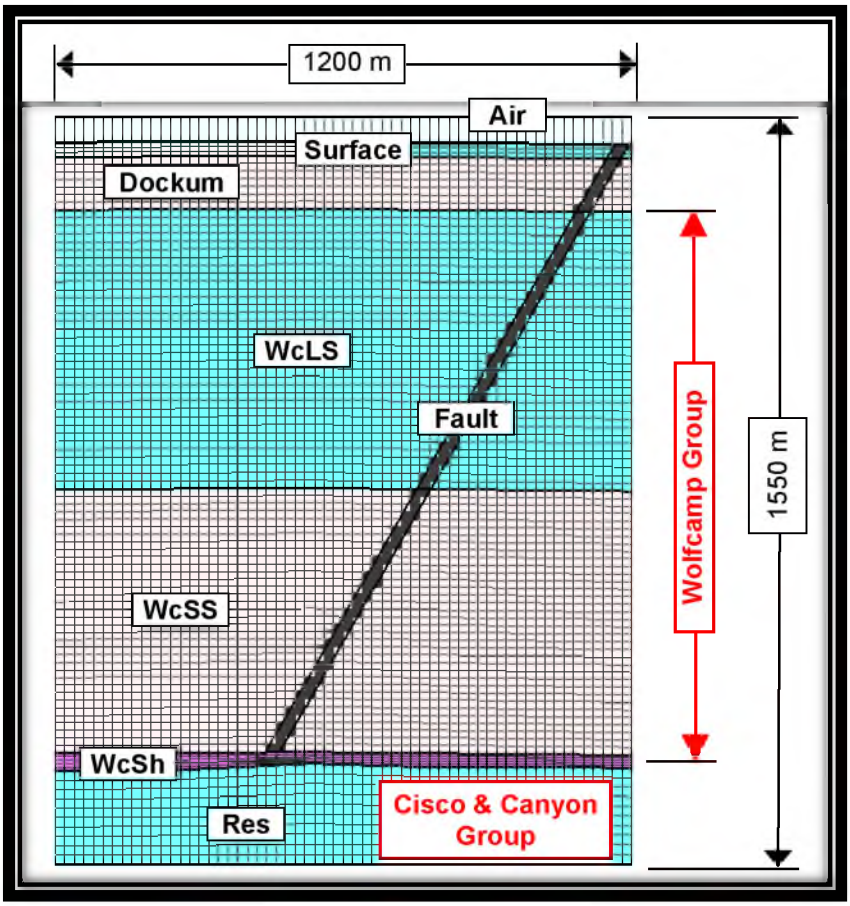

Figure 9. Dual porosity conceptual model including all formations and dimensions.

Table 2. Unpenetrated-Seal matrix and fracture porosity values for dual porosity model simulations. Values are based on (Schwartz, et al., 2003).

Material	Matrix Porosity (%)	Fracture		
		Volume fraction (%)	Flow in fraction (%)	Effective Porosity (%)
Air	100	2	80	1.6
Surface	10	2	80	1.6
Dockum	20	2	80	1.6
WcLS	10	2	80	1.6
WcSS	15	2	80	1.6
WcSh	2	2	40	0.8
Res	10	2	80	1.6
Fault	60	2	85	1.7

Table 3. Fault-Penetrating-Seal matrix and fracture porosity values for dual porosity model simulations. Values are based on (Schwartz, et al., 2003).

Material	Matrix Porosity (%)	Fracture		
		Volume fraction (%)	Flow in fraction (%)	Effective Porosity (%)
Air	100	2	80	1.6
Surface	10	2	80	1.6
Dockum	20	2	80	1.6
WcLS	10	2	80	1.6
WcSS	15	2	80	1.6
WcSh	2	2	80	1.6
Res	10	2	80	1.6
Fault	60	2	85	1.7

Table 4. Permeability values assigned to the bottom three formations of the model, as permutations in the sensitivity analysis.

Case	Permutation			Res (R) (m^2)	WcSh (H) (m^2)	WcSS (S) (m^2)
1	R 1	H 1	S 1	1.0E-13	1.0E-18	1.0E-17
2	R 1	H 1	S 2	1.0E-13	1.0E-18	1.0E-18
3	R 1	H 2	S 1	1.0E-13	1.0E-16	1.0E-17
4	R 1	H 2	S 2	1.0E-13	1.0E-16	1.0E-18
5	R 2	H 1	S 1	1.0E-15	1.0E-18	1.0E-17
6	R 2	H 1	S 2	1.0E-15	1.0E-18	1.0E-18
7	R 2	H 2	S 1	1.0E-15	1.0E-16	1.0E-17
8	R 2	H 2	S 2	1.0E-15	1.0E-16	1.0E-18

Table 5. Porosity values assigned to the bottom three formations of the model, as permutations in the sensitivity analysis.

Case	Permutation				Res (R) (%)	WcSh (H) (%)	WcSS (S) (%)
		R 1	H 1	S 1	10	2	15
9	p 1	R 1	H 1	S 1	5	5	5
10	p 2	R 1	H 1	S 1	15	15	15

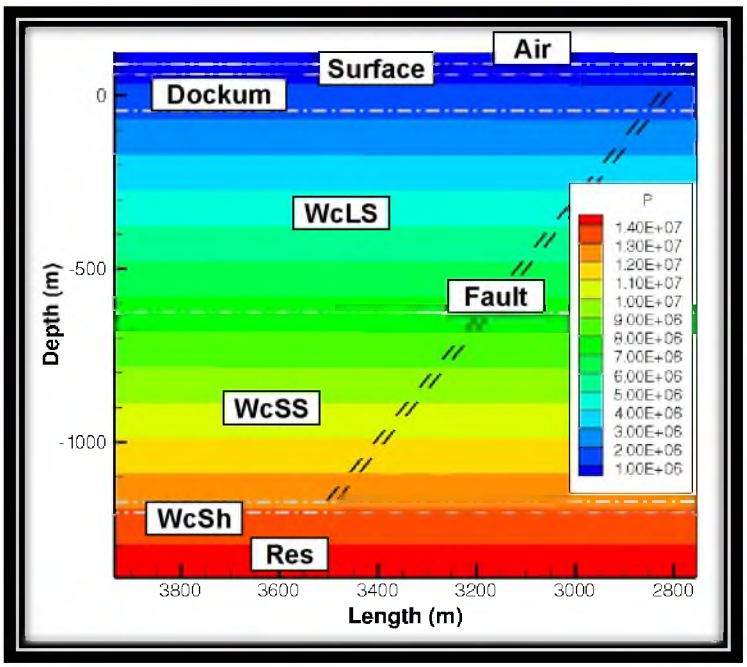

Figure 10. Simulated steady-state pressure distribution corresponding to a model reservoir with an unpenetrated seal.
See text for details.

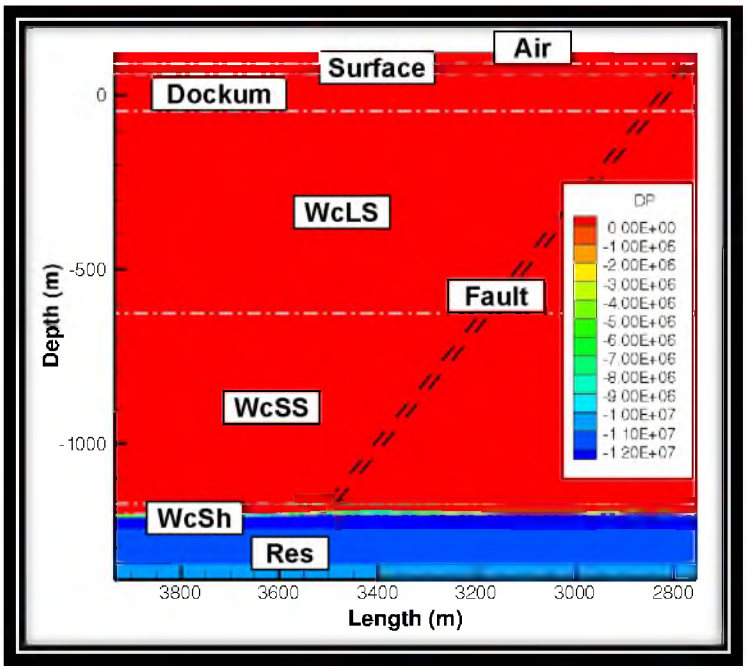

Figure 11. Simulated distribution of total pressure change corresponding to a model reservoir with an unpenetrated seal.
See text for details.

Table 6. Time to reach steady-state for different permeability permutations in the sensitivity analysis of pressure dissipation in a reservoir model with an unfractured seal. See text for more details.

Case	Permutation			Res (R) (m^2)	WcSh (H) (m^2)	WcSS (S) (m^2)	Years to steady state
1	R 1	H 1	S 1	1.0E-13	1.0E-18	1.0E-17	1317.1
2	R 1	H 1	S 2	1.0E-13	1.0E-18	1.0E-18	1821.0
3	R 1	H 2	S 1	1.0E-13	1.0E-16	1.0E-17	1037.5
4	R 1	H 2	S 2	1.0E-13	1.0E-16	1.0E-18	1270.4
5	R 2	H 1	S 1	1.0E-15	1.0E-18	1.0E-17	1153.1
6	R 2	H 1	S 2	1.0E-15	1.0E-18	1.0E-18	1685.9
7	R 2	H 2	S 1	1.0E-15	1.0E-16	1.0E-17	1210.1
8	R 2	H 2	S 2	1.0E-15	1.0E-16	1.0E-18	1269.1

Table 7. Time to reach steady-state for different porosity permutations in the sensitivity analysis of pressure dissipation in a reservoir model with an unfractured seal. See text for more details.

Case	Permutation				Res (R) (%)	WcSh (H) (%)	WcSS (S) (%)	Years to steady state
9	p 1	R 1	H 1	S 1	5	5	5	1080.8
10	p 2	R 1	H 1	S 1	15	15	15	1343.6

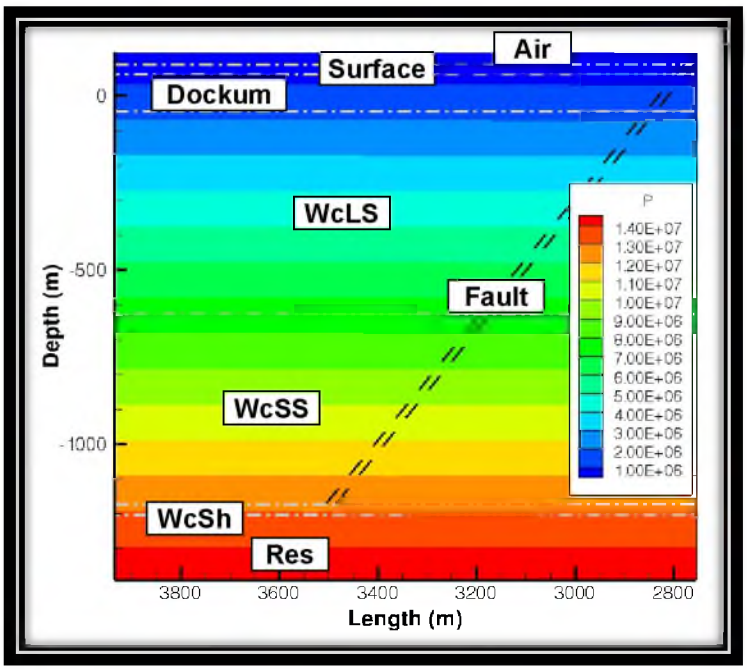

Figure 12. Simulated distribution of fluid pressure corresponding to a model reservoir with a fault penetrating its seal.
See text for details.

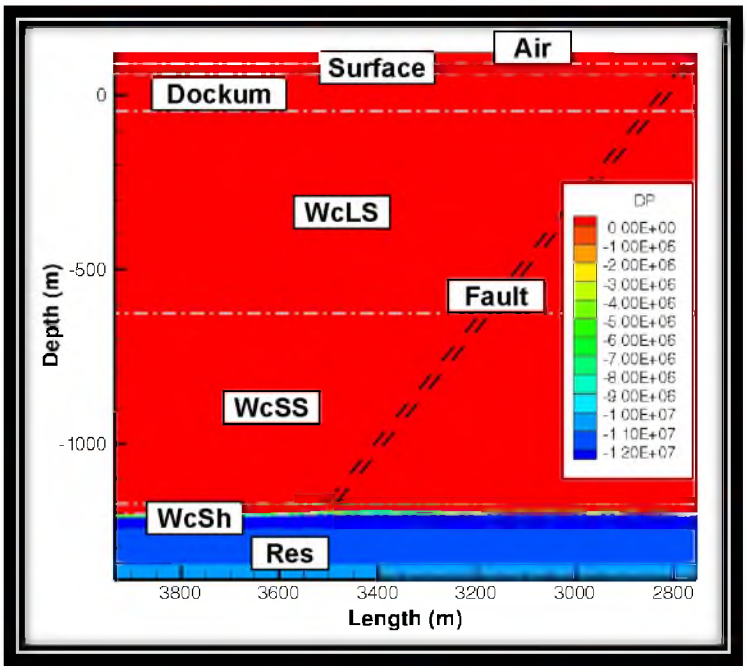

Figure 13. Simulated distribution of total pressure change corresponding to a model reservoir with a fault penetrating its seal.
See text for details

Table 8. Time to reach steady-state for different permeability permutations in the sensitivity analysis of pressure dissipation in a reservoir model with a fractured seal. See text for more details.

Case	Permutation			Res (R) (m^2)	WcSh (H) (m^2)	WcSS (S) (m^2)	Years to steady state
1	R 1	H 1	S 1	1.0E-13	1.0E-18	1.0E-17	1153.1
2	R 1	H 1	S 2	1.0E-13	1.0E-18	1.0E-18	1823.0
3	R 1	H 2	S 1	1.0E-13	1.0E-16	1.0E-17	1093.8
4	R 1	H 2	S 2	1.0E-13	1.0E-16	1.0E-18	1299.7
5	R 2	H 1	S 1	1.0E-15	1.0E-18	1.0E-17	1314.8
6	R 2	H 1	S 2	1.0E-15	1.0E-18	1.0E-18	1656.5
7	R 2	H 2	S 1	1.0E-15	1.0E-16	1.0E-17	1218.4
8	R 2	H 2	S 2	1.0E-15	1.0E-16	1.0E-18	1271.6

Table 9. Time to reach steady-state for different porosity permutations in the sensitivity analysis of pressure dissipation in a reservoir model with a fractured seal. See text for more details.

Case	Permutation				Res (R) (%)	WcSh (H) (%)	WcSS (S) (%)	Years to steady state
9	p 1	R 1	H 1	S 1	5	5	5	1091.8
10	p 2	R 1	H 1	S 1	15	15	15	1353.8

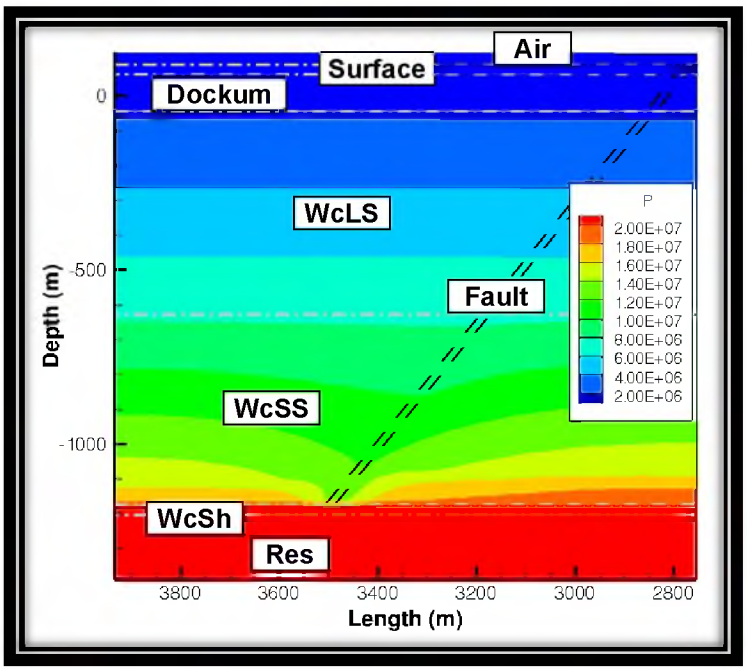

Figure 14. Simulated steady-state pressure distribution corresponding to simulated multiphase CO2 flow in a model reservoir with an unpenetrated seal.
See text for details.

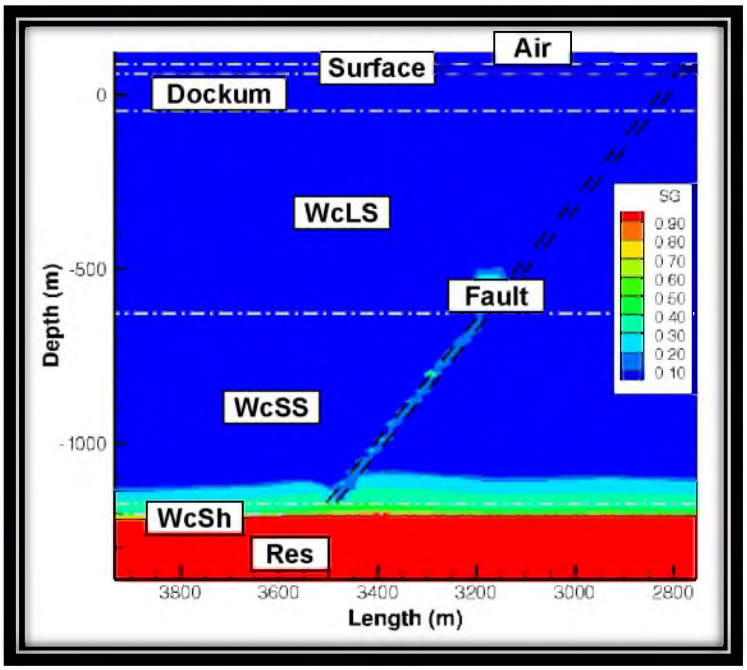

Figure 15. Simulated steady-state distribution of supercritical CO2 corresponding to simulated multiphase CO2 flow in a model reservoir with an unpenetrated seal.
See text for details.

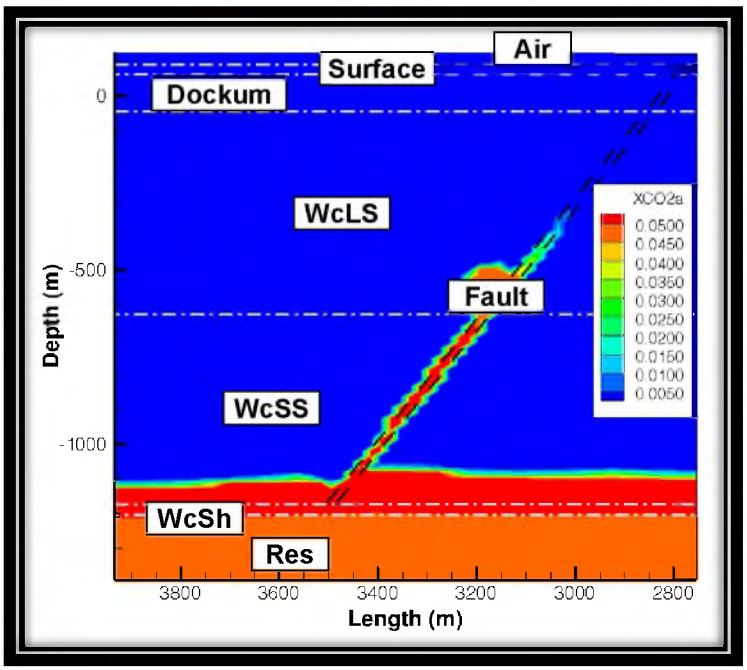

Figure 16. Simulated steady-state distribution of dissolved (aqueous) CO2 corresponding to simulated multiphase CO2 flow in a model reservoir with an unpenetrated seal. See text for details.

Table 10. Time to reach steady-state for different permeability permutations in the sensitivity analysis of CO2 migration in a reservoir model with an unbreached seal. See text for more details.

Case	Permutation			Res (R) (m^2)	WcSh (H) (m^2)	WcSS (S) (m^2)	Years to end of Simulation
1	R 1	H 1	S 1	1.0E-13	1.0E-18	1.0E-17	115.5
2	R 1	H 1	S 2	1.0E-13	1.0E-18	1.0E-18	151.5
3	R 1	H 2	S 1	1.0E-13	1.0E-16	1.0E-17	1.9
4	R 1	H 2	S 2	1.0E-13	1.0E-16	1.0E-18	2.1
5	R 2	H 1	S 1	1.0E-15	1.0E-18	1.0E-17	115.5
6	R 2	H 1	S 2	1.0E-15	1.0E-18	1.0E-18	151.6
7	R 2	H 2	S 1	1.0E-15	1.0E-16	1.0E-17	1.9
8	R 2	H 2	S 2	1.0E-15	1.0E-16	1.0E-18	2.2

Table 11. Time to reach steady-state for different porosity permutations in the sensitivity analysis of CO2 migration in a reservoir model with an unbreached seal. See text for more details.

Case	Permutation				Res (R) (%)	WcSh (H) (%)	WcSS (S) (%)	Years to end of Simulation
9	p 1	R 1	H 1	S 1	5	5	5	118.8
10	p 2	R 1	H 1	S 1	15	15	15	112.9

Table 12. Calculated specific discharge values for flow across the seal corresponding to the sensitivity analysis of CO2 migration in a reservoir model with an unbreached seal.

Depth at 1165m		Depth at 1200m		Darcy's flow velocity
y (m)	Pressure (Pa)	y (m)	Pressure (Pa)	q (m/s)
3805	1.80E+07	3805	2.25E+07	1.29E-13
3491	1.47E+07	3491	2.25E+07	2.23E-13
2863	1.91E+07	2863	2.25E+07	9.71E-14

Table 13. Coordinates of model grid points plotted in Figure 17, Figure 18 and Figure 19.

Cell Number	Coordinates		
	X	Y	Z
597	2413.10	3493.65	-1205.86
969		3493.65	-1160.06
3123		3173.65	-614.68

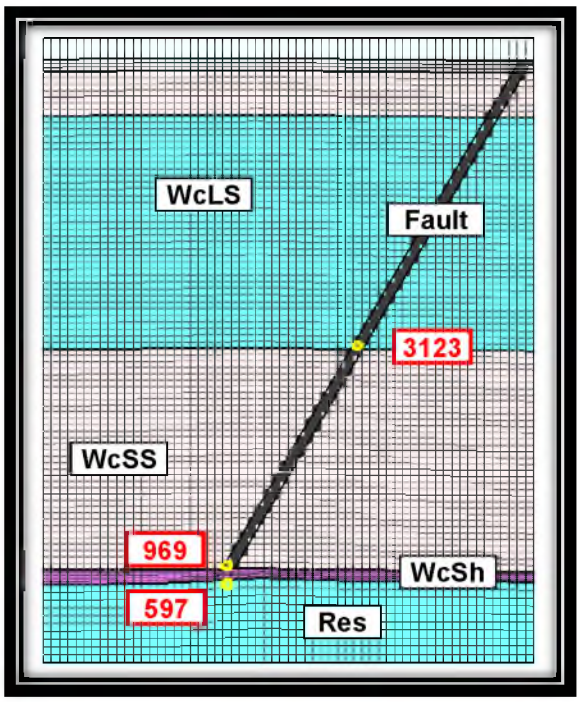

Figure 17. Locations of points corresponding to breakthrough curves plotted in Figure 18 and Figure 19.

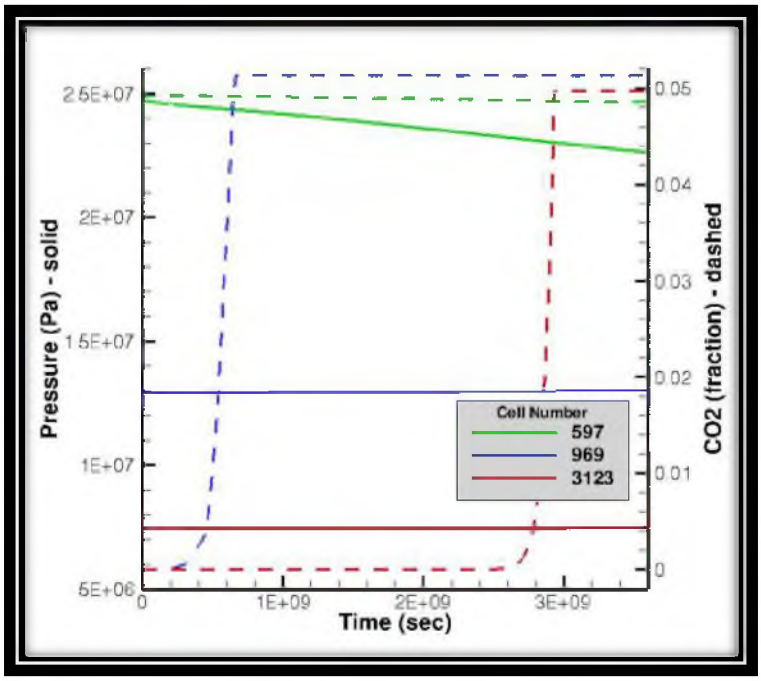

Figure 18. Breakthrough curves of pressure and CO2 corresponding to the results summarized in Table 14.
See text for details.

Table 14. Summary of breakthrough analysis results for a model reservoir with an unbreached seal, with typical values of permeability (case R1H1S1 of Table 4).

Cell Number	CO2 Time (sec)	CO2 Time (year)	Pressure (Pa) initial	Pressure (Pa) change	Pressure (Pa) difference
597	saturated		2.55E+07	2.30E+07	-2.42E+06
969	6.62E+08	20.98	1.22E+07	1.29E+07	7.10E+05
3123	2.93E+09	92.91	6.85E+06	7.47E+06	6.25E+05

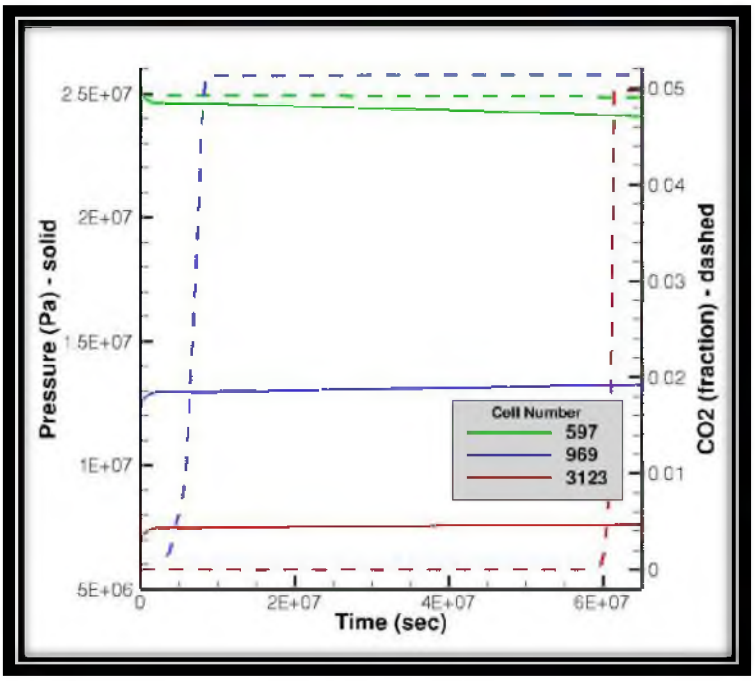

Figure 19. Breakthrough curves of pressure and CO2 corresponding to the results summarized in Table 15.
See text for details.

Table 15. Summary of breakthrough analysis results for a model reservoir with an unbreached seal, with more-extreme values of permeability (case R2H2S2 of Table 4)

Cell Number	CO2 Time (sec)	CO2 Time (year)	Pressure (Pa) initial	Pressure (Pa) change	Pressure (Pa) difference
597	saturated		2.55E+07	2.41E+07	-1.37E+06
969	8.52E+06	0.27	1.22E+07	1.30E+07	7.40E+05
3123	6.14E+07	1.94	6.85E+06	7.57E+06	7.26E+05

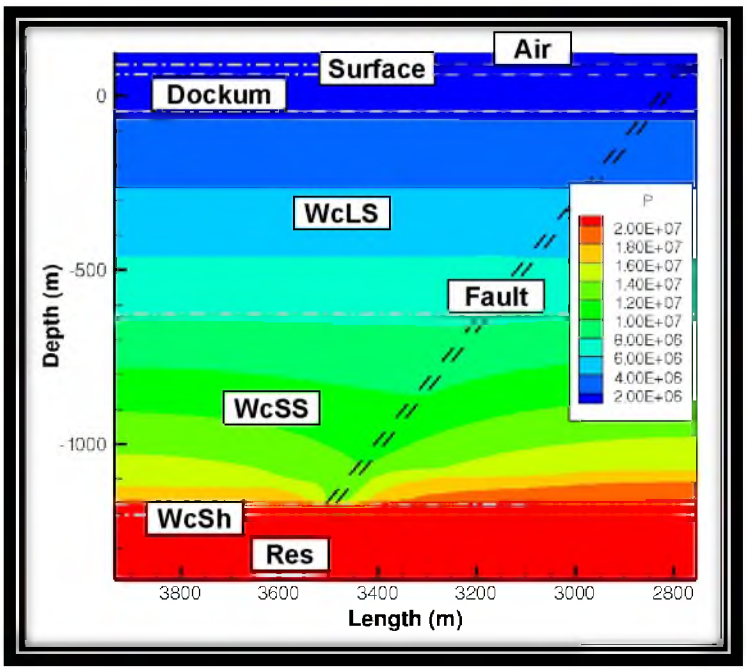

Figure 20. Simulated steady-state pressure distribution corresponding to simulated multiphase CO2 flow in a model reservoir with a breached seal.
See text for details.

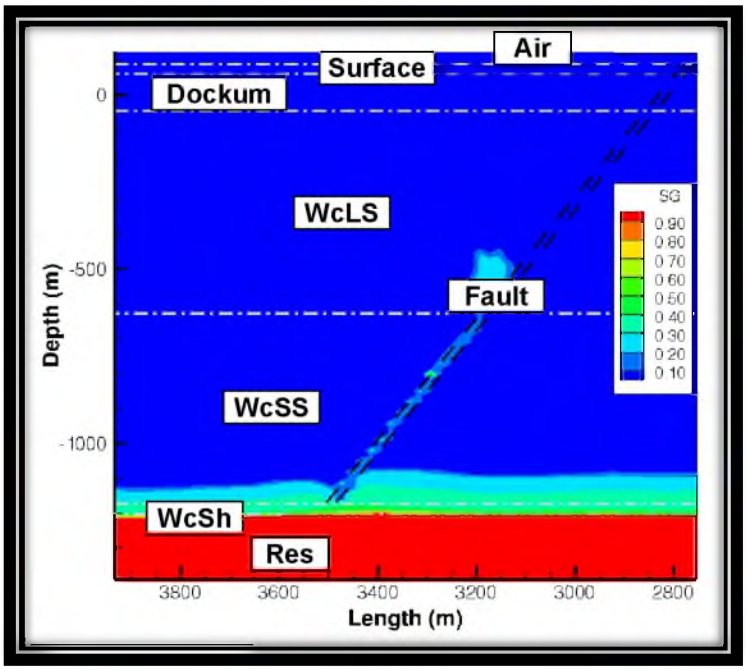

Figure 21. Simulated steady-state distribution of supercritical CO2 corresponding to simulated multiphase CO2 flow in a model reservoir with a breached seal.
See text for details.

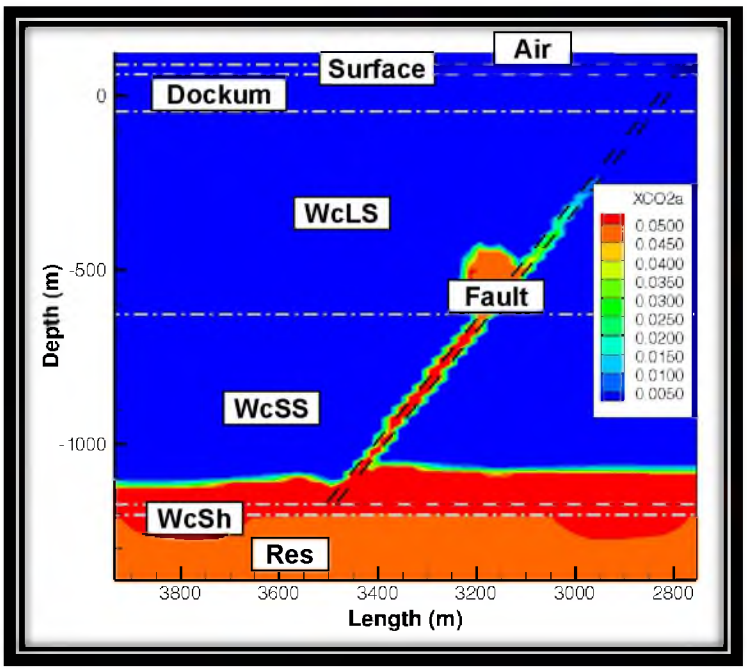

Figure 22. Simulated steady-state distribution of dissolved (aqueous) CO2 corresponding to simulated multiphase CO2 flow in a model reservoir with a breached seal. See text for details.

Table 16. Time to reach steady-state for different permeability permutations in the sensitivity analysis of CO2 migration in a reservoir model with a faulted seal. See text for more details.

Case	Permutation			Res (R) (m^2)	WcSh (H) (m^2)	WcSS (S) (m^2)	Years to end of Simulation
1	R 1	H 1	S 1	1.0E-13	1.0E-18	1.0E-17	147.5
2	R 1	H 1	S 2	1.0E-13	1.0E-18	1.0E-18	188.6
3	R 1	H 2	S 1	1.0E-13	1.0E-16	1.0E-17	2.4
4	R 1	H 2	S 2	1.0E-13	1.0E-16	1.0E-18	3.0
5	R 2	H 1	S 1	1.0E-15	1.0E-18	1.0E-17	147.6
6	R 2	H 1	S 2	1.0E-15	1.0E-18	1.0E-18	188.8
7	R 2	H 2	S 1	1.0E-15	1.0E-16	1.0E-17	2.5
8	R 2	H 2	S 2	1.0E-15	1.0E-16	1.0E-18	3.0

Table 17. Time to reach steady-state for different porosity permutations in the sensitivity analysis of CO2 migration in a reservoir model with a faulted seal.
See text for more details.

Case	Permutation				Res (R) (%)	WcSh (H) (%)	WcSS (S) (%)	Years to end of Simulation
9	p 1	R 1	H 1	S 1	5	5	5	146.8
10	p 2	R 1	H 1	S 1	15	15	15	145.9

Table 18. Coordinates of model grid points plotted in Figure 23, Figure 24 and Figure 25.

Cell Number	Coordinates		
	X	Y	Z
597	2413.10	3493.65	-1205.86
969		3493.65	-1160.06
3123		3173.65	-614.68

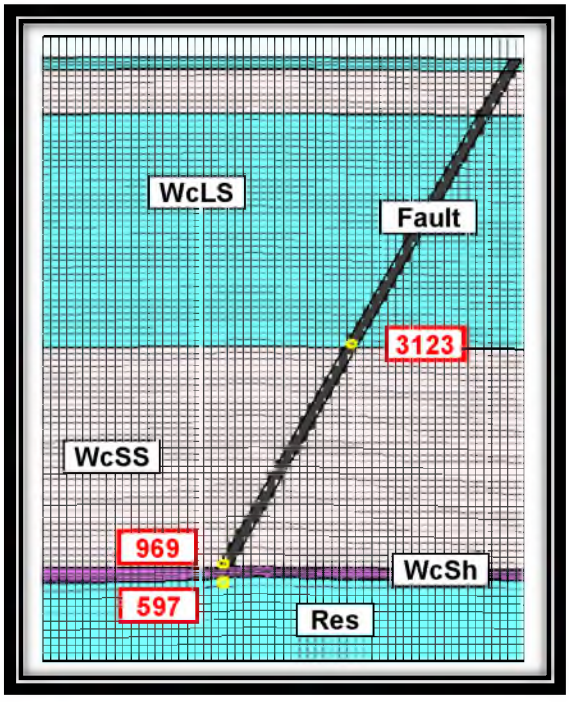

Figure 23. Locations of points corresponding to breakthrough curves plotted in Figure 24 and Figure 25.

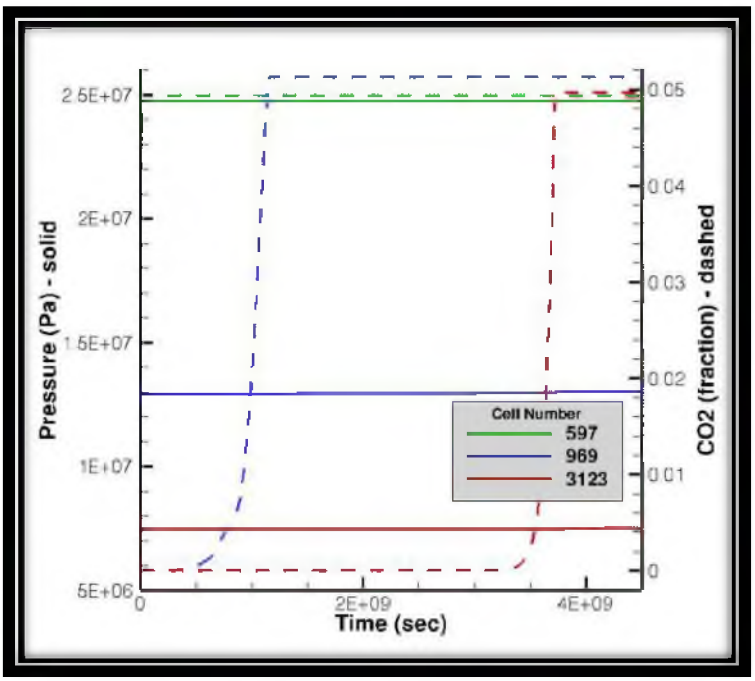

Figure 24. Breakthrough curves of pressure and CO2 corresponding to the results summarized in Table 19.
See text for details.

Table 19. Summary of breakthrough analysis results for a model reservoir with a faulted seal, with typical values of permeability (case R1H1S1 of Table 4).

Cell Number	CO2 Time (sec)	CO2 Time (year)	Pressure (Pa) initial	Pressure (Pa) change	Pressure (Pa) difference
597	saturated		2.55E+07	2.48E+07	-7.50E+05
969	1.15E+09	36.51	1.22E+07	1.29E+07	7.10E+05
3123	3.72E+09	117.93	6.85E+06	7.47E+06	6.26E+05

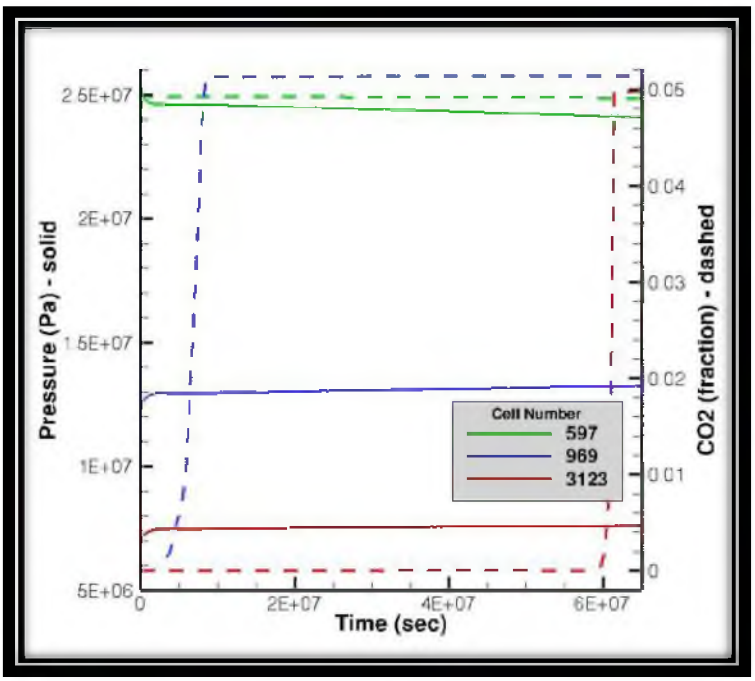

Figure 25. Breakthrough curves of pressure and CO2 corresponding to the results summarized in Table 20.
See text for details.

Table 20. Summary of breakthrough analysis results for a model reservoir with a faulted seal, with more-extreme values of permeability (case R2H2S2 of Table 4).

Cell Number	CO2 Time (sec)	CO2 Time (year)	Pressure (Pa) initial	Pressure (Pa) change	Pressure (Pa) difference
597	saturated		2.55E+07	2.45E+07	-9.80E+05
969	1.47E+07	0.47	1.22E+07	1.30E+07	7.50E+05
3123	8.43E+07	2.67	6.85E+06	7.56E+06	7.10E+05

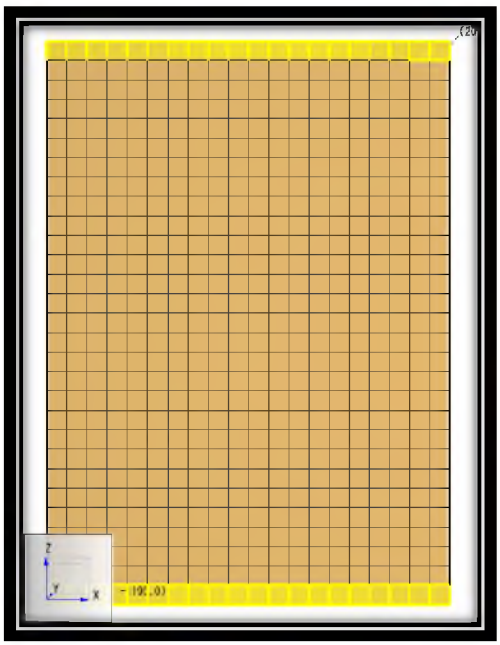

Figure 26. Schematic of model grid used for seal-only analysis.

Table 21. Multiphase CO2 seal simulated migration times for case 1 and case 8

Case	Permutation			WcSh (H) (m^2)	Time	
					(sec)	(year)
1	R 1	H 1	S 1	1.0E-18	8.46E+08	26.81
8	R 2	H 2	S 2	1.0E-16	8.47E+06	0.27

Table 22. Numerical simulation results of travel time through a generic seal layer. See text for more details.

Case	Permutation			WcSh (H) (m^2)	Length (m)	CO2	
						Density (kg/m^3)	Viscosity (kg/(ms))
1	R 1	H 1	S 1	1.0E-18	27	821	7.6E-05
8	R 2	H 2	S 2	1.0E-16			

Table 23. Analytical results of travel time through a generic seal layer. See text for more details.

Case	Permutation			K (m/s)	S_s (1/m)	Time (sec)	Time (days)
1	R 1	H 1	S 1	1.06E-10	1.0E-06	1.72E+06	19.90
8	R 2	H 2	S 2	1.06E-08		1.72E+04	0.20

CONCLUSION

The purpose of this research was focused on potential CO2 leakage through known (or unforeseen) faults in a target area of storage, and addressed the following four critical questions. Each of the following research questions is followed by the primary conclusions drawn from the simulation results of this study.

(1) Under what conditions CO2 will leak through a fault and how much will leak under different conditions?

CO2 exists as a gas at Earth's standard atmospheric temperature and pressure. It is a greenhouse gas of interest at the present time because of its documented effects on global warming and as a possible fuel extraction resource. Therefore it is of great benefit to investigate the behavior of CO2 in underground environments, especially whether leakage is possible. Leakage of CO2 from a geologic storage site is of concern because several potential hazards exist in connection to CO2, including acidification of ground water, asphyxiation when CO2 in high concentrations is leaked at the land surface and increases in atmospheric concentrations of CO2. The inexpensive and plentiful sources of CO2 make it an attractive item in such industry as oil recovery. Therefore it is worth investigating the leakage potential of CO2 and the factors that influence leakage and flow rates of CO2 from geologic storage sites. CO2 responds to many environmental factors such as temperature and pressure. It is less dense than water and pressure (head) is the driving force for leakage and a fault above a reservoir will increase the seepage velocity from the reservoir to a fault. Simulations suggest that a fault will increase leakage from a given area.

(2) How much time is required for CO2 to migrate through an un-broken seal formation?

CO2, like most gases, is capable of diverse rates of migration, depending on the structure of the material it is moving through. It is helpful to know how fast CO2 is capable of moving through various types of strata. In particular, the porosity of the strata and the overall thickness of the strata have the greatest potential for influencing migration time. Highly porous strata may allow CO2 to move faster than nonporous or minimally porous strata, but thickness of the strata also affects migration time, depending on how far the CO2 has to travel to reach the surface. Migration time depends primarily on permeability, porosity and thickness of the target storage formation and can be estimated using simple diffusion calculations.

(3) Under what conditions will permeable reservoirs above the target reservoir intercept or "catch" CO2 leaking through a fault?

Upward migration of CO2 will occur whenever appropriate subvertical permeability is present. Geologic formations that are well suited for CO2 storage generally display a caprock of low permeability and significant gas entry pressure. CO2 has larger compressibility than water, so small pressure reductions can cause large volumetric expansion. In this study, simulation results suggest that, in general, if permeability of a reservoir adjacent (and connected) to the fault is two orders of magnitude higher than that fault, the efficiency at capturing leaking CO2 in the formation above will be greater and thus reduce migration or escape of CO2 through the fault. Details of this analysis are outlined in Appendix A.

(4) Is injecting into two reservoirs preferable to injection into one?

Injection into a single-reservoir would be preferable, for managing pressure and facilitating effective monitoring, especially in a setting where multiple "stacked" reservoirs above would decrease risk of CO2 leakage (issue (3) above). Managing pressure is extremely important because CO2 is particularly responsive to pressure changes in the strata through which it is migrating. Injection into a single, rather than a double, reservoir reduces the number of factors influencing the behavior of CO2

and creates a more manageable system than injection into a double reservoir. Details of this analysis are outlined in Appendix B.

Even though this study was primarily focused on these four questions, other conclusions may be drawn from the results of this study. Specifically, a fault will likely increase risk of leakage, regardless of type of injection fluid or depth of a target reservoir. For example, if a fault is located immediately above an unbroken seal formation, simulations suggest that hydraulic head gradients (through the seal) tend to increase, thus increasing seepage velocity through the seal layer. Water quality is an important issue when sequestering CO2 and requires extensive evaluation if the fault is near underground drinking water reservoirs. Gathering accurate data is extremely important for evaluating the rate and amount of CO2 leakage potential in target formations.

This study also suggests that when CO2 is used for enhanced oil recovery and a fault runs through the production site, the problem of pressure build-up may be increased and, in turn, seepage velocity may also be increased.

Some limitations of this study include application of homogeneous permeability that cannot represent the complexity of heterogeneous rock formations in nature.

Recommendations based on this study include further investigations of fault systems utilizing chemical reactions, non-isothermal processes and heterogeneous mediums to determine effects on CO2 leakage through a fault system. The answers to these questions can be determined through further research.

APPENDIX A

WHETHER SECONDARY RESERVOIRS WILL"CATCH" CO2 LEAKING THROUGH A FAULT (CRITICAL QUESTION 3)

The analysis and results described in this section pertain to Critical Question 3 (Introduction), under what conditions will permeable reservoirs above the target reservoir intercept or "catch" CO2 leaking through a fault? The model boundary dimensions are: in the horizontal direction 71m and in the vertical direction 2667m below the surface. The horizontal direction is broken into 3 sections: 14m media, 3m fault, and 44m media. There are 5 to 6 different formations in the vertical direction with appropriate porosity and permeability values (see Table 24 for medium values and Figure 27 for conceptual layout). The fault has its own porosity and permeability values. Boundaries on either side in the horizontal direction are no flow, along with the bottom in the vertical direction. The top in the vertical direction is constant head of 101kPa. Injection into the lower reservoir was divided into 4 cells that are shown hatched in Figure 27. The model was simulated in TOUGH2 using multiphase CO2; isothermal conditions, and chemical reactions were neglected, consistent with all other analysis in this study.

Model Simulation Analysis

The model was injected with CO2 at a rate of 7.922E-3 kg/sec (1,000 tonne/yr total) in each injection cell for 3 years and ran for a total of 100 years. To perform the analysis, three scenarios were used to evaluate a faults porosity and permeability Table 25 through Table 27).

After running the simulations for the nine different scenarios, a pattern emerged. When the fault is given a permeability of 1.0E-11, CO2 flows up the fault but only slightly reaching the rock formation during 3 years of injection, shown in Figure 28. The simulation then ran for another 28 years postinjection before coming to an end, seen in Figure 29. The thought for the simulation ending is that CO2 reaches equilibrium in the fault and no longer flows. When the fault was given a permeability of 1.0E-13, CO2 flows up the fault but only to the upper reservoir during 3 years of injection, shown in Figure 30. The simulation then ran the remaining 97 years postinjection before ending, seen in Figure 31. Although CO2 did travel up the fault, it did not go any further than the upper reservoir.

When the fault was given a permeability of 1.0E-15, the simulation ended after 3 months. The fault became a barrier and the section of the reservoir filled up with CO2, not allowing for any more to be injected. It seemed that as the porosity for the different scenarios was changed with the permeability, the results of the simulations were the same as summarized above. Two final simulations were run changing the injection time and the injection rate to evaluate what kind of effect this would have. The results were that the injection time pushed CO2 further up the fault, and a larger rate of injection also pushed more CO2 through the fault.

Therefore, (Table 28) a fault to medium permeability ratio was developed to explain why CO2 flows into adjacent formations as it follows the fault. A ratio of 0.1 to 10 shows that a resistance of flow in either direction is not that significant, but a ratio greater than this will improve or hinder capture of CO2 into lateral formations that a fault passes through.

Discussion of Results

After running all nine different scenarios to simulate how porosity and permeability would affect a fault, it was concluded that the porosity had no effect on the flow of CO2. The permeability of a fault dictated how far the CO2 flowed and amount. Boundary conditions, maximum injection flow and location of injection had an effect on the results. CO2 moves through the fault and the USDWs if a significant amount of CO2 is injected near a fault. Finally, since

chemical reactions were not included in simulations, there is a large chance that the reactions will reduce the permeability of a fault and hinder, if not seal, any fault conduits.

Table 24. Single continuum single reservoir medium values.

Material	Porosity (%)	Horizontal direction (m^2)	Permeability in Vertical direction (m^2)
USDW	5	1.0E-15	1.0E-16
GAS	2	1.0E-13	1.0E-14
CO2	20	1.0E-13	1.0E-14
ROCK	2	1.0E-15	1.0E-16
SEAL	2	1.0E-16	1.0E-18
FAULT	40	1.0E-11	1.0E-11

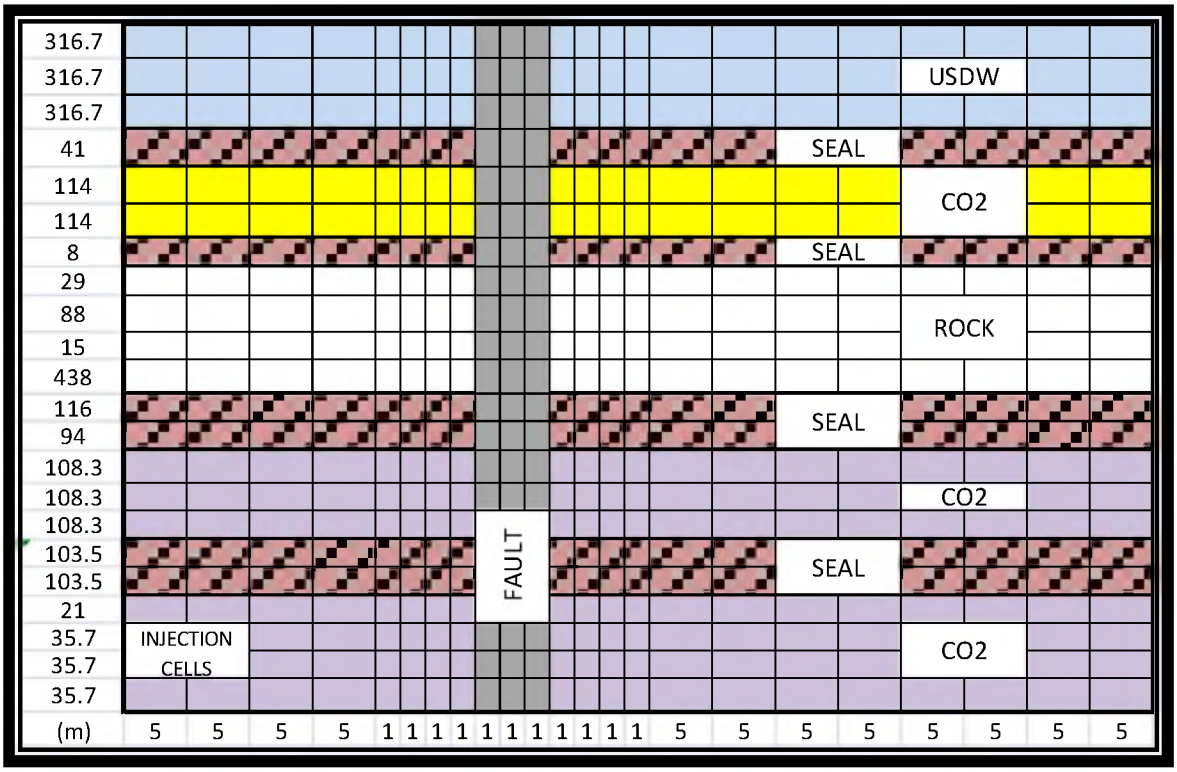

Figure 27. Single continuum single reservoir conceptual layout.

Table 25. Scenarios 11 through 13.

Scenario	Porosity (%)	Permeability in Horizontal & Vertical direction (m^2)
11	40	1.0E-11
12	40	1.0E-13
13	40	1.0E-15

Table 26. Scenarios 21 through 23.

Scenario	Porosity (%)	Permeability in Horizontal & Vertical direction (m^2)
21	30	1.0E-11
22	30	1.0E-13
23	30	1.0E-15

Table 27. Scenarios 31 through 33.

Scenario	Porosity (%)	Permeability in Horizontal & Vertical direction (m^2)
31	20	1.0E-11
32	20	1.0E-13
33	20	1.0E-15

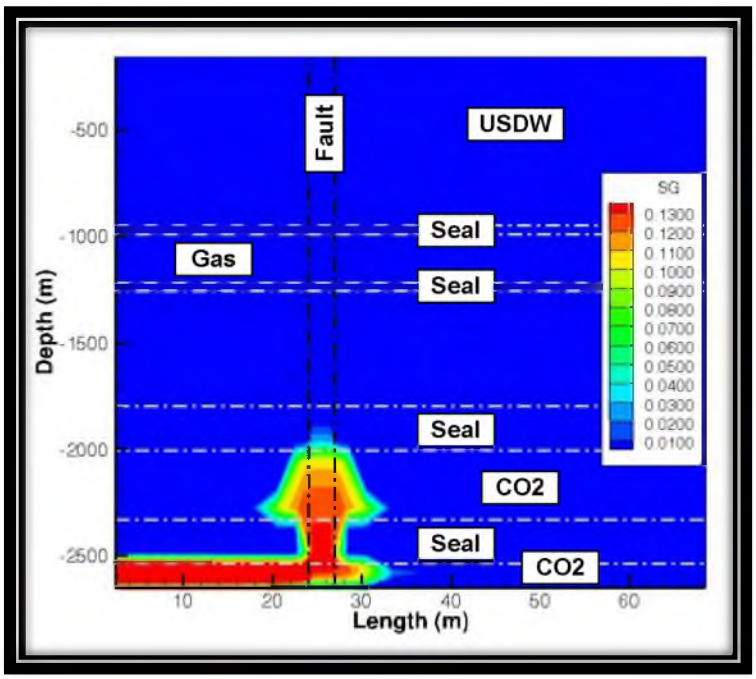

Figure 28. Scenario 11 - 3yr Injection.

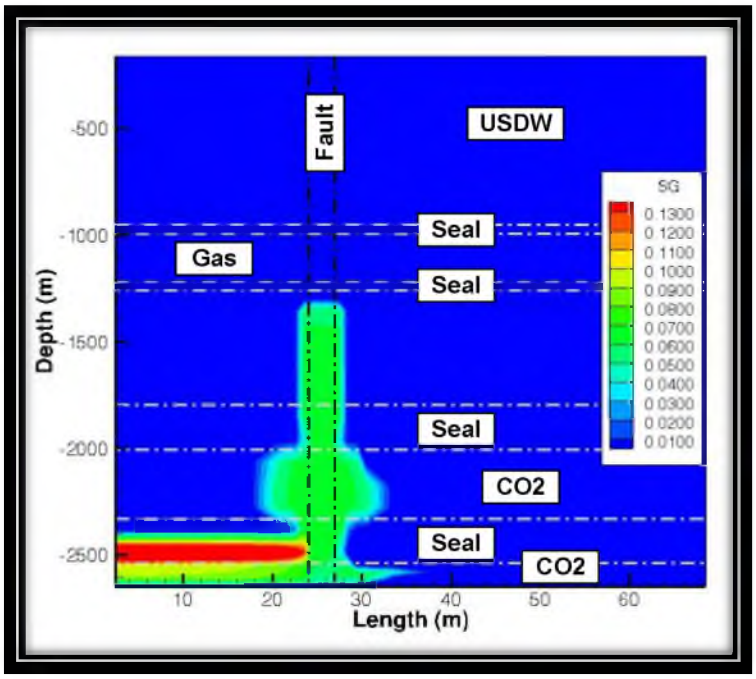

Figure 29. Scenario 11 - 28yr Postinjection.

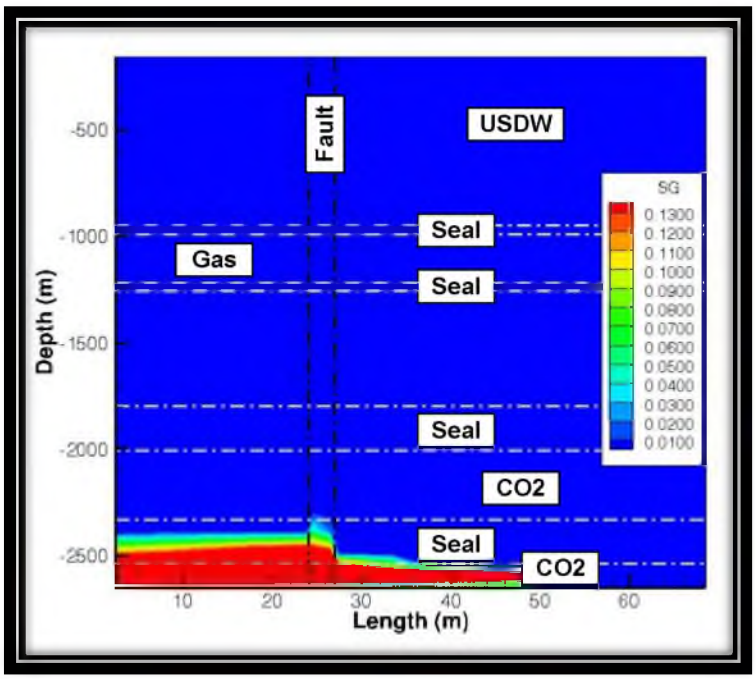

Figure 30. Scenario 12 - 3yr Injection.

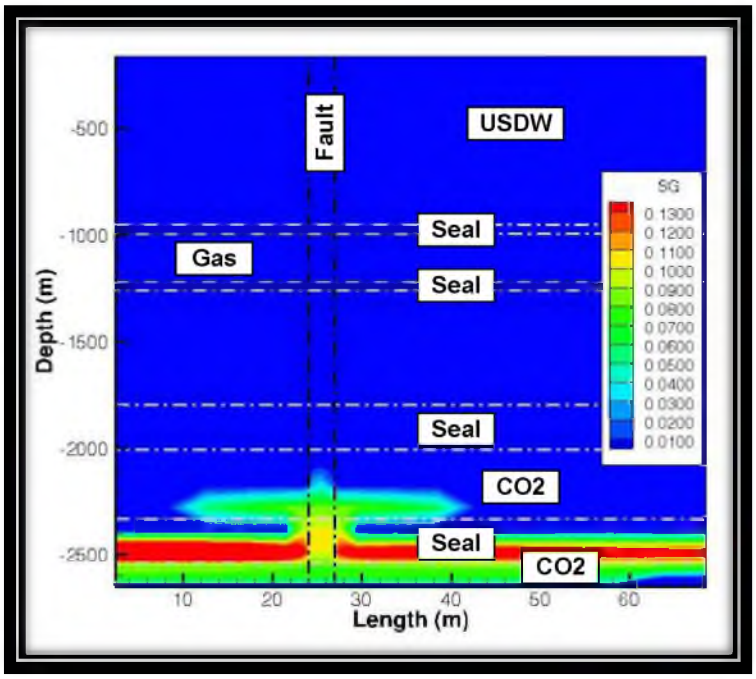

Figure 31. Scenario 12 - 97yr Postinjection.

Table 28. Fault to medium permeability ratio.

Fault (m^2) \ Medium (m^2)	1.0E-11	1.0E-12	1.0E-13	1.0E-14	1.0E-15	1.0E-16
1.0E-11	1	0.1	0.01	0.001	0.0001	0.00001
1.0E-12	10	1	0.1	0.01	0.001	0.0001
1.0E-13	100	10	1	0.1	0.01	0.001
1.0E-14	1000	100	10	1	0.1	0.01
1.0E-15	10000	1000	100	10	1	0.1
1.0E-16	0.00001	0.0001	0.001	100	10	1

APPENDIX B

IS INJECTING IN TWO RESERVOIRS BETTER THAT ONE?

(CRITICAL QUESTION 4)

The analysis and results described in this section pertain to Critical Question 4 (Introduction), is injecting into two reservoirs preferable to injection into one? The model consisted of 15 different formations in the z-direction and a fault medium with appropriate porosity and permeability values (see Table 29 for medium values and Figure 32 for conceptual grid section). This model is intended to represent those of an actual candidate CCS site in central Utah, the Gordon Creek field (Morgan, et al., 1991). Different injection rates were simulated using a single injection point (Figure 33 for conceptual single injection layout) or a dual injection point (Figure 34 for conceptual dual injection layout).

The model boundary dimensions are; in the x-direction 126km, in the y-direction 500m and in the z-direction 3.7km. The boundary on either side in the x-direction and bottom in the z-direction is no flow. The top in the z-direction is constant head of 101kPa.

For a single injection the location was in the Navajo (JNS) reservoir shown hatched in Figure 33. For a dual injection the locations were in the Navajo (JNS) and Entrada (JES) reservoirs shown hatched in Figure 34. The model was simulated in TOUGH2 using multiphase CO2; isothermal conditions and chemical reactions were neglected.

Simulation Analysis

To perform the analysis the model was injected for 3 years at the different rates of 1k, 10k, 50k, 100k, 250k, 500k, 1Mtonne/yr. For the dual injection simulations the injection rate was

split evenly between the two reservoirs. Figure 35 through Figure 44 show the results of the varying injection rates and single verses dual injections. The single injection into the Navajo reservoir ran to completion in all case except for 1M tonne/yr which failed after 10 months, seen in Figure 44. The dual injection into both the Navajo and Entrada reservoirs ran to completion for the rates up to 50k tonne/yr, all other simulations failed at or before 1 month.

Since the Entrada has a lower permeability than the Navajo, the fault conduits between the reservoirs allowed the CO2 to flow from the Entrada into the Navajo, making the majority of stored CO2 in the lower reservoir. If the fault conduits were removed from the model, the dual injection simulations would need to be reevaluated. An injection rate of 50k may be too high of an injection rate for the Entrada reservoir. Also the simulation may have to have a 25/75 split in the injection rate to complete a 3-year injection period.

Finally, more simulations need to be done on a dual injection scenario to evaluate how efficiently this would work. Pressure and temperature changes of a dual simulation will also need to be evaluated.

Discussion of Results

From the simulation results, it seems that a dual injection into the reservoirs will work but that the majority of CO2 storage will occur in the Navajo reservoir. Although the Entrada does seem to have a greater storage capacity then the Navajo, the permeability of the Entrada is limiting the injection rate. Therefore, to achieve a large volume of storage, one of two options is available. Inject CO2 only into the Navajo reservoir at a larger rate or inject into both reservoirs at a lower rate and a longer injection time. Dual inject into the area without the fault conduits need to be reevaluated as well.

Table 29. Single continuum dual reservoir medium values.

Formation / Member		Material Code	Density (kg/m^3)	Porosity (%)	Permeability in Horizontal direction (m^2)	Permeability in Vertical direction (m^2)
Atmosphere		Air	2650	50	1.0E-10	1.0E-10
Mancos Shale	Emery Sandstone	CES	2323	5	1.0E-15	1.0E-16
	Blue Gate Shale	CBGS	2675	2	1.0E-16	1.0E-18
	Ferron Sandstone	CFS	2323	2	1.0E-13	1.0E-14
	Tunuk Shale	CTS	2675	2	1.0E-16	1.0E-18
Dakota Sandstone		CDS	2323	10	1.0E-15	1.0E-16
Cedar Mountian Formation		CCMF	2650	10	1.0E-16	1.0E-17
Morrison Formation		JMF	2650	2	1.0E-16	1.0E-17
San Rafael Group	Summerville Formation	JSF	2675	2	1.0E-16	1.0E-18
	Curtis Formation	JCuF	2675	2	1.0E-16	1.0E-18
	Entrada Sandstone	JES	2323	10	1.0E-16	1.0E-17
	Carmel Formation	JCaF	2675	2	1.0E-16	1.0E-18
Glen Canyon Group	Navajo Sandstone	JNS	2323	20	1.0E-13	1.0E-14
	Kayenta	TK	2323	20	1.0E-16	1.0E-17
	Wingate	TW	2323	20	1.0E-16	1.0E-17
Fault	Basalt, broken	Fault	1954	40	1.0E-12	1.0E-12

Material Code	cells per layer	thk per layer
Air	1	0.01
CES	1	950
CBGS	1	11
CFS	1	228
CTS	1	8
CDS	1	29
CCMF	1	103
JMF	1	438
JSF	2	58
JCuF	2	47
JES	5	65
JCaF	4	57
JNS	5	21.4
TK	1	41
TW	1	104

Figure 32. Single continuum dual reservoir conceptual grid section.

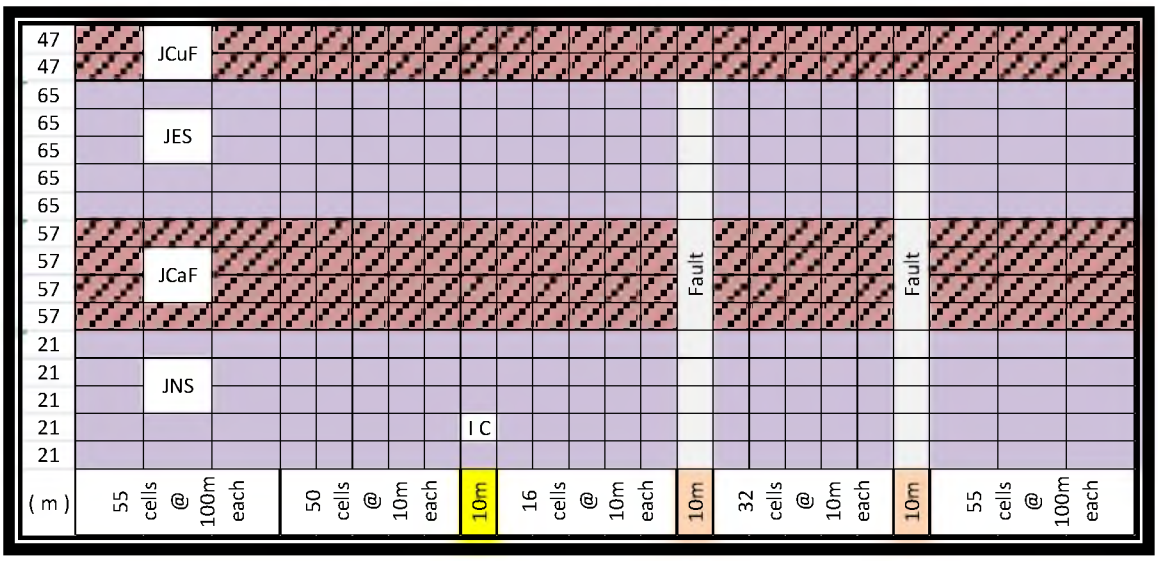

Figure 33. Single continuum dual reservoir conceptual single injection layout.

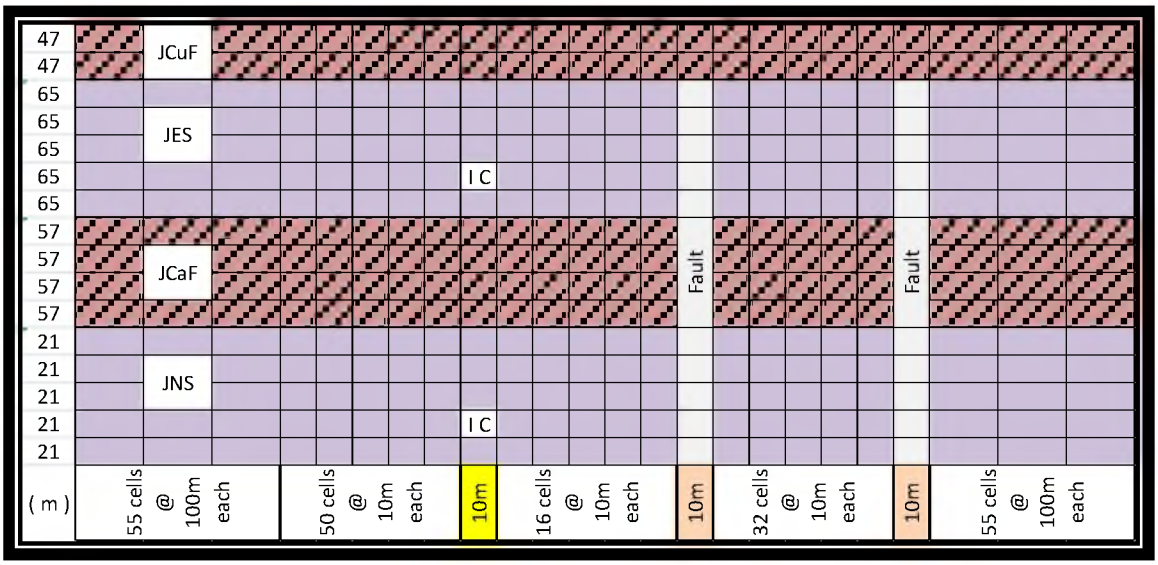

Figure 34. Single continuum dual reservoir conceptual dual injection layout.

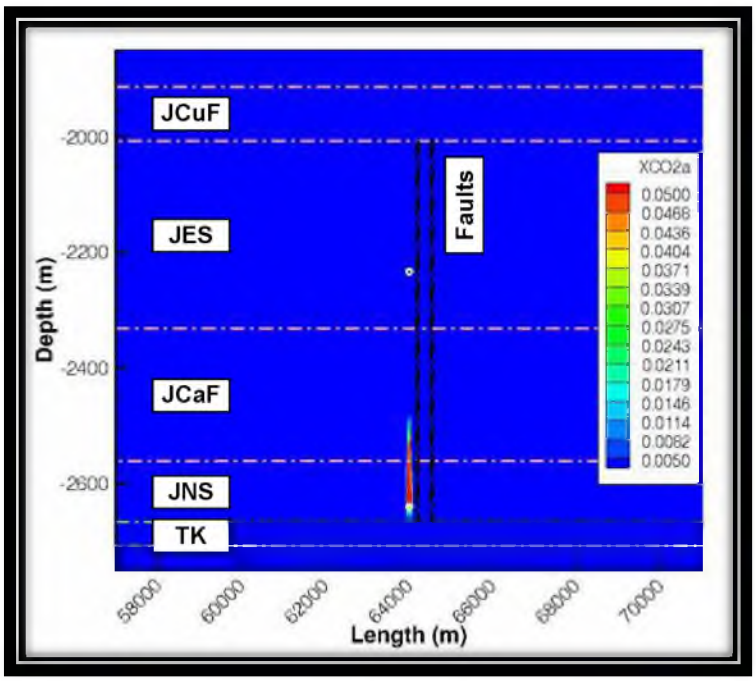

Figure 35. 1k Single injection.

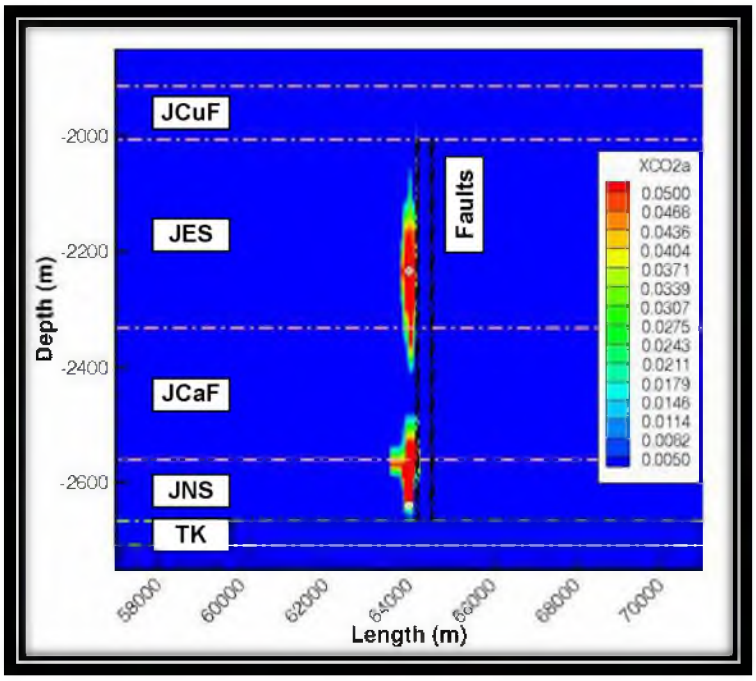

Figure 36. 1k Dual injection.

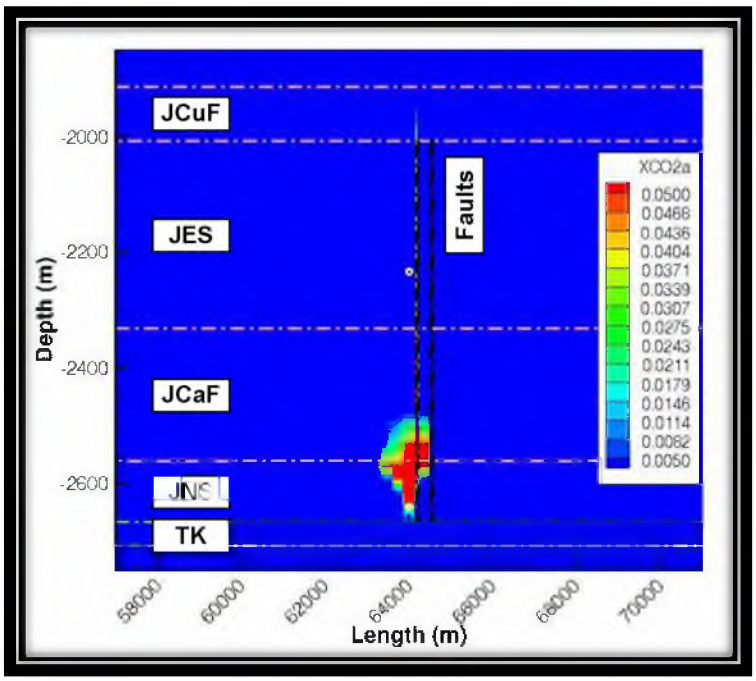

Figure 37. 10k Single injection.

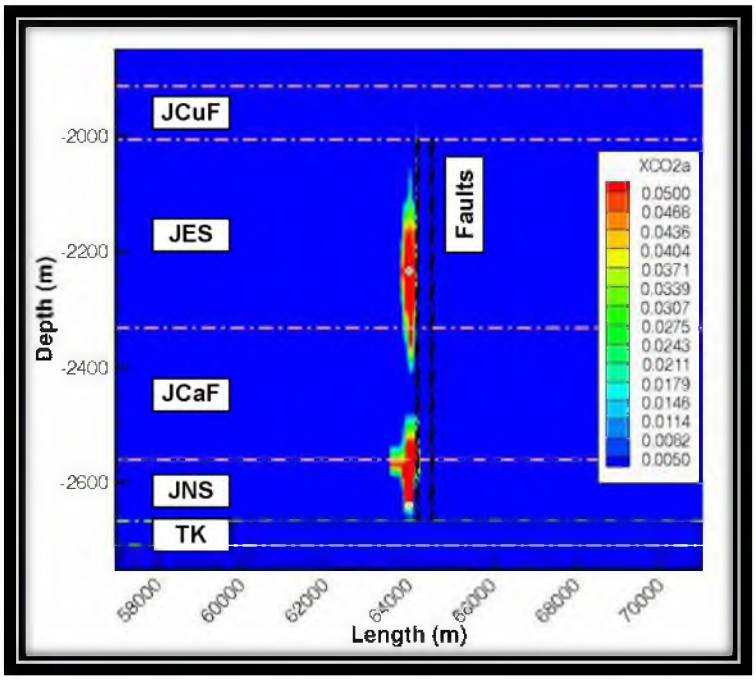

Figure 38. 10k Dual injection.

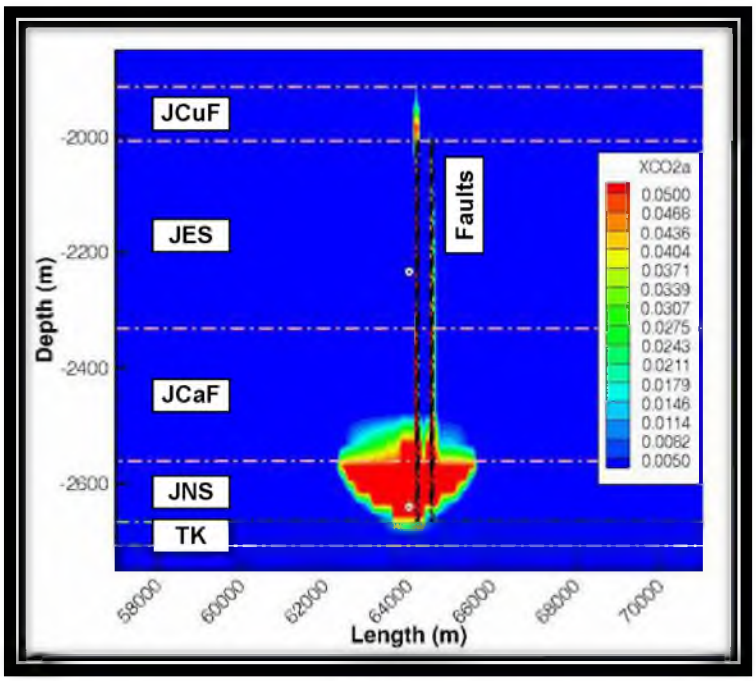

Figure 39. 50k Single injection.

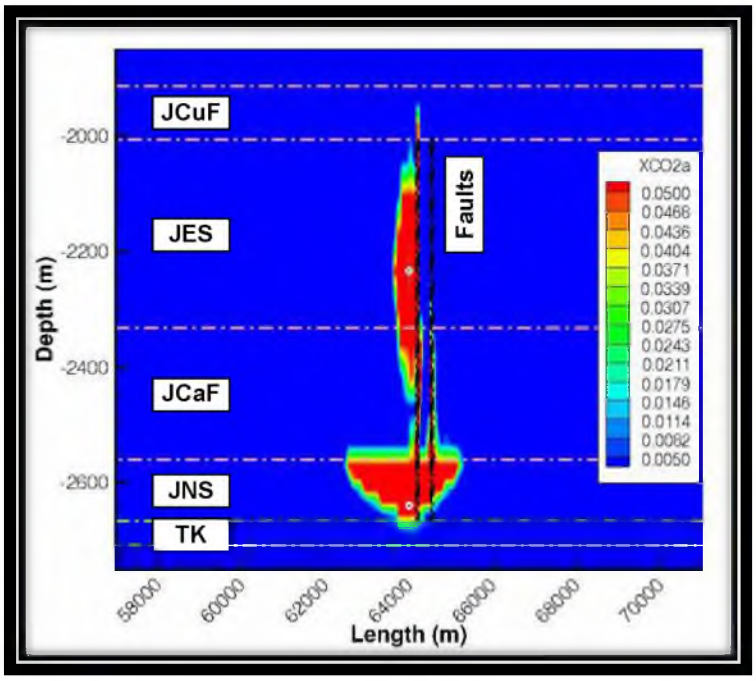

Figure 40. 50k Dual injection.

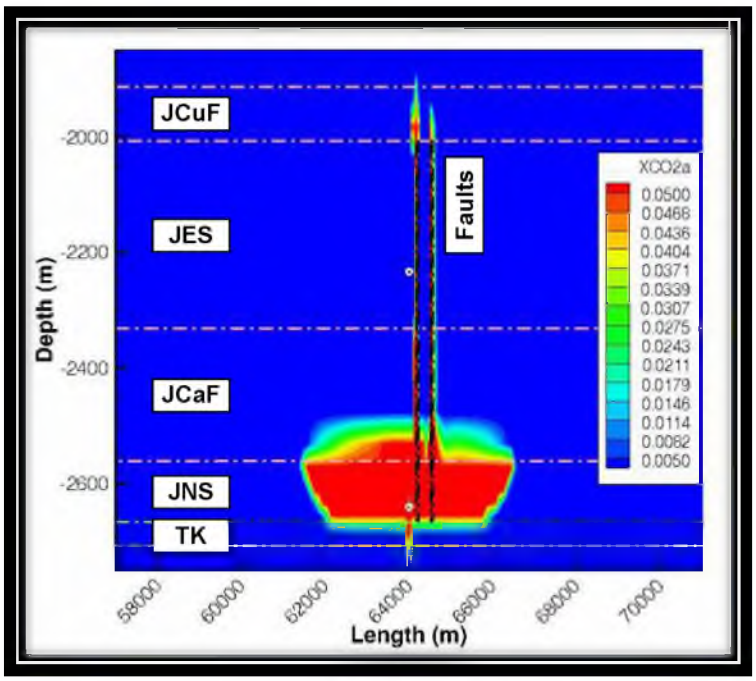

Figure 41. 100k Single injection.

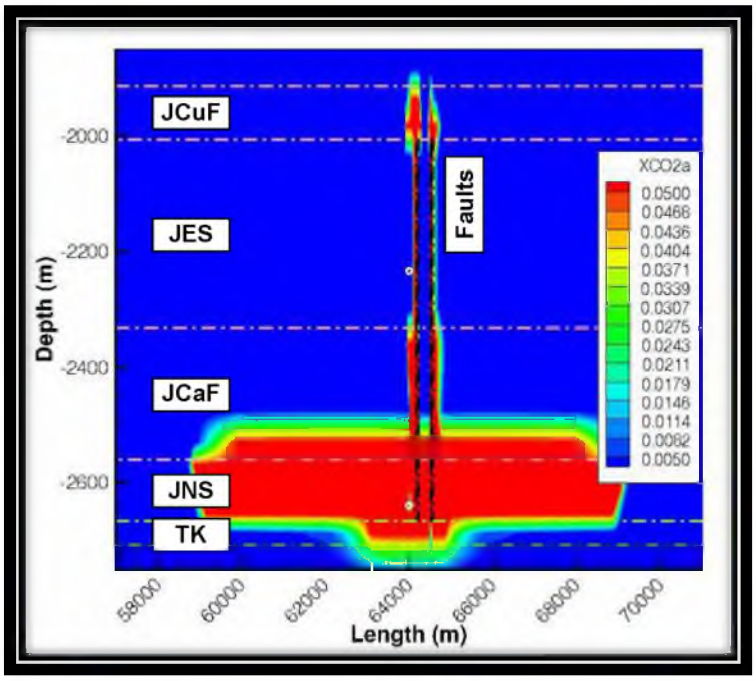

Figure 42. 250k Single injection.

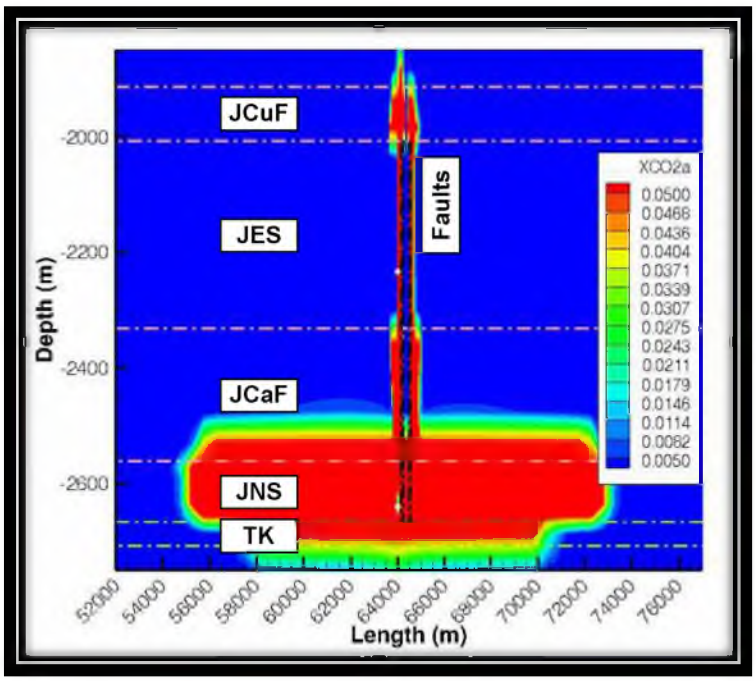

Figure 43. 500k Single injection.

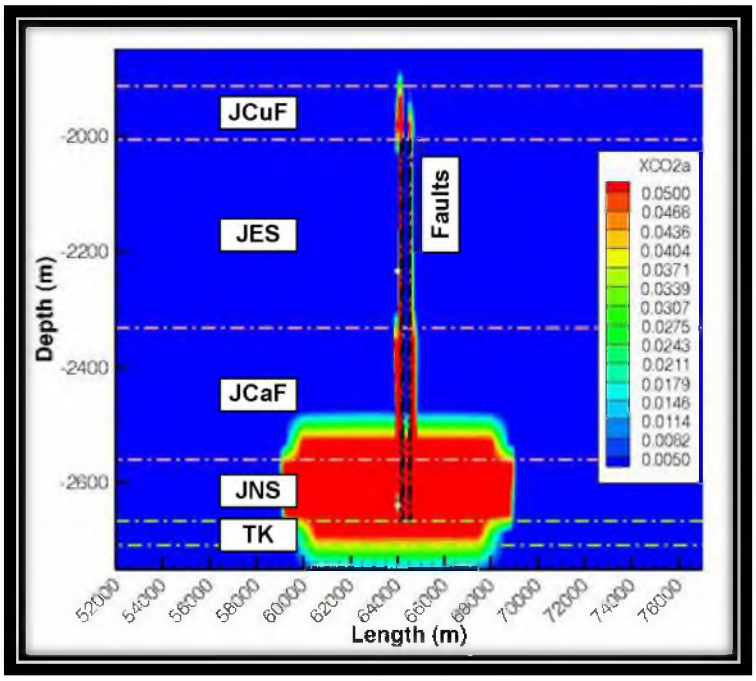

Figure 44. 1M Single injection (10 months).

APPENDIX C

SINGLE PHASE WATER UNPENETRATED-SEAL PRESSURE IN THE RESERVOIR

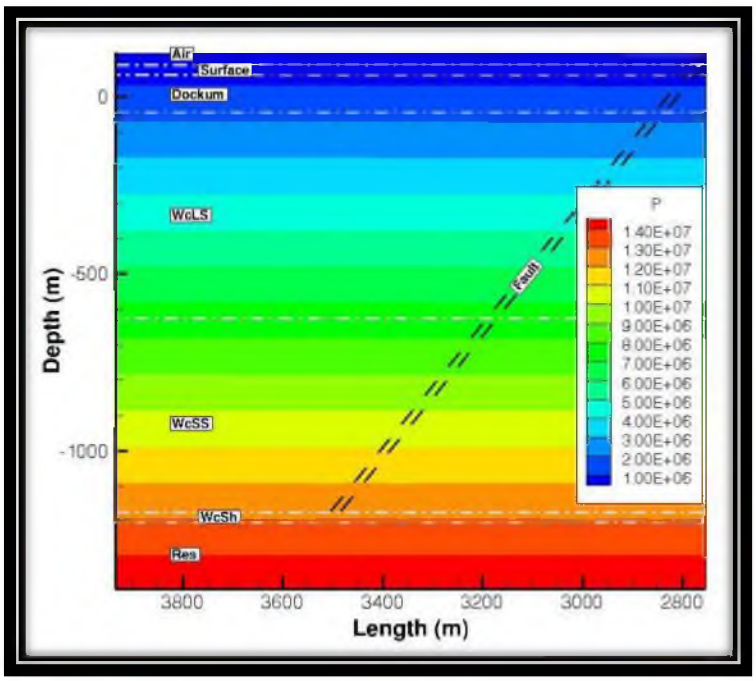

Case 1 (R1H1S1) Single Phase Water Unpenetrated-Seal Pressure in the Reservoir

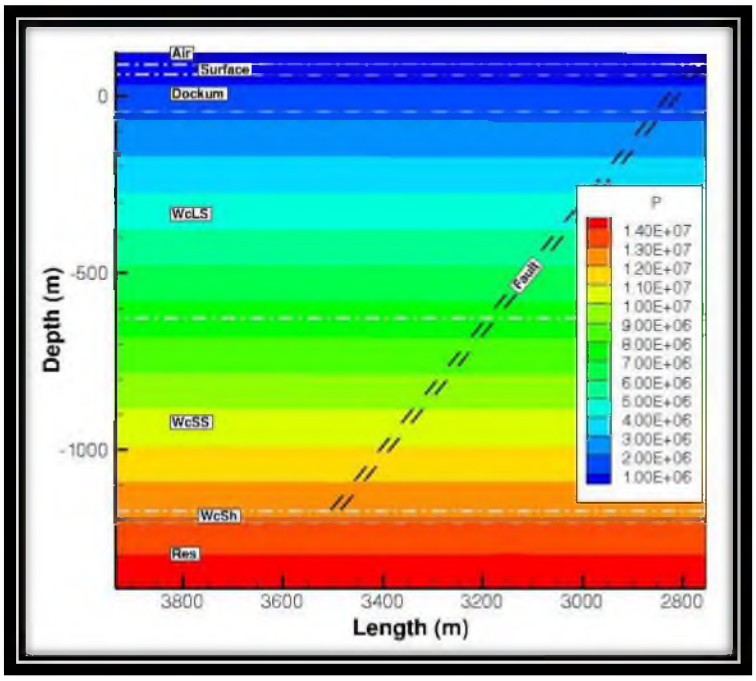

Case 2 (R1H1S2) Single Phase Water Unpenetrated-Seal Pressure in the Reservoir

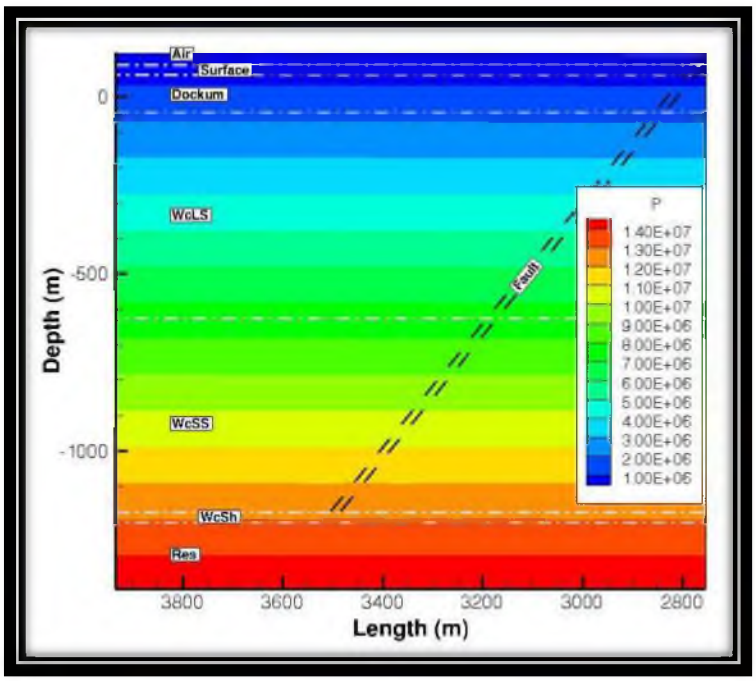

Case 3 (R1H2S1) Single Phase Water Unpenetrated-Seal Pressure in the Reservoir

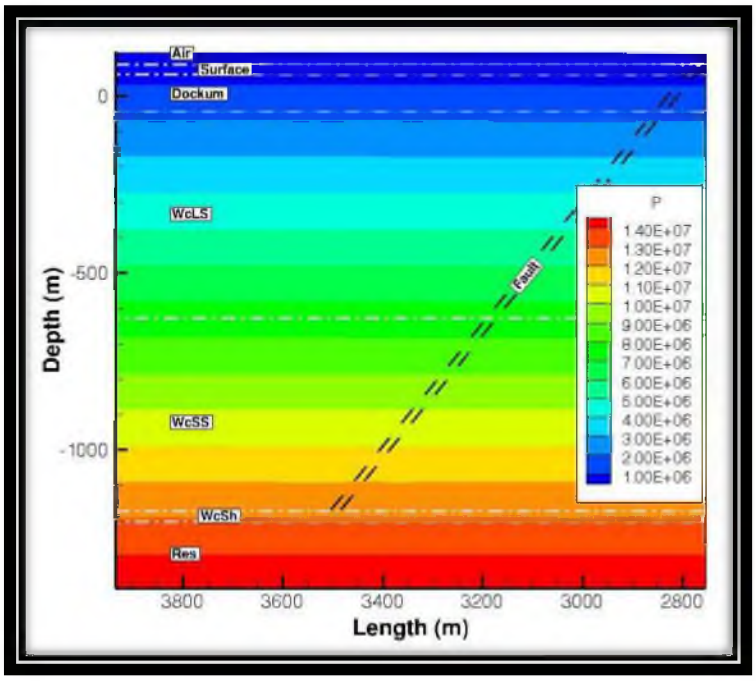

Case 4 (R1H2S2) Single Phase Water Unpenetrated-Seal Pressure in the Reservoir

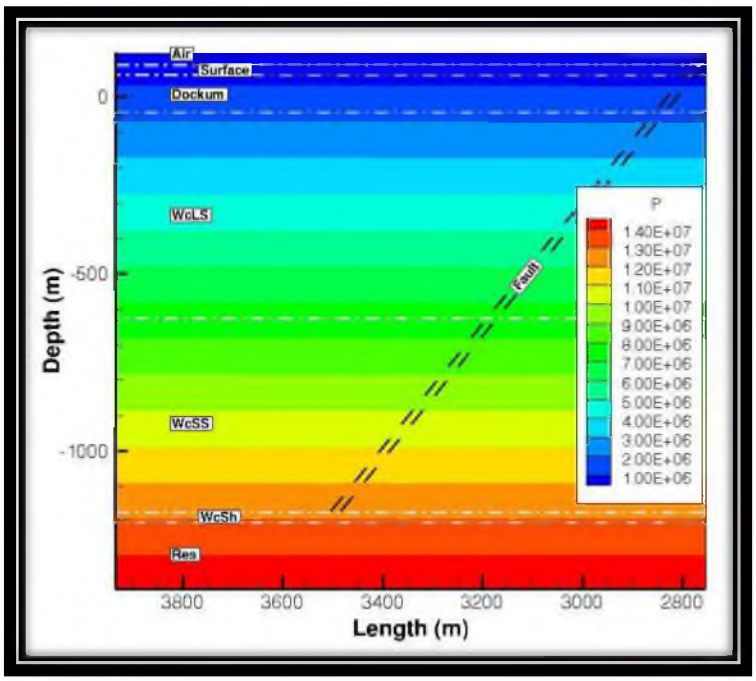

Case 5 (R2H1S1) Single Phase Water Unpenetrated-Seal Pressure in the Reservoir

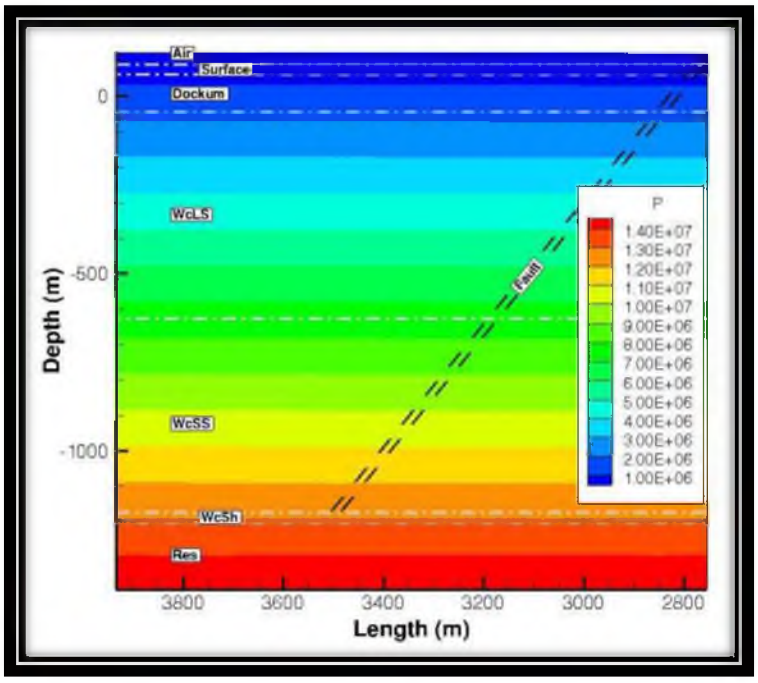

Case 6 (R2H1S2) Single Phase Water Unpenetrated-Seal Pressure in the Reservoir

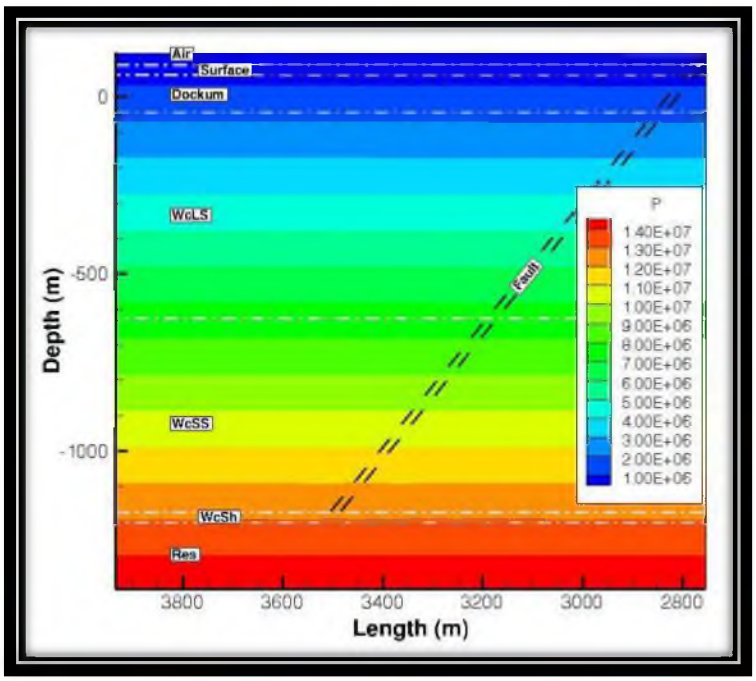

Case 7 (R2H2S1) Single Phase Water Unpenetrated-Seal Pressure in the Reservoir

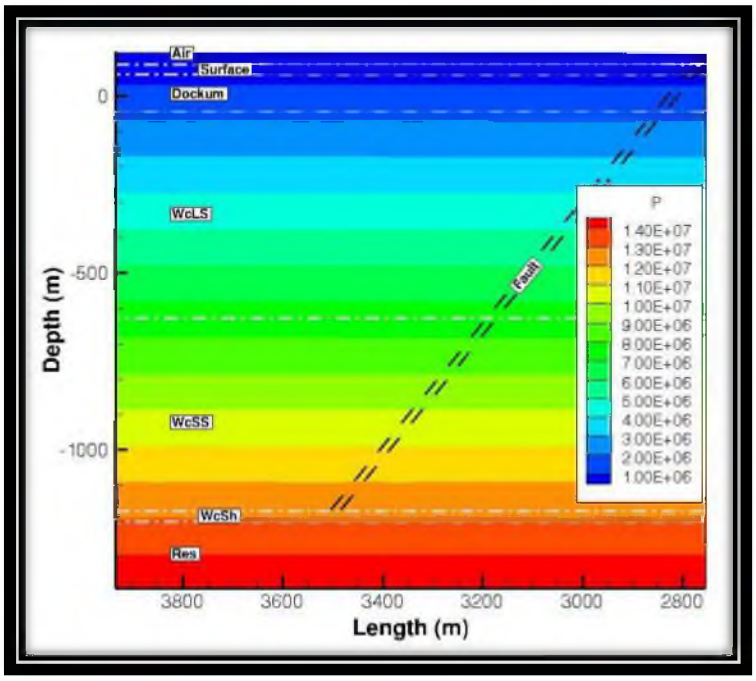

Case 8 (R2H2S2) Single Phase Water Unpenetrated-Seal Pressure in the Reservoir

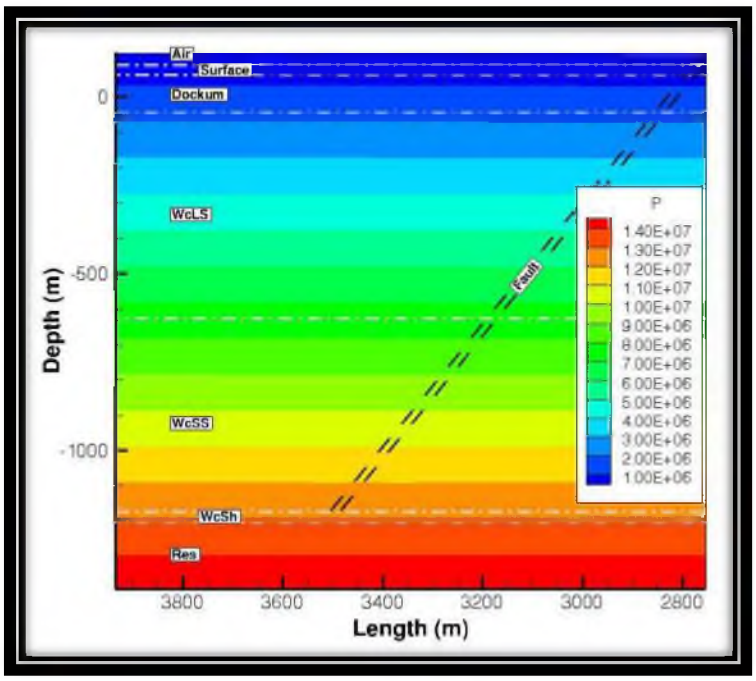

Case 9 (p1R1H1S1) Single Phase Water Unpenetrated-Seal Pressure in the Reservoir

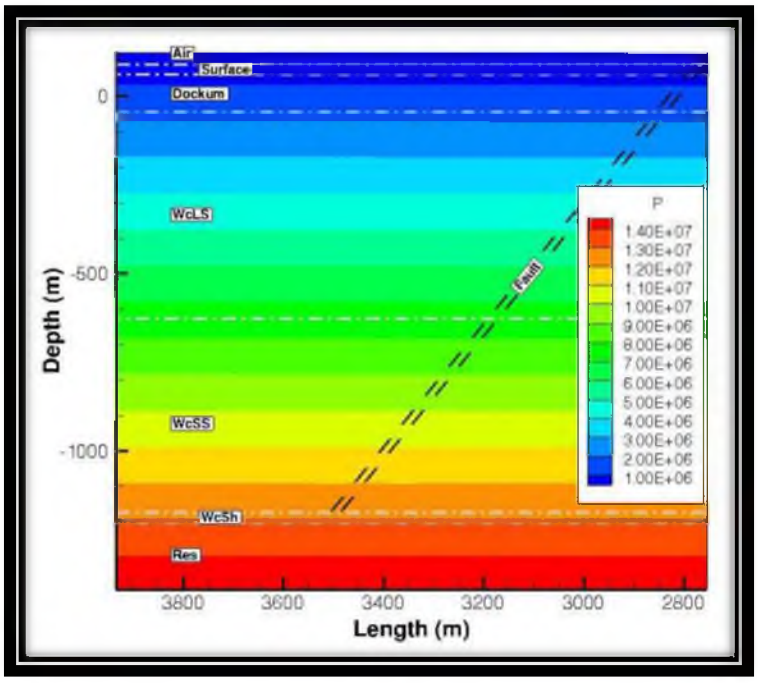

Case 10 (p2R1H1S1) Single Phase Water Unpenetrated-Seal Pressure in the Reservoir

APPENDIX D

SINGLE PHASE WATER UNPENETRATED-SEAL

CHANGE IN PRESSURE

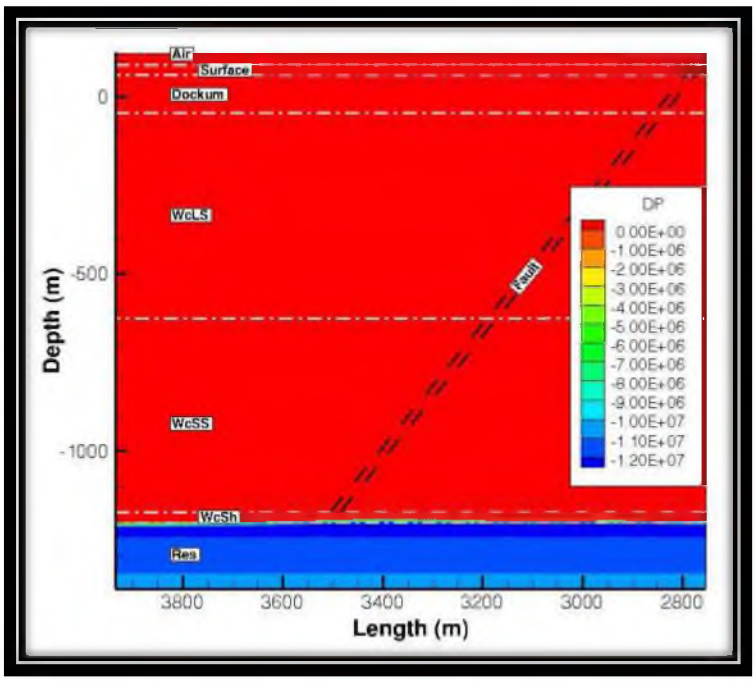

Case 1 (R1H1S1) Single Phase Water Unpenetrated-Seal Change in Pressure

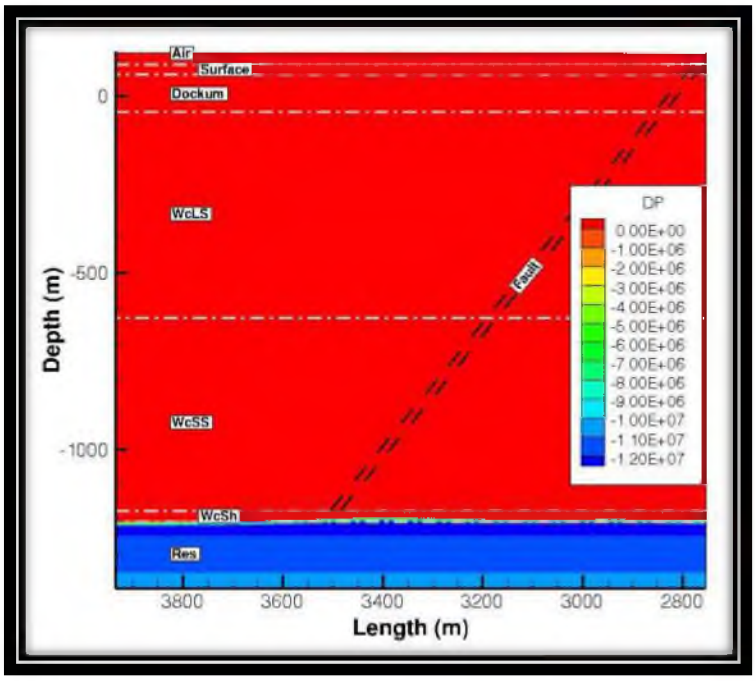

Case 2 (R1H1S2) Single Phase Water Unpenetrated-Seal Change in Pressure

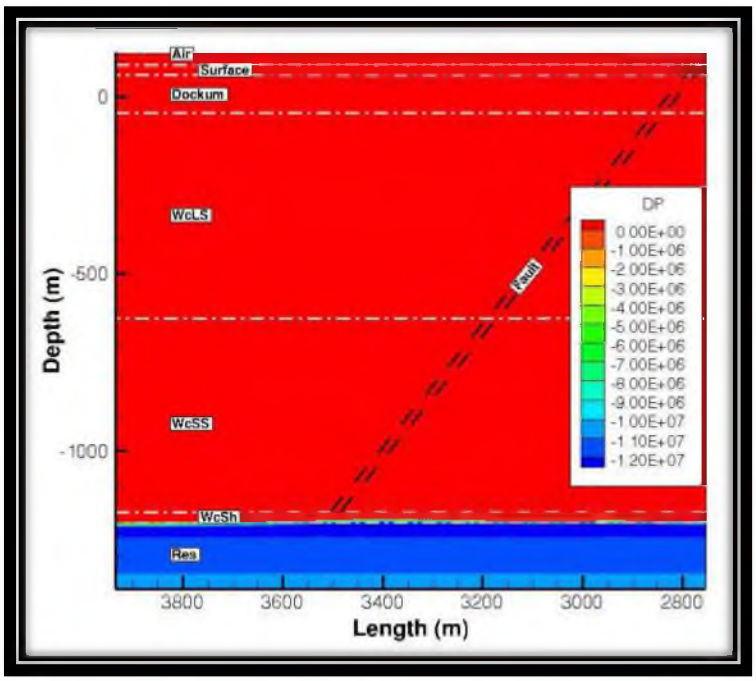

Case 3 (R1H2S1) Single Phase Water Unpenetrated-Seal Change in Pressure

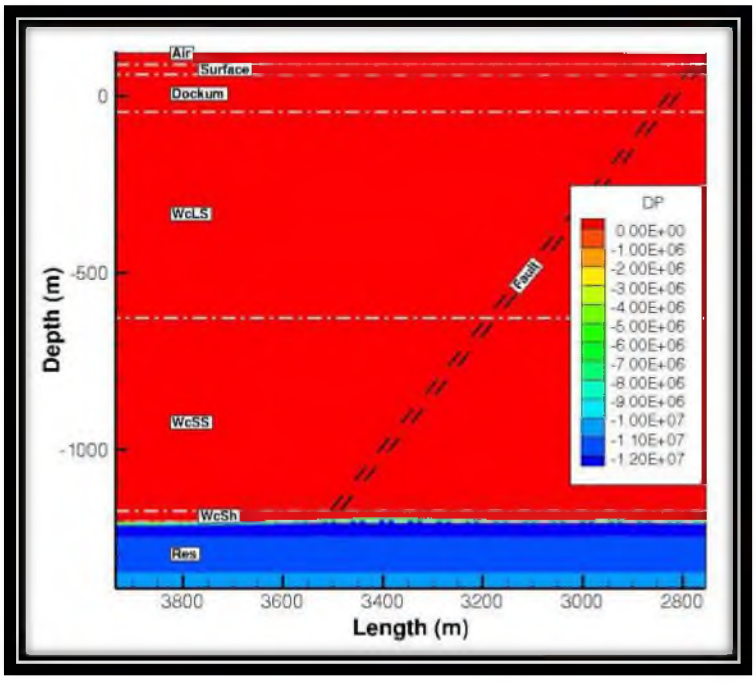

Case 4 (R1H2S2) Single Phase Water Unpenetrated-Seal Change in Pressure

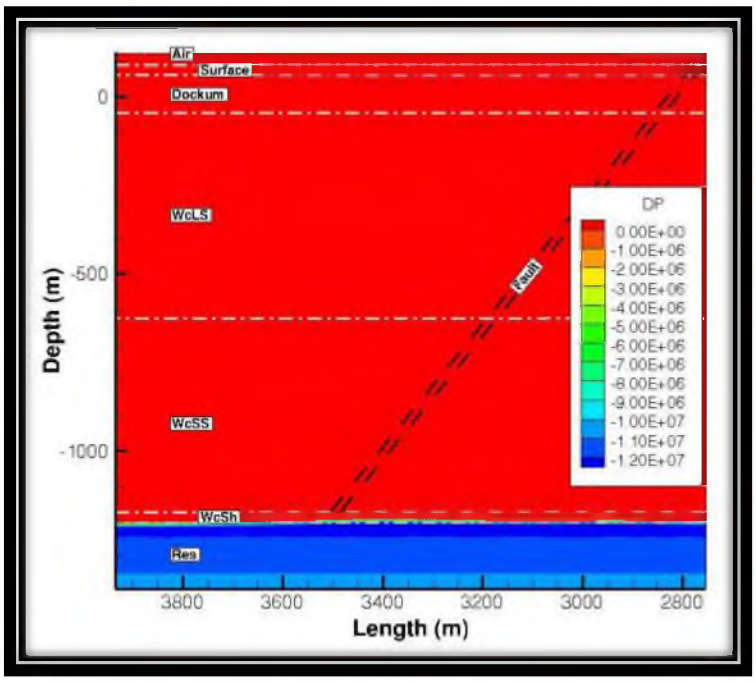

Case 5 (R2H1S1) Single Phase Water Unpenetrated-Seal Change in Pressure

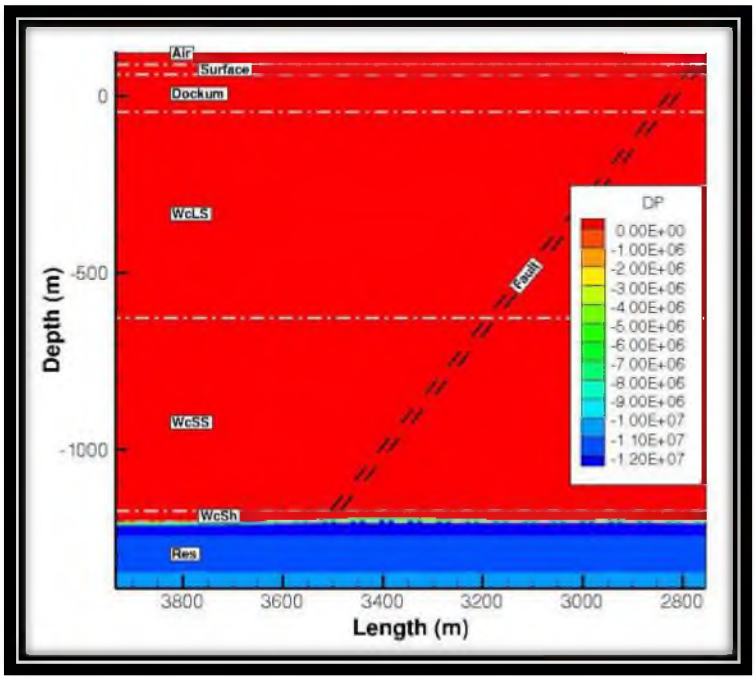

Case 6 (R2H1S2) Single Phase Water Unpenetrated-Seal Change in Pressure

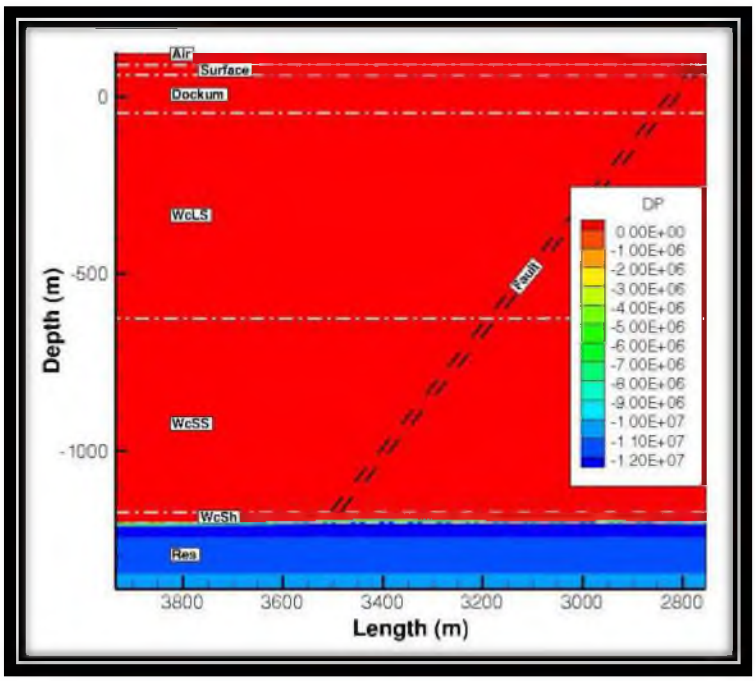

Case 7 (R2H2S1) Single Phase Water Unpenetrated-Seal Change in Pressure

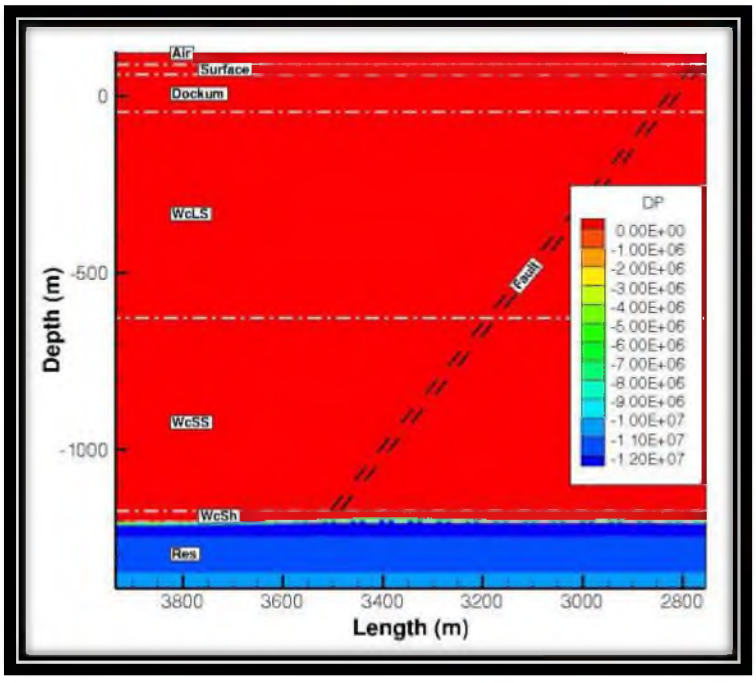

Case 8 (R2H2S2) Single Phase Water Unpenetrated-Seal Change in Pressure

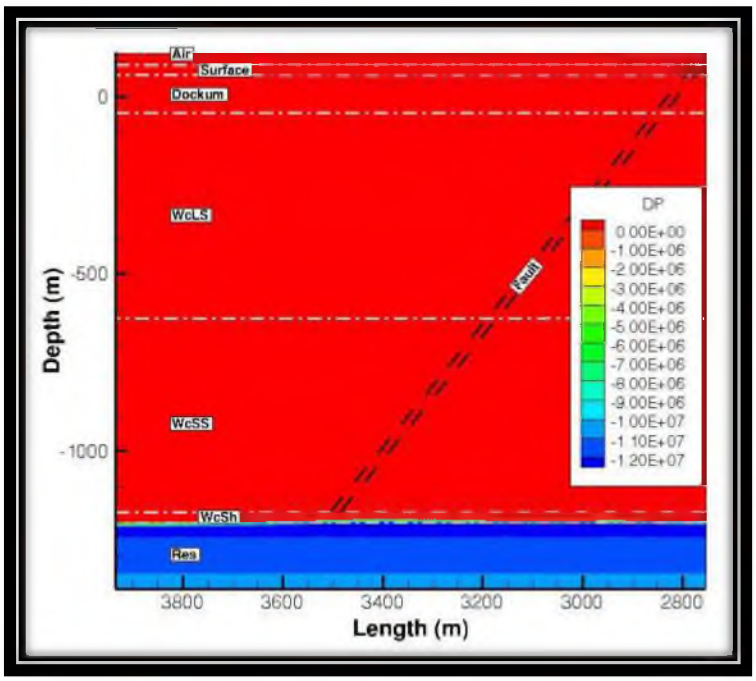

Case 9 (p1R1H1S1) Single Phase Water Unpenetrated-Seal Change in Pressure

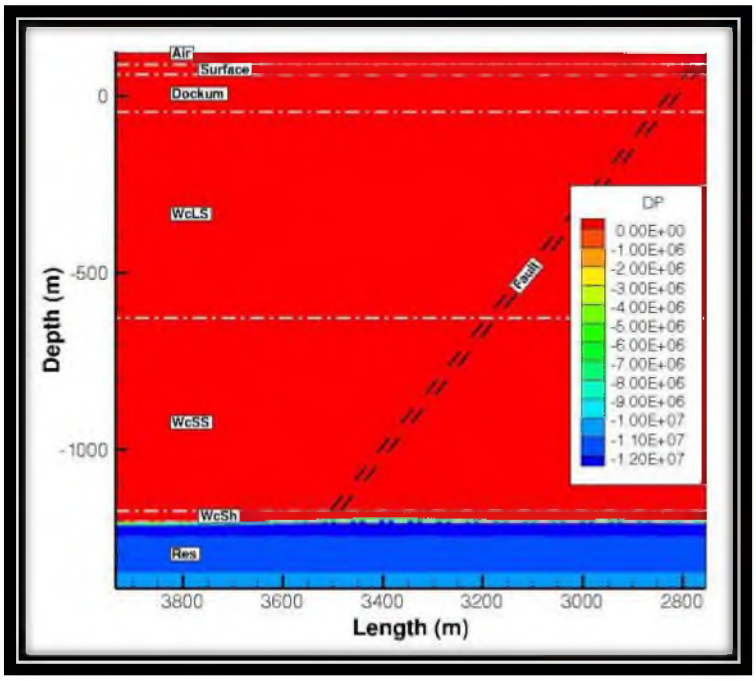

Case 10 (p2R1H1S1) Single Phase Water Unpenetrated-Seal Change in Pressure

APPENDIX E

SINGLE PHASE WATER FAULT-PENETRATING-SEAL

PRESSURE IN THE RESERVOIR

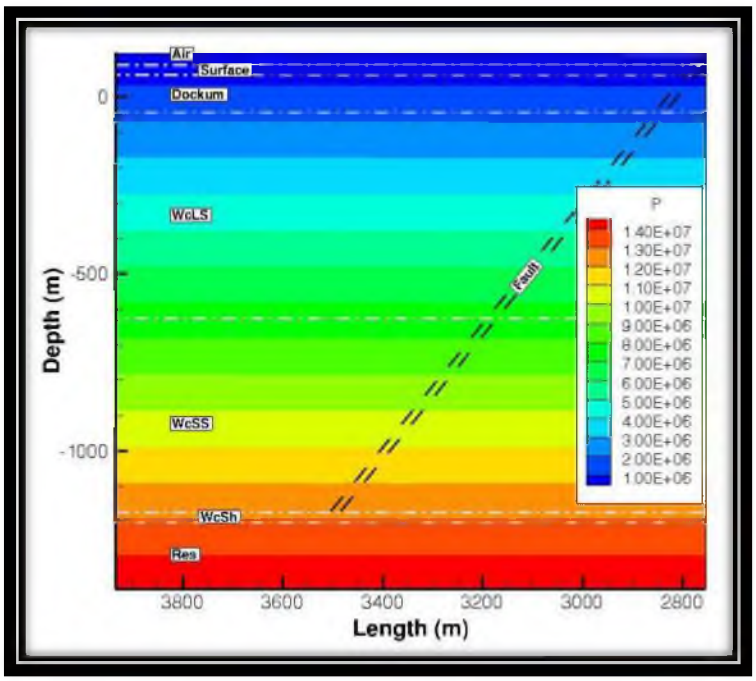

Case 1 (R1H1S1) Single Phase Water Fault-Penetrating-Seal Pressure in the Reservoir

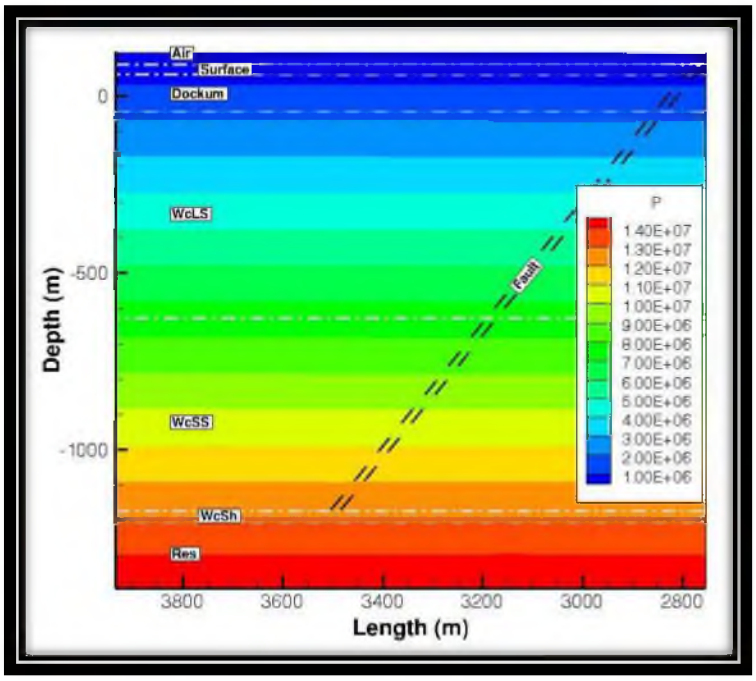

Case 2 (R1H1S2) Single Phase Water Fault-Penetrating-Seal Pressure in the Reservoir

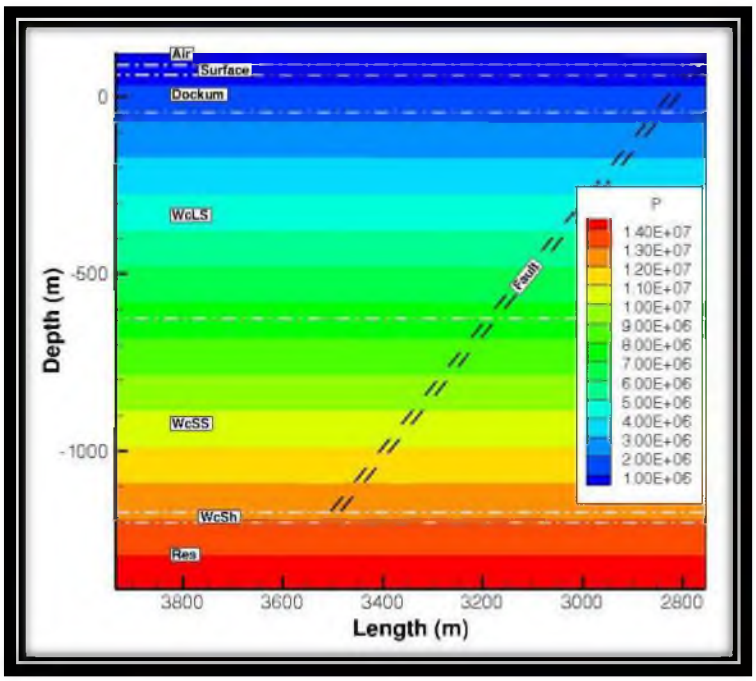

Case 3 (R1H2S1) Single Phase Water Fault-Penetrating-Seal Pressure in the Reservoir

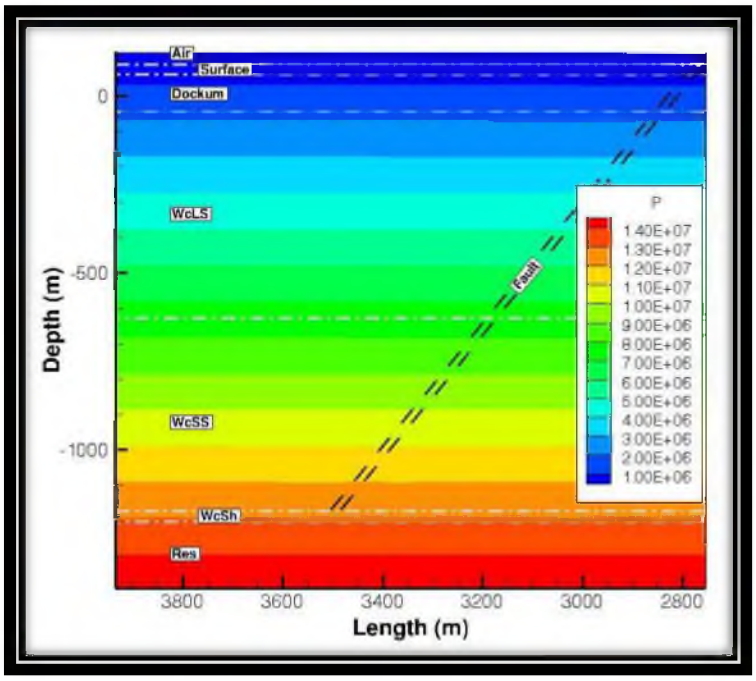

Case 4 (R1H2S2) Single Phase Water Fault-Penetrating-Seal Pressure in the Reservoir

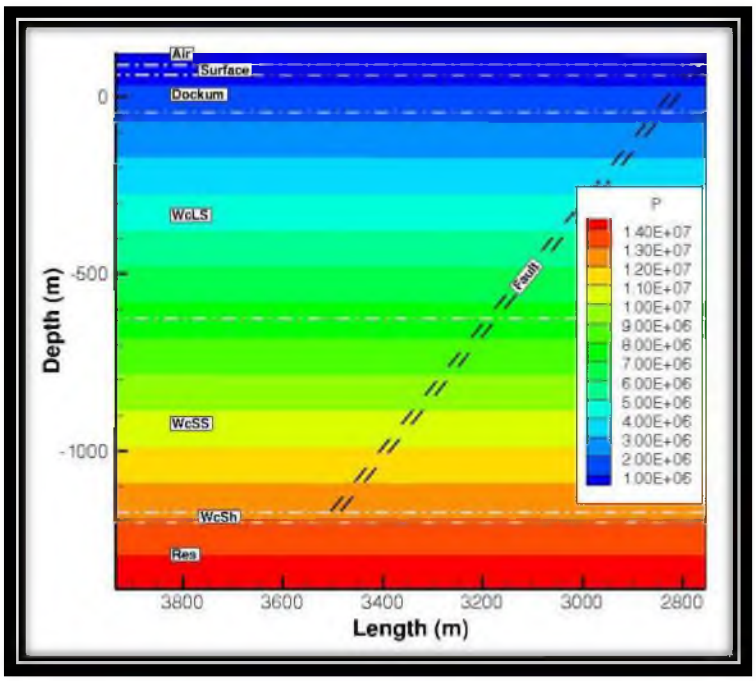

Case 5 (R2H1S1) Single Phase Water Fault-Penetrating-Seal Pressure in the Reservoir

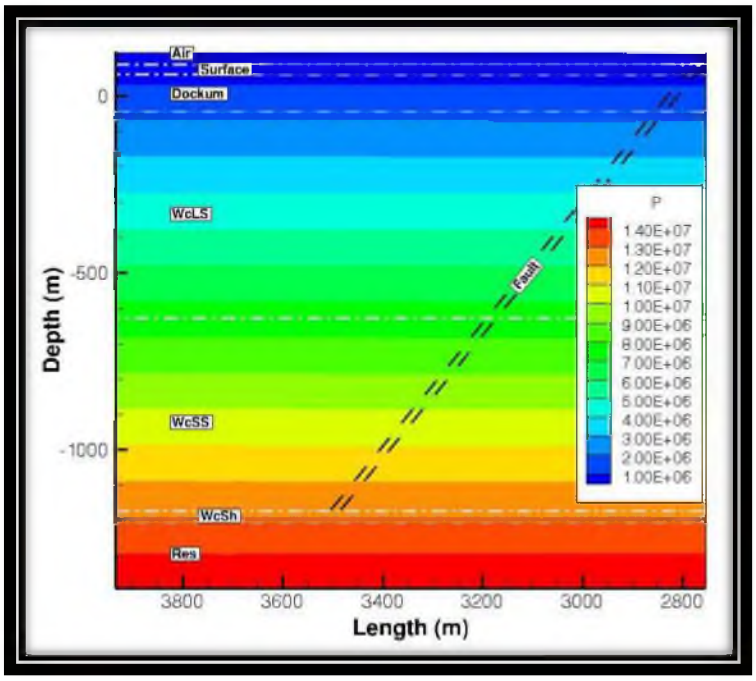

Case 6 (R2H1S2) Single Phase Water Fault-Penetrating-Seal Pressure in the Reservoir

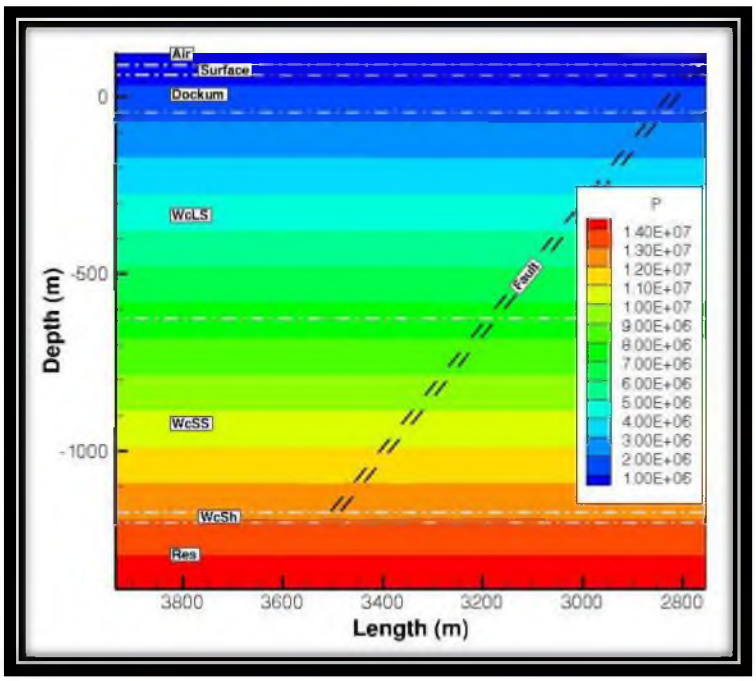

Case 7 (R2H2S1) Single Phase Water Fault-Penetrating-Seal Pressure in the Reservoir

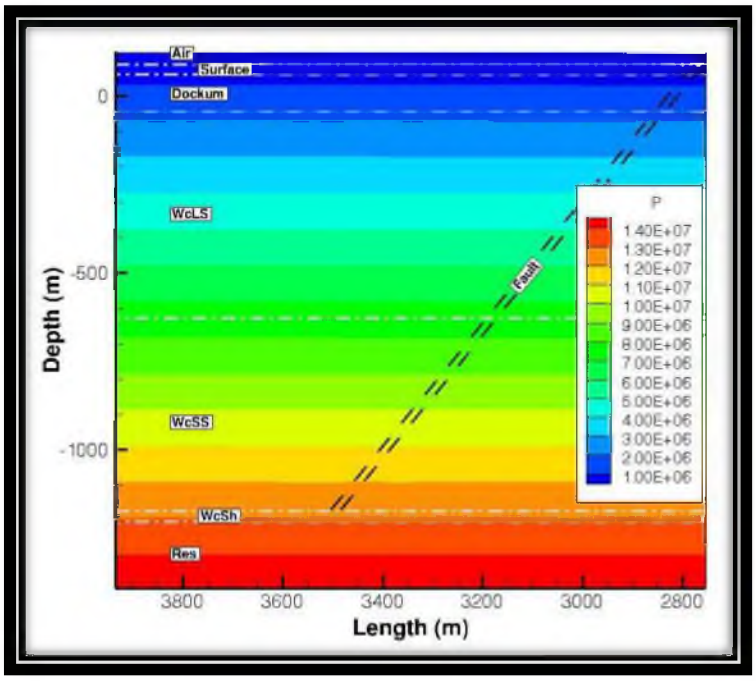

Case 8 (R2H2S2) Single Phase Water Fault-Penetrating-Seal Pressure in the Reservoir

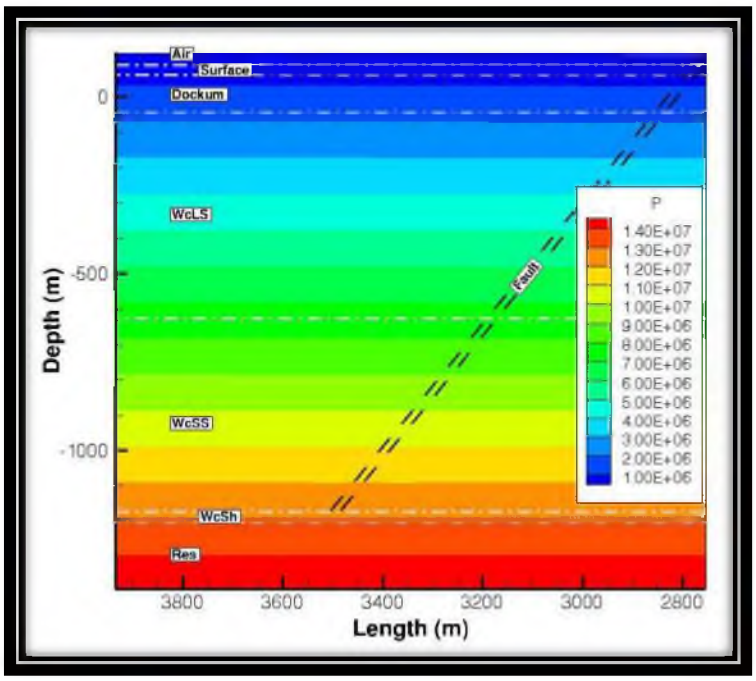

Case 9 (p1R1H1S1) Single Phase Water Fault-Penetrating-Seal Pressure in the Reservoir

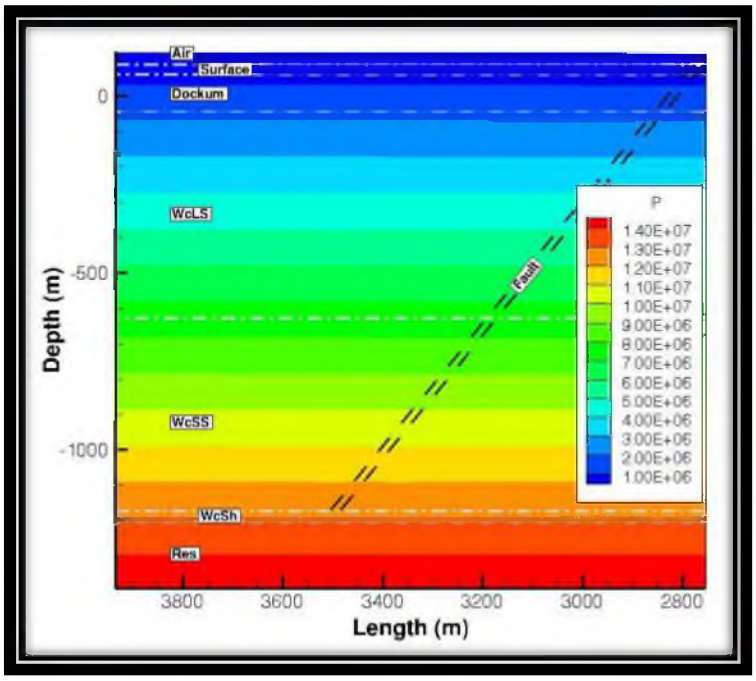

Case 10 (p2R1H1S1) Single Phase Water Fault-Penetrating-Seal Pressure in the Reservoir

APPENDIX F

SINGLE PHASE WATER FAULT-PENETRATING-SEAL

CHANGE IN PRESSURE

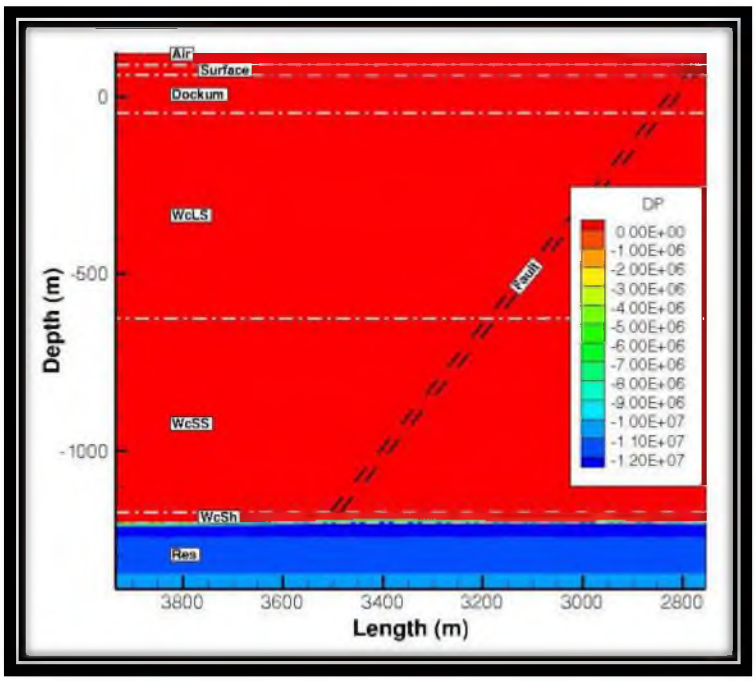

Case 1 (R1H1S1) Single Phase Water Fault-Penetrating-Seal Change in Pressure

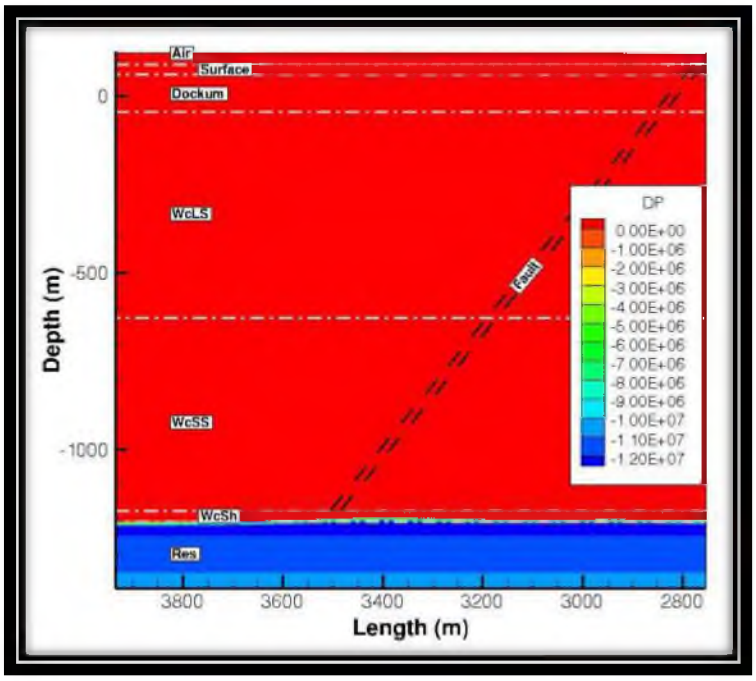

Case 2 (R1H1S2) Single Phase Water Fault-Penetrating-Seal Change in Pressure

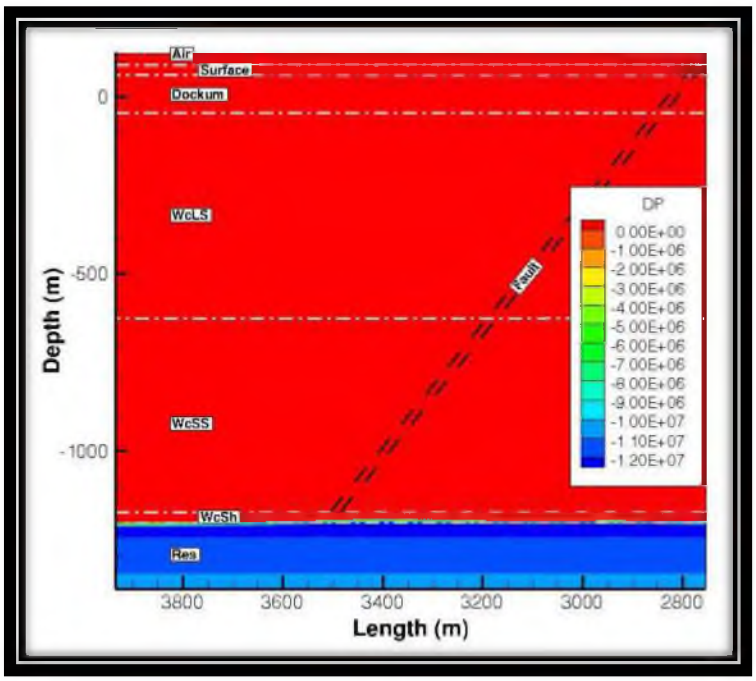

Case 3 (R1H2S1) Single Phase Water Fault-Penetrating-Seal Change in Pressure

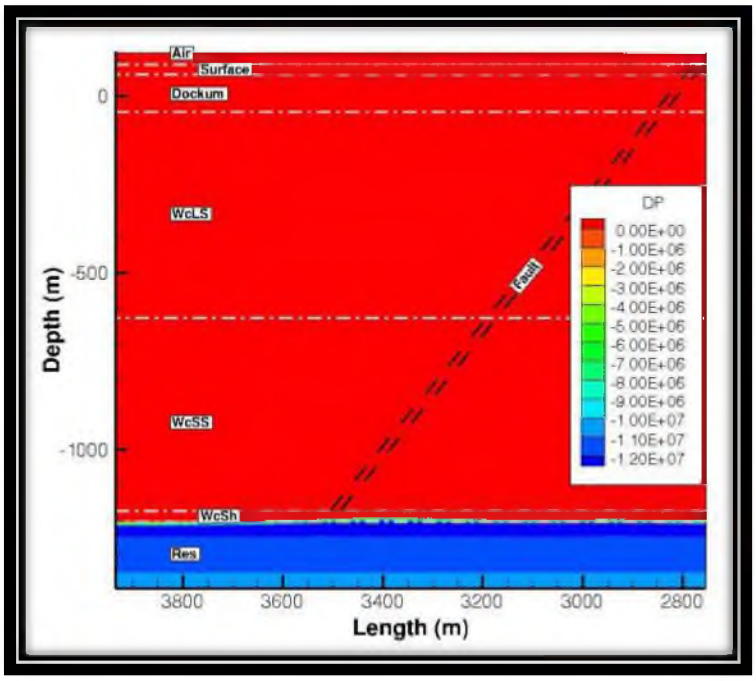

Case 4 (R1H2S2) Single Phase Water Fault-Penetrating-Seal Change in Pressure

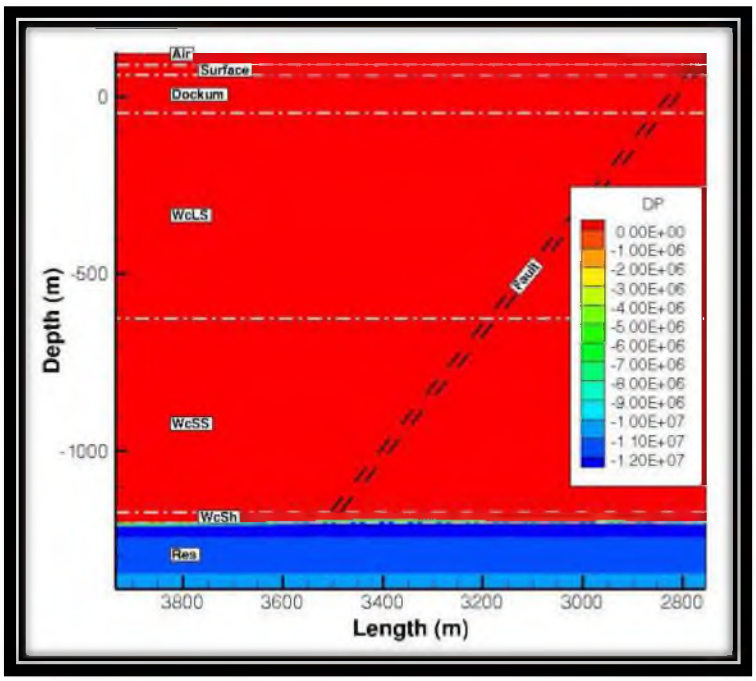

Case 5 (R2H1S1) Single Phase Water Fault-Penetrating-Seal Change in Pressure

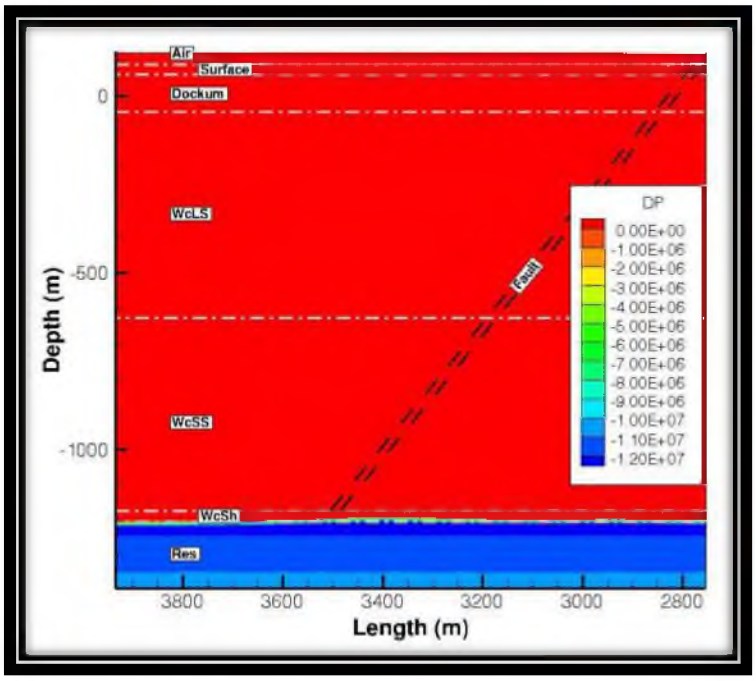

Case 6 (R2H1S2) Single Phase Water Fault-Penetrating-Seal Change in Pressure

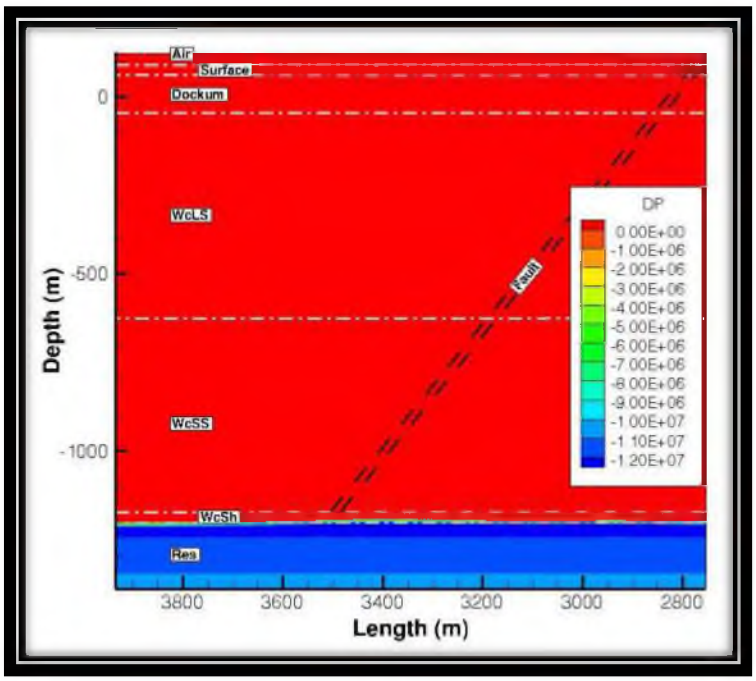

Case 7 (R2H2S1) Single Phase Water Fault-Penetrating-Seal Change in Pressure

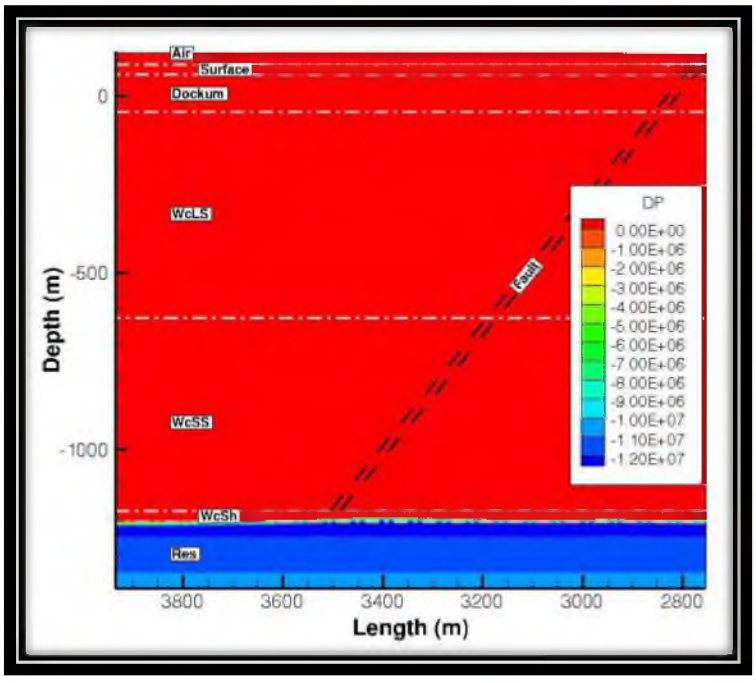

Case 8 (R2H2S2) Single Phase Water Fault-Penetrating-Seal Change in Pressure

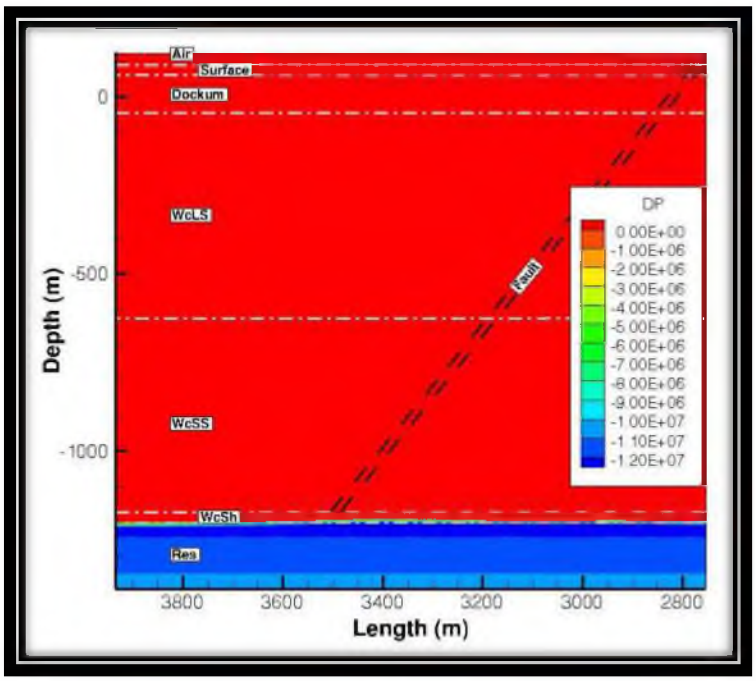

Case 9 (p1R1H1S1) Single Phase Water Fault-Penetrating-Seal Change in Pressure

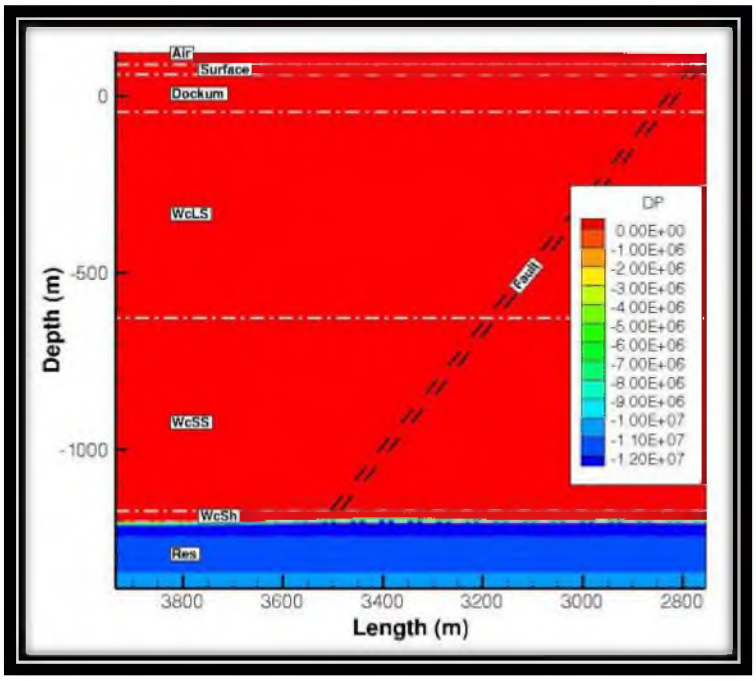

Case 10 (p2R1H1S1) Single Phase Water Fault-Penetrating-Seal Change in Pressure

APPENDIX G

MULTIPHASE CO_2 UNPENETRATED-SEAL PRESSURE IN THE RESERVOIR

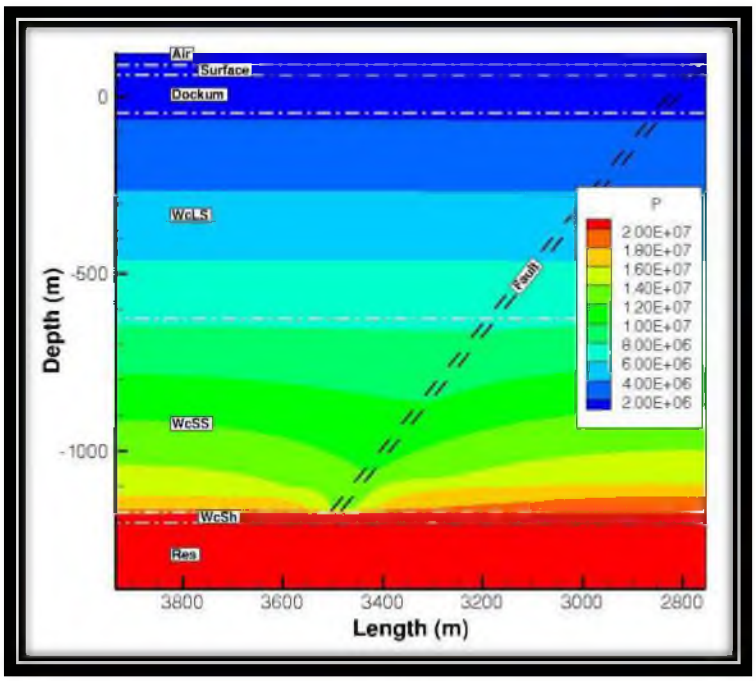

Case 1 (R1H1S1) Multiphase CO2 Unpenetrated-Seal Pressure in the Reservoir

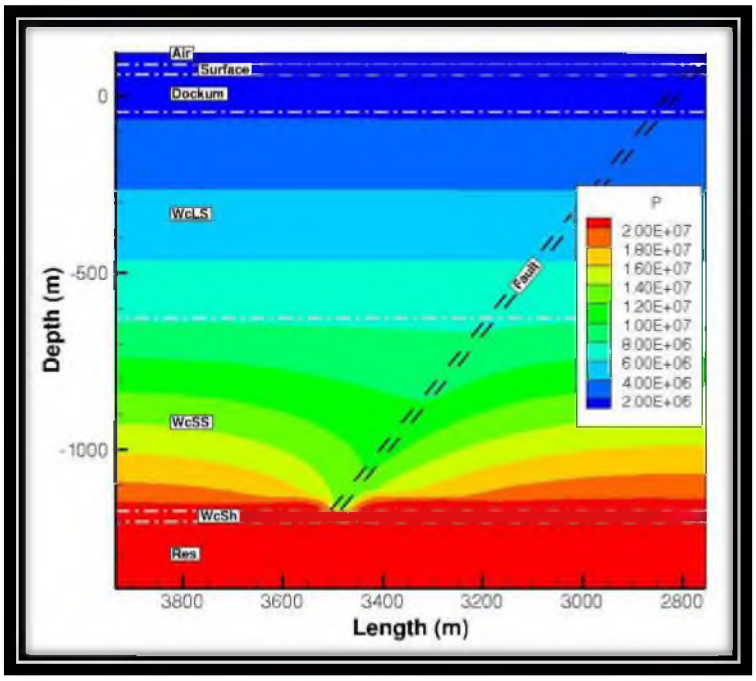

Case 2 (R1H1S2) Multiphase CO2 Unpenetrated-Seal Pressure in the Reservoir

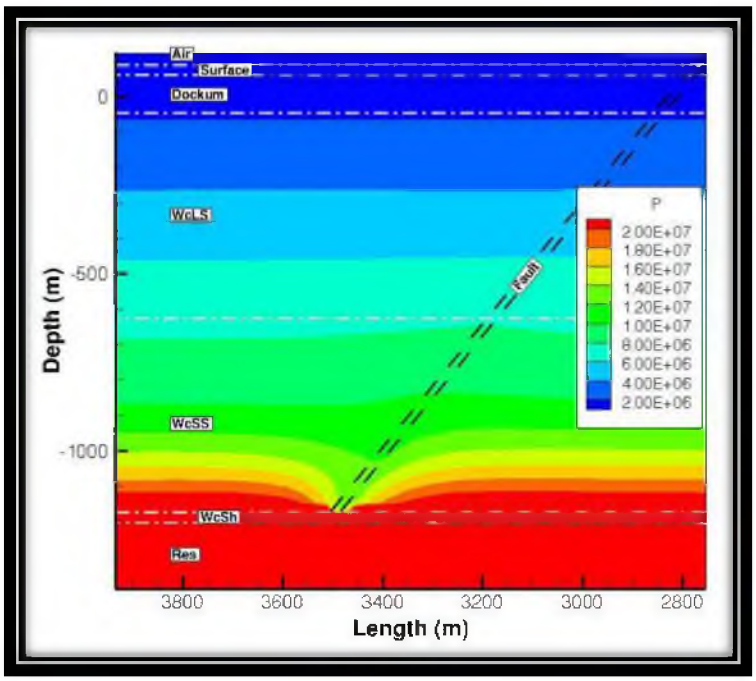

Case 3 (R1H2S1) Multiphase CO2 Unpenetrated-Seal Pressure in the Reservoir

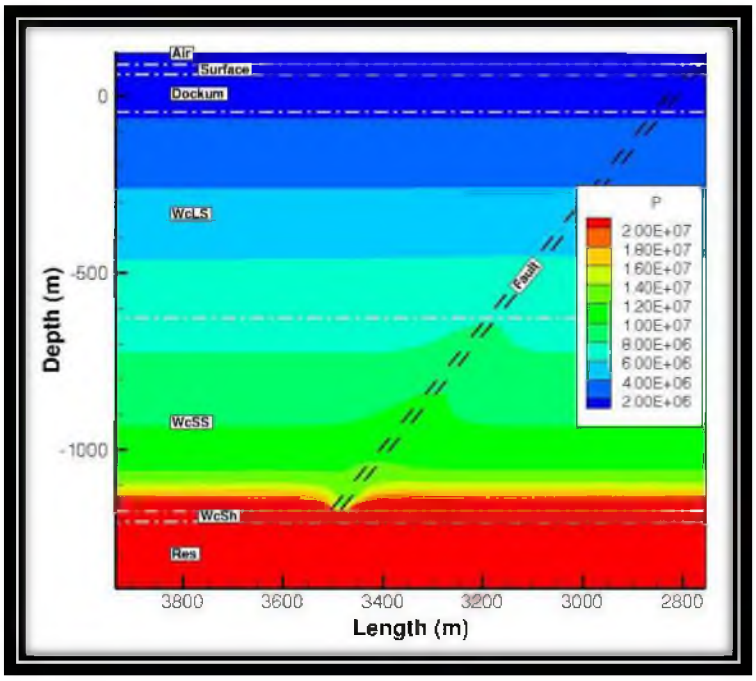

Case 4 (R1H2S2) Multiphase CO2 Unpenetrated-Seal Pressure in the Reservoir

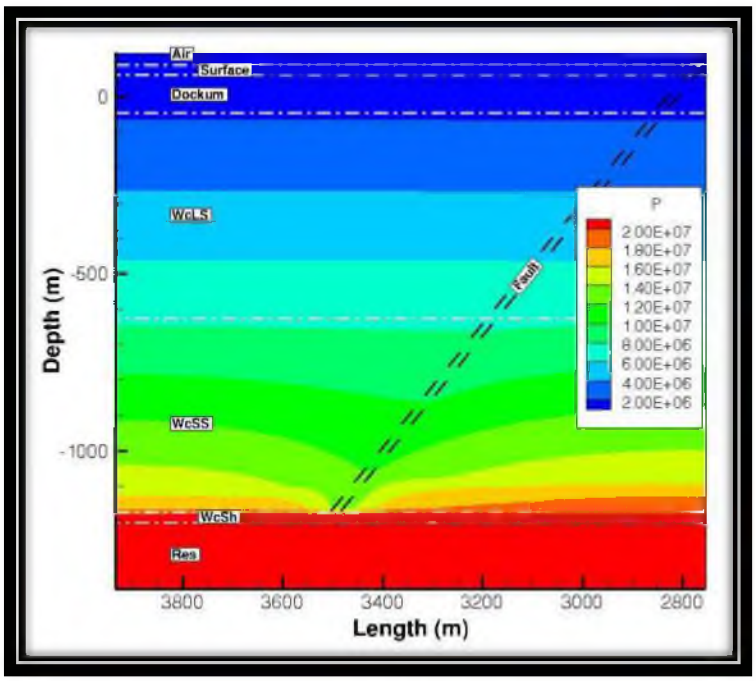

Case 5 (R2H1S1) Multiphase CO2 Unpenetrated-Seal Pressure in the Reservoir

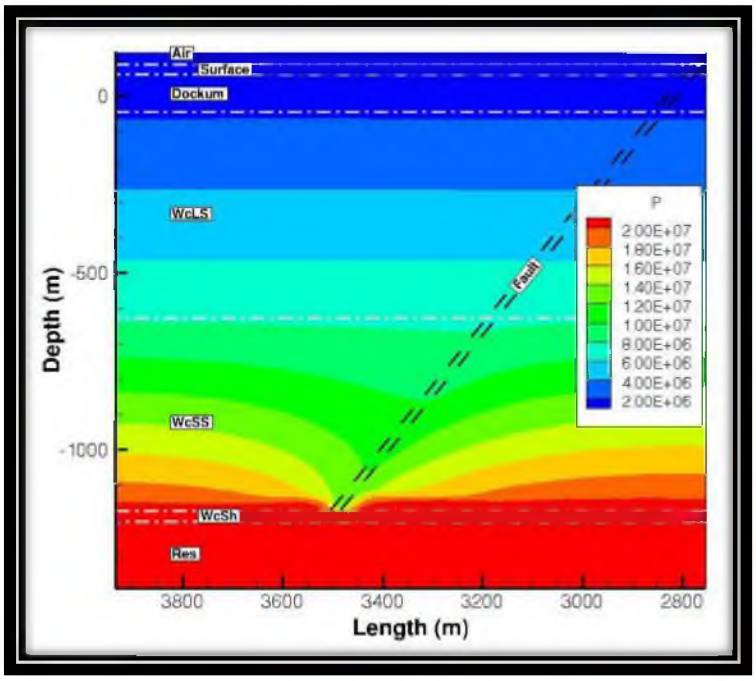

Case 6 (R2H1S2) Multiphase CO2 Unpenetrated-Seal Pressure in the Reservoir

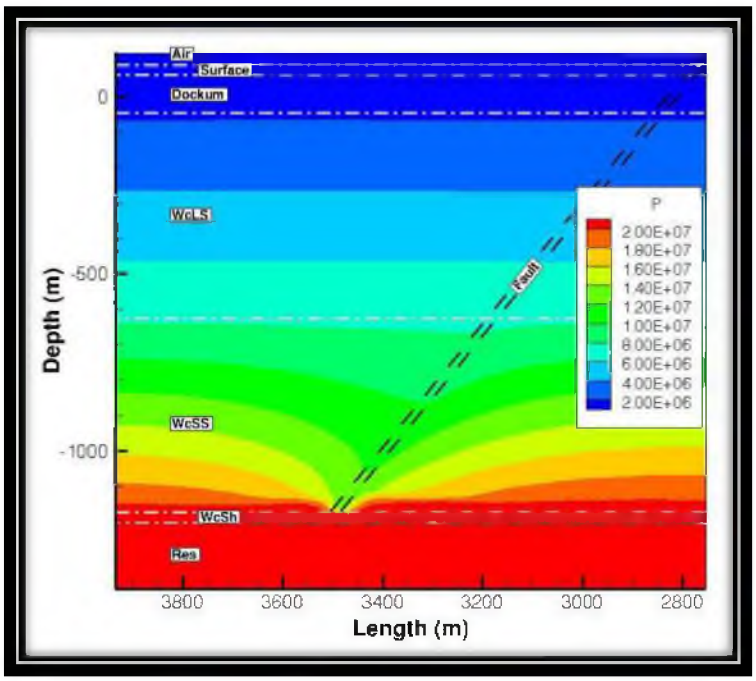

Case 7 (R2H2S1) Multiphase CO2 Unpenetrated-Seal Pressure in the Reservoir

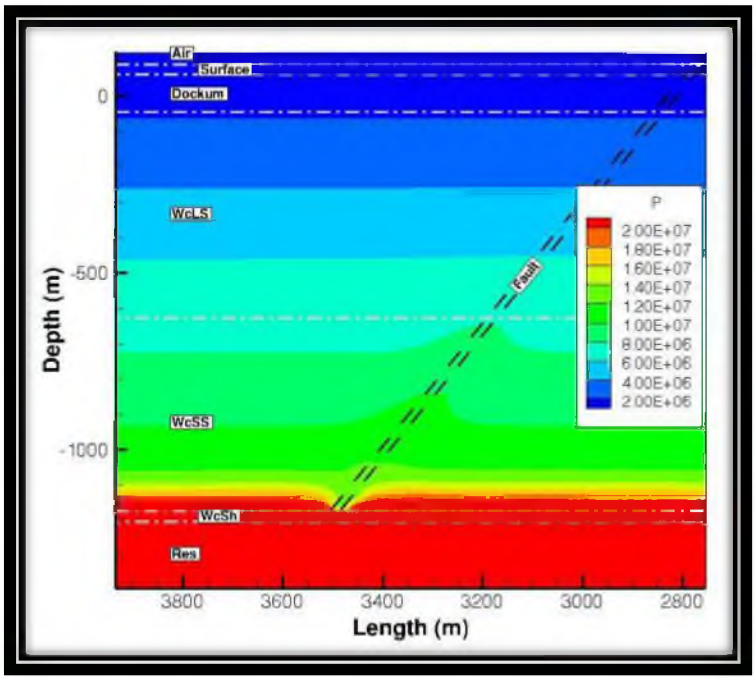

Case 8 (R2H2S2) Multiphase CO2 Unpenetrated-Seal Pressure in the Reservoir

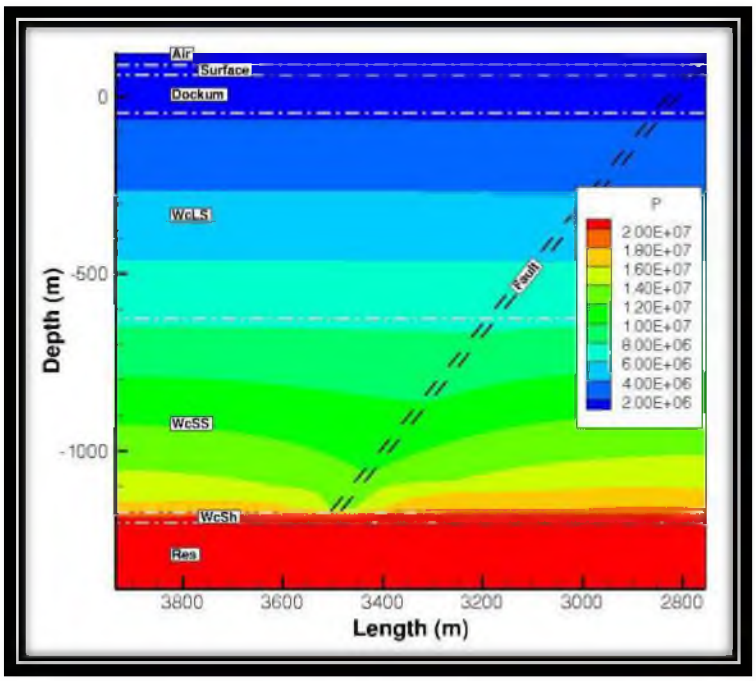

Case 9 (p1R1H1S1) Multiphase CO2 Unpenetrated-Seal Pressure in the Reservoir

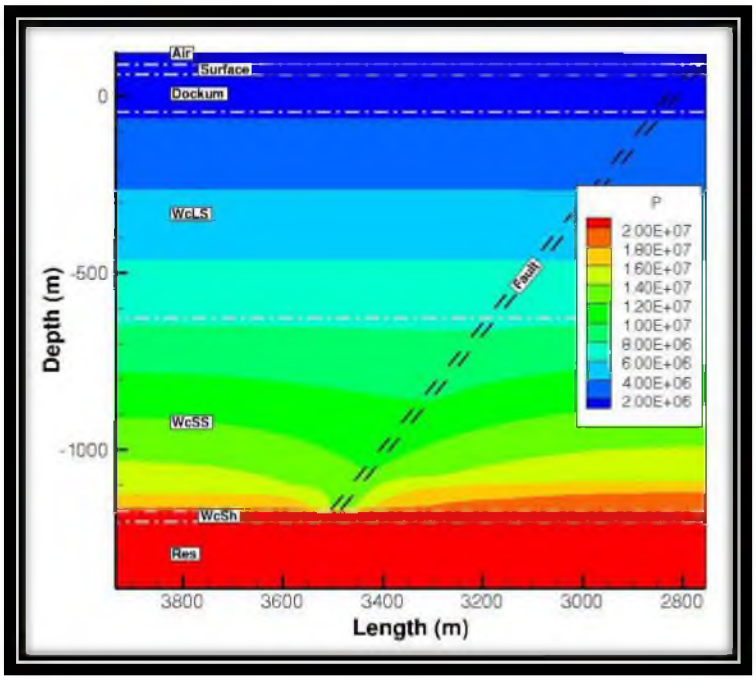

Case 10 (p2R1H1S1) Multiphase CO2 Unpenetrated-Seal Pressure in the Reservoir

APPENDIX H

MULTIPHASE CO2 UNPENETRATED-SEAL

IN THE RESERVOIR

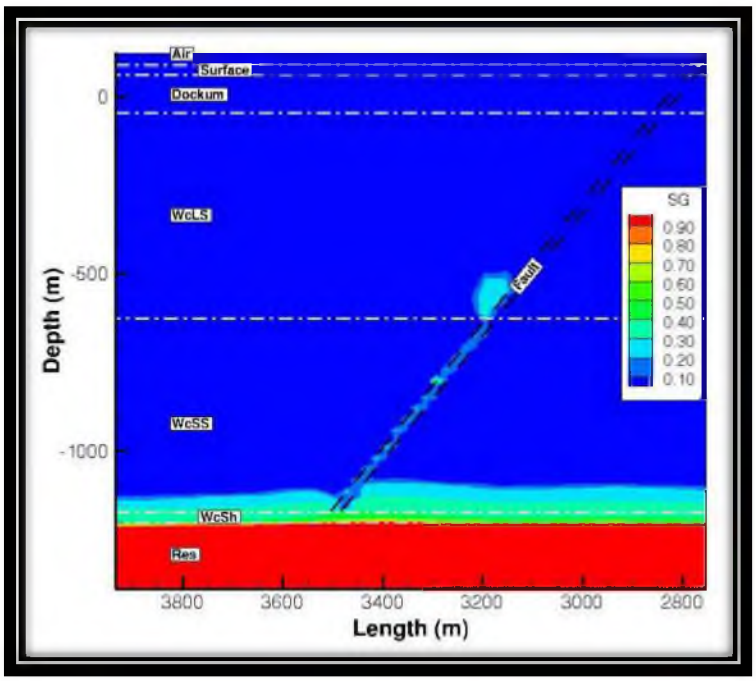

Case 1 (R1H1S1) Multiphase CO2 Unpenetrated-Seal in the Reservoir

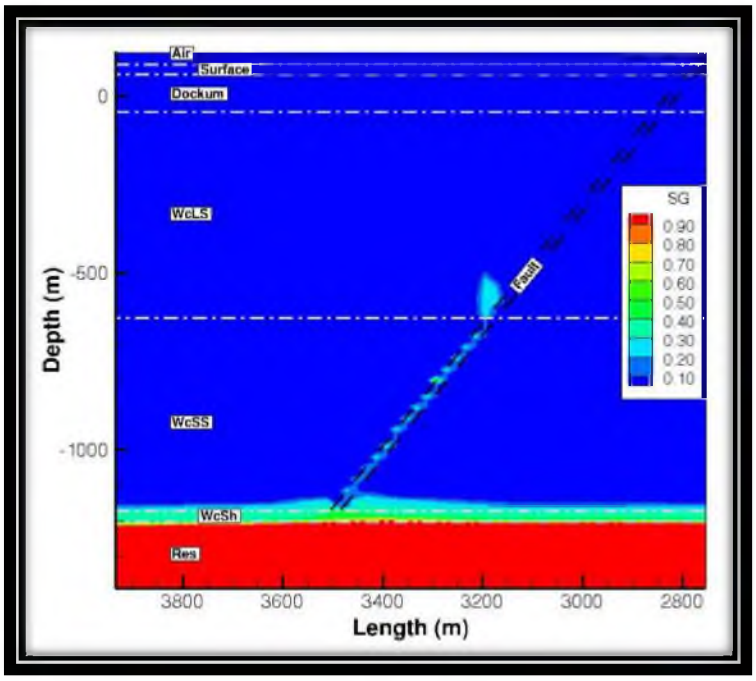

Case 2 (R1H1S2) Multiphase CO2 Unpenetrated-Seal in the Reservoir

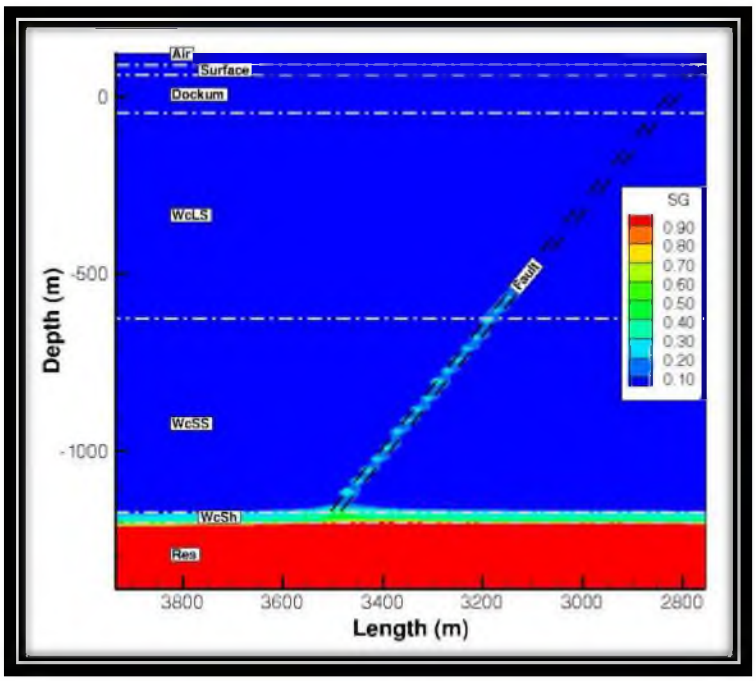

Case 3 (R1H2S1) Multiphase CO2 Unpenetrated-Seal in the Reservoir

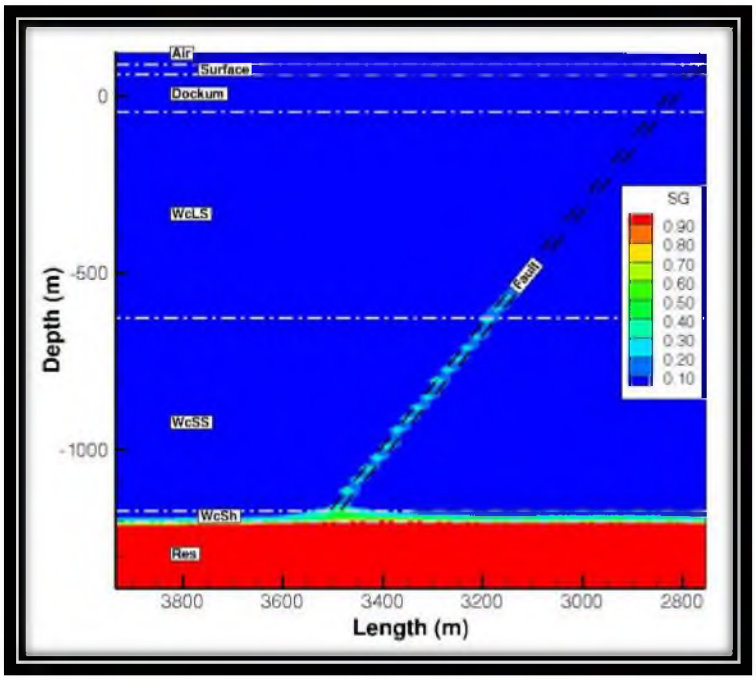

Case 4 (R1H2S2) Multiphase CO2 Unpenetrated-Seal in the Reservoir

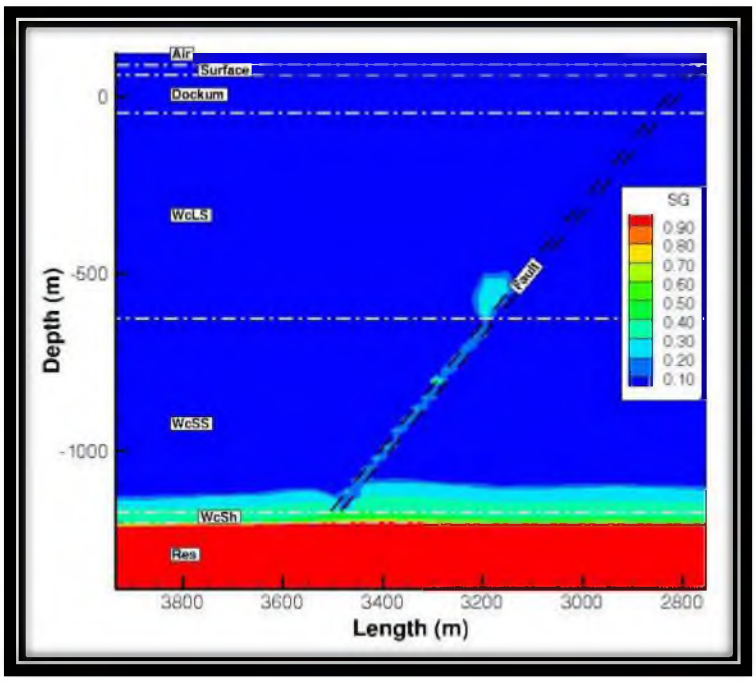

Case 5 (R2H1S1) Multiphase CO2 Unpenetrated-Seal in the Reservoir

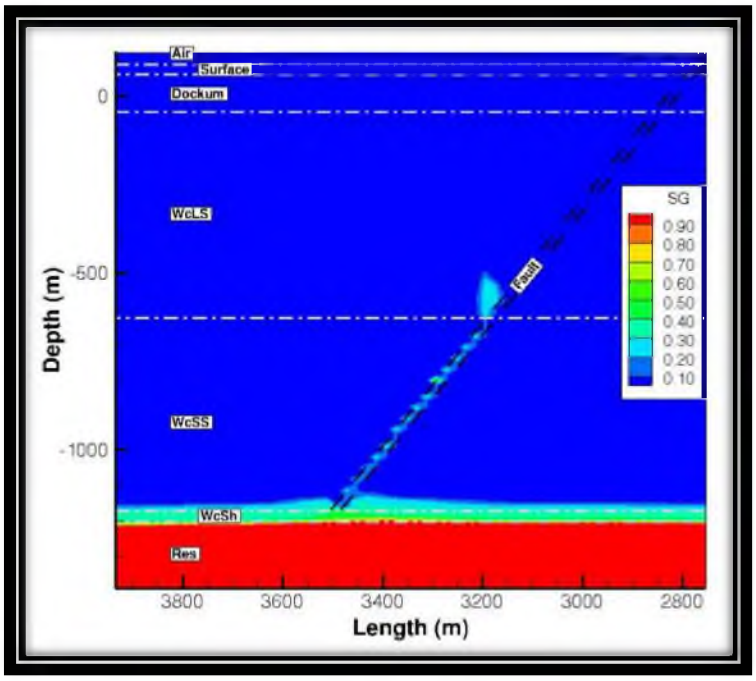

Case 6 (R2H1S2) Multiphase CO2 Unpenetrated-Seal in the Reservoir

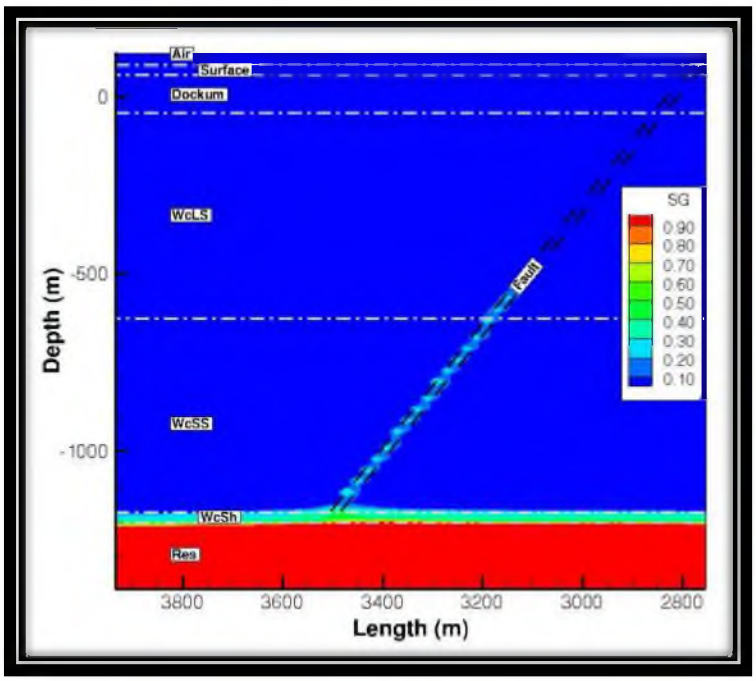

Case 7 (R2H2S1) Multiphase CO2 Unpenetrated-Seal in the Reservoir

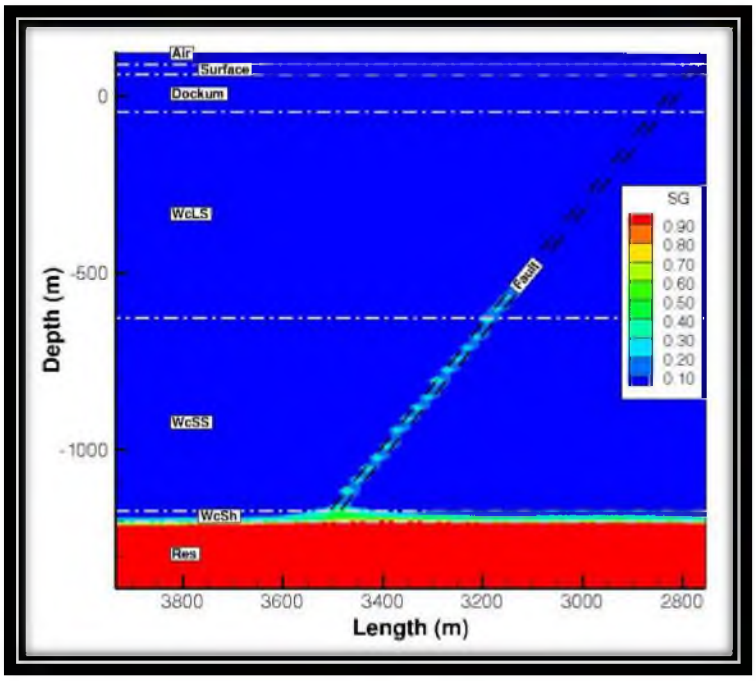

Case 8 (R2H2S2) Multiphase CO2 Unpenetrated-Seal in the Reservoir

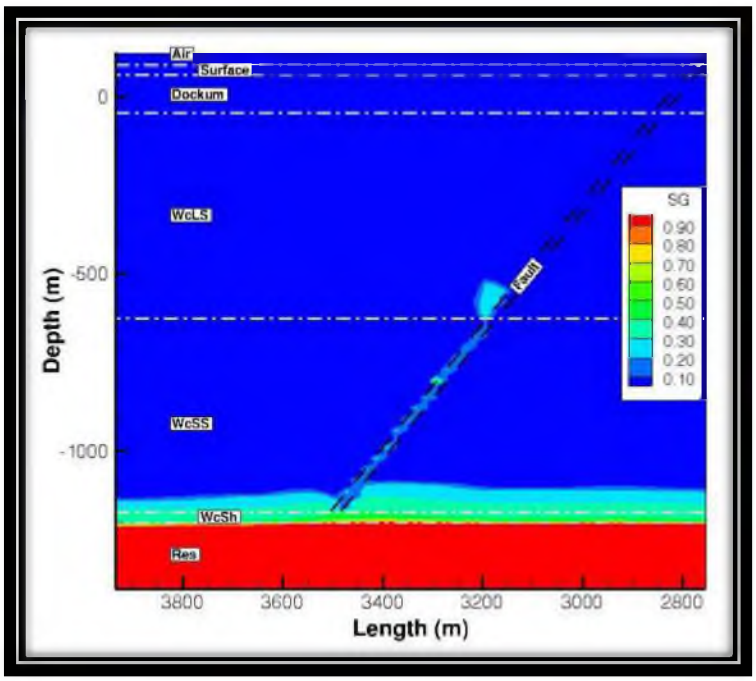

Case 9 (p1R1H1S1) Multiphase CO2 Unpenetrated-Seal in the Reservoir

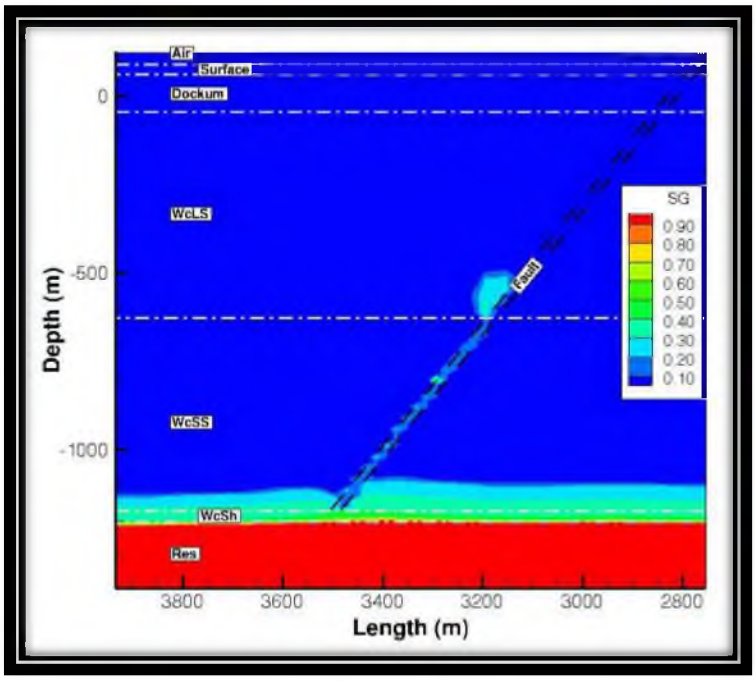

Case 10 (p2R1H1S1) Multiphase CO2 Unpenetrated-Seal in the Reservoir

APPENDIX I

MULTIPHASE CO2 UNPENETRATED-SEAL

DISSOLVED PLUME

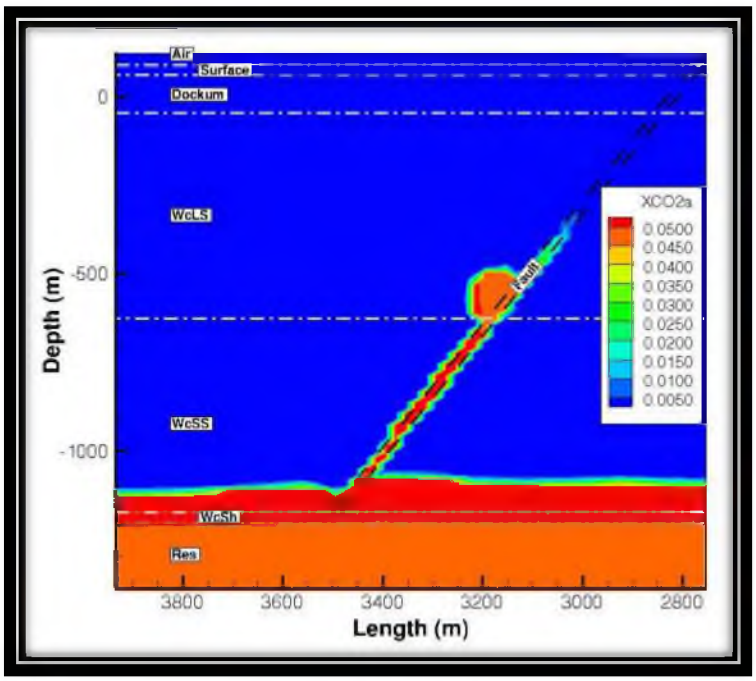

Case 1 (R1H1S1) Multiphase CO2 Unpenetrated-Seal Dissolved Plume

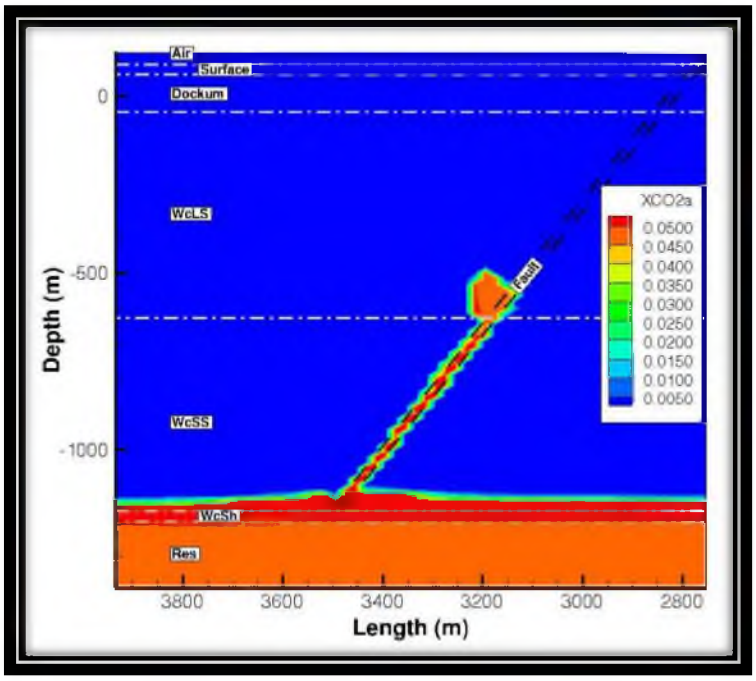

Case 2 (R1H1S2) Multiphase CO2 Unpenetrated-Seal Dissolved Plume

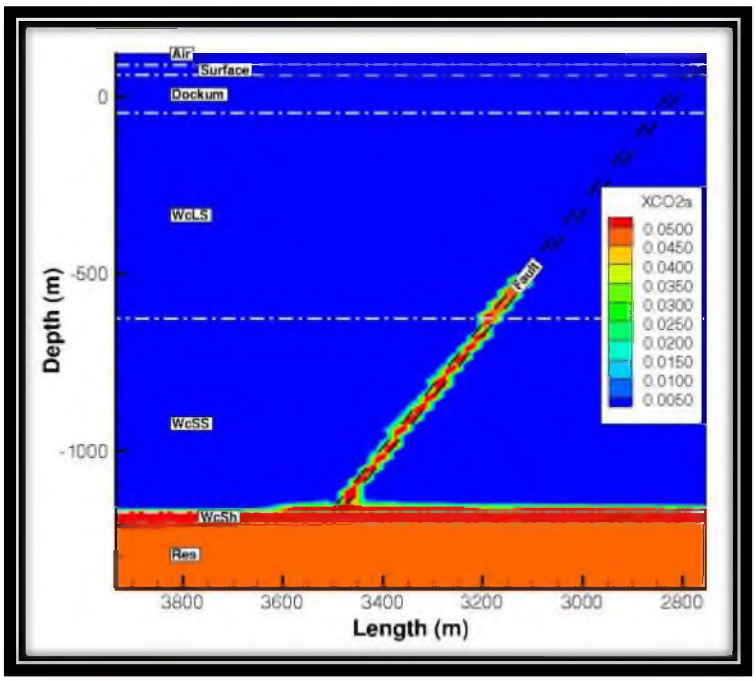

Case 3 (R1H2S1) Multiphase CO2 Unpenetrated-Seal Dissolved Plume

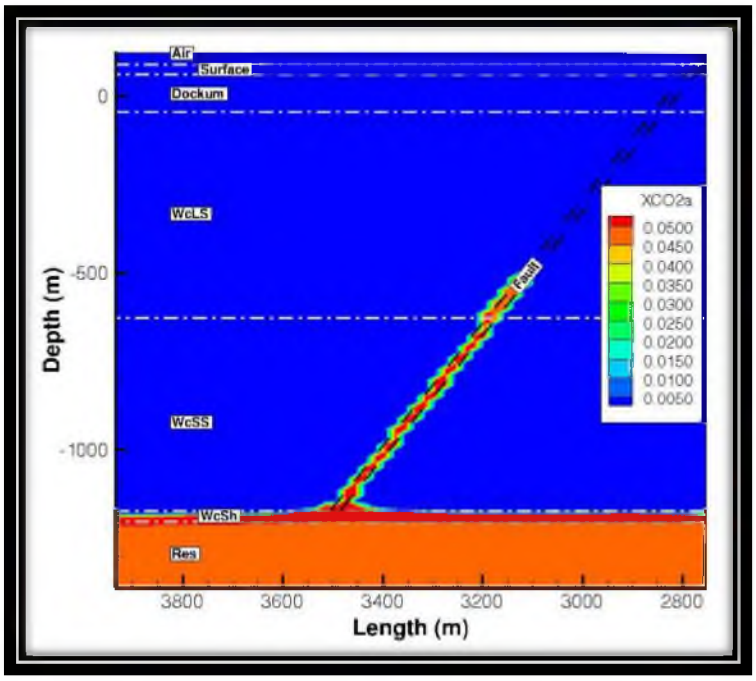

Case 4 (R1H2S2) Multiphase CO2 Unpenetrated-Seal Dissolved Plume

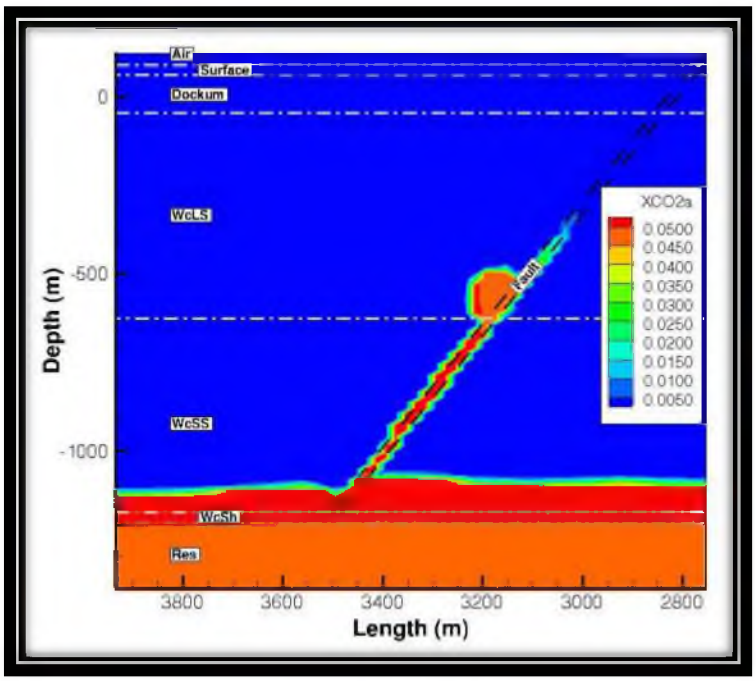

Case 5 (R2H1S1) Multiphase CO2 Unpenetrated-Seal Dissolved Plume

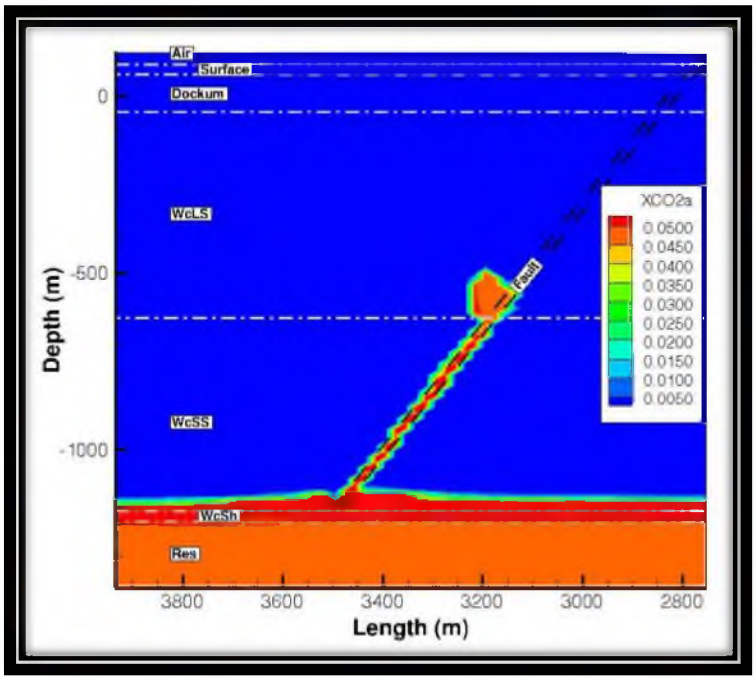

Case 6 (R2H1S2) Multiphase CO2 Unpenetrated-Seal Dissolved Plume

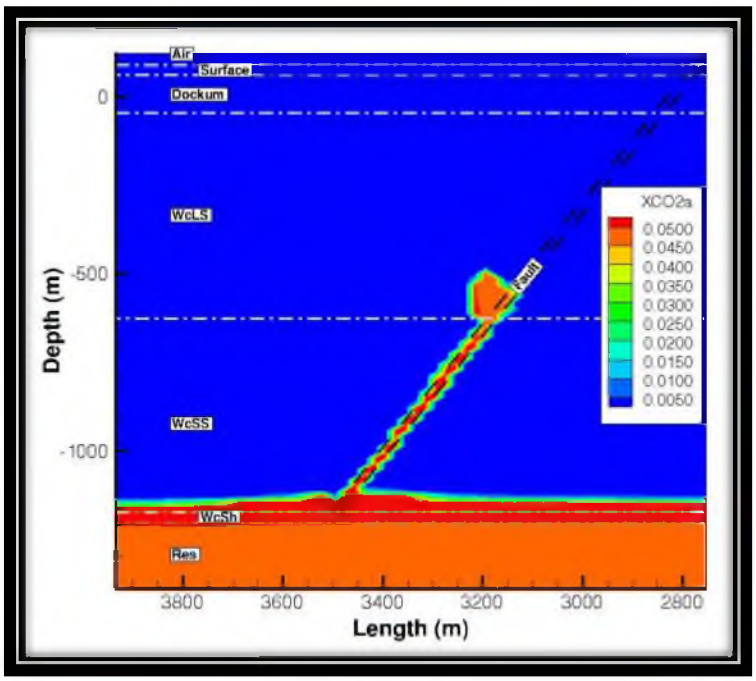

Case 7 (R2H2S1) Multiphase CO2 Unpenetrated-Seal Dissolved Plume

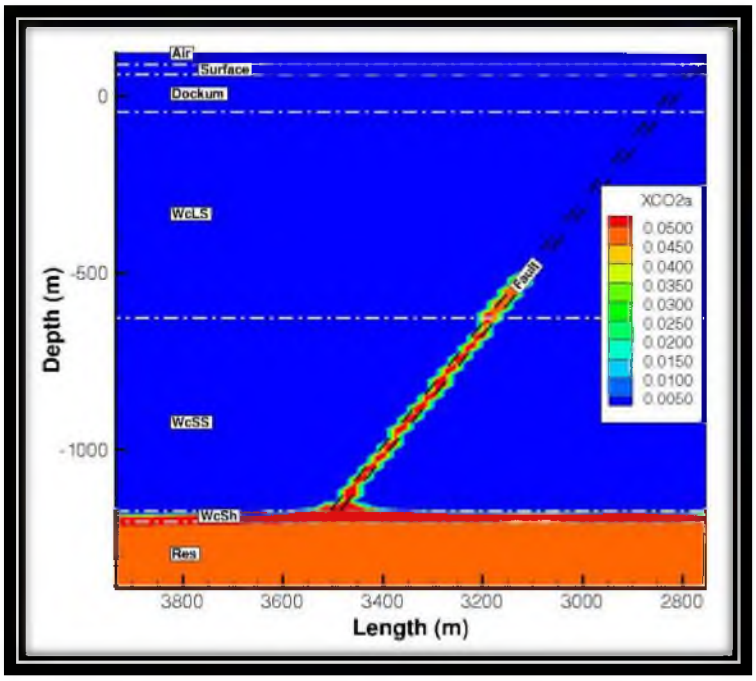

Case 8 (R2H2S2) Multiphase CO2 Unpenetrated-Seal Dissolved Plume

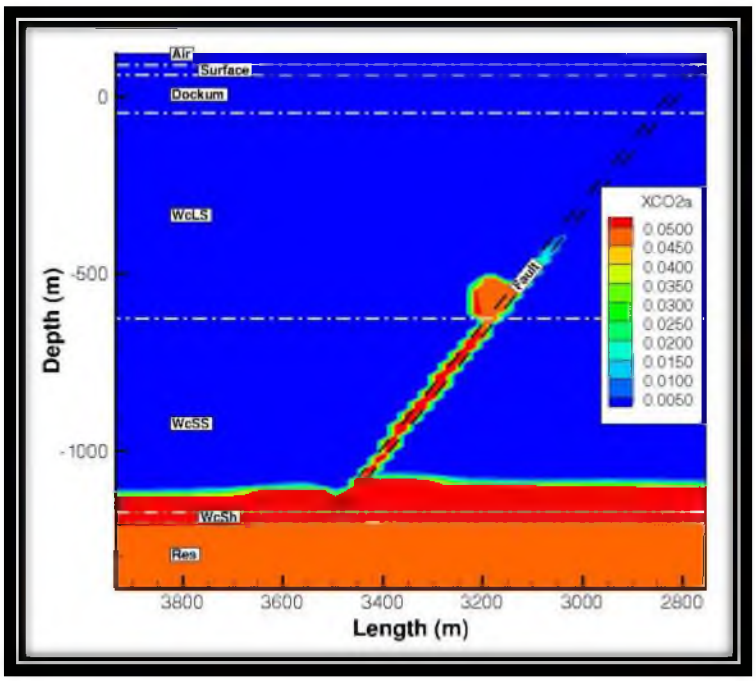

Case 9 (p1R1H1S1) Multiphase CO2 Unpenetrated-Seal Dissolved Plume

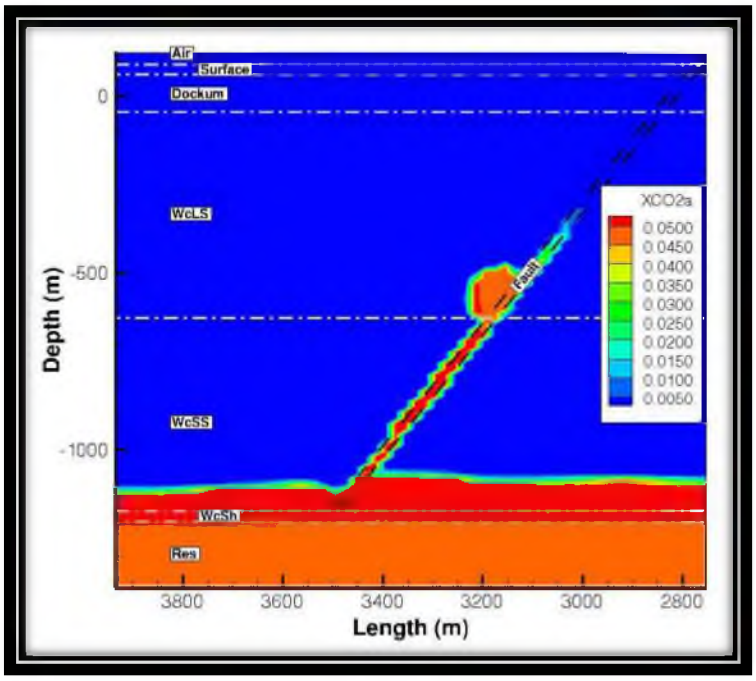

Case 10 (p2R1H1S1) Multiphase CO2 Unpenetrated-Seal Dissolved Plume

APPENDIX J

MULTIPHASE CO2 FAULT-PENETRATING-SEAL PRESSURE IN THE RESERVOIR

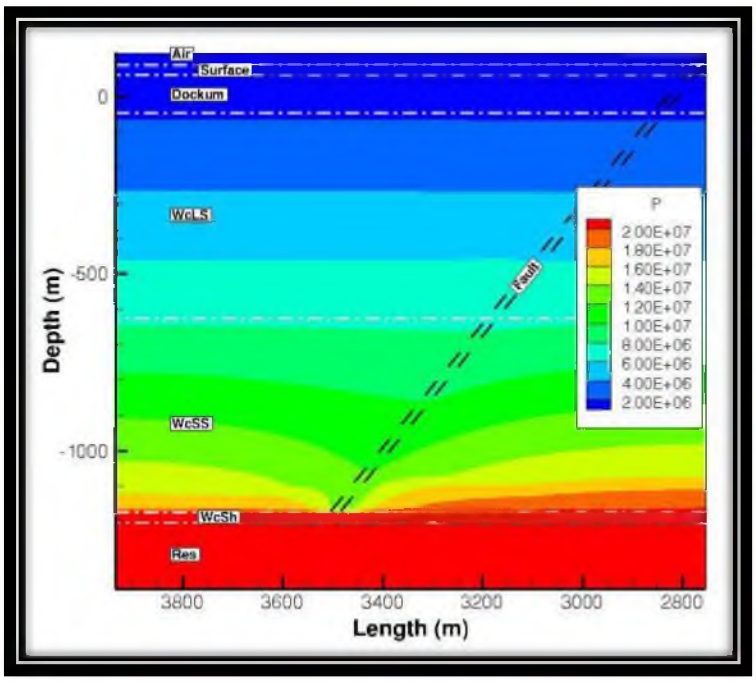

Case 1 (R1H1S1) Multiphase CO2 Fault-Penetrating-Seal Pressure in the Reservoir

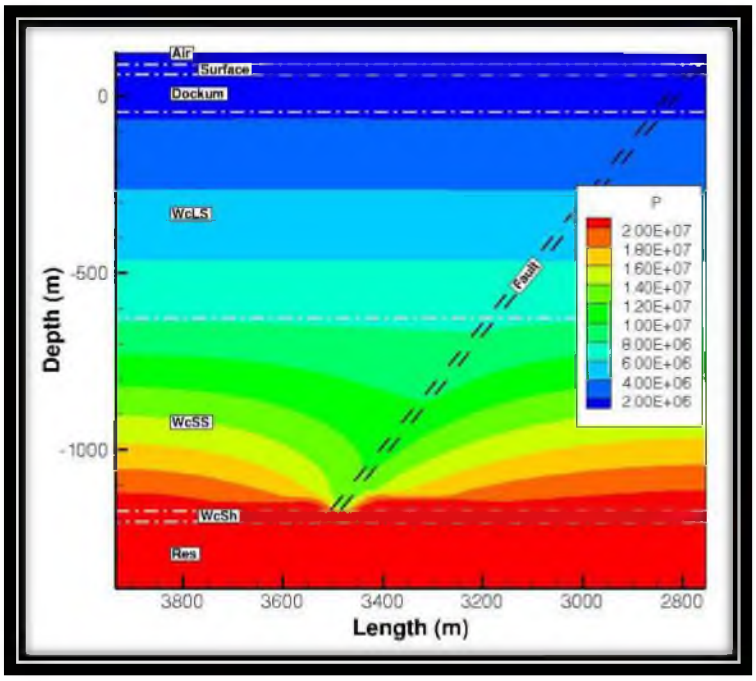

Case 2 (R1H1S2) Multiphase CO2 Fault-Penetrating-Seal Pressure in the Reservoir

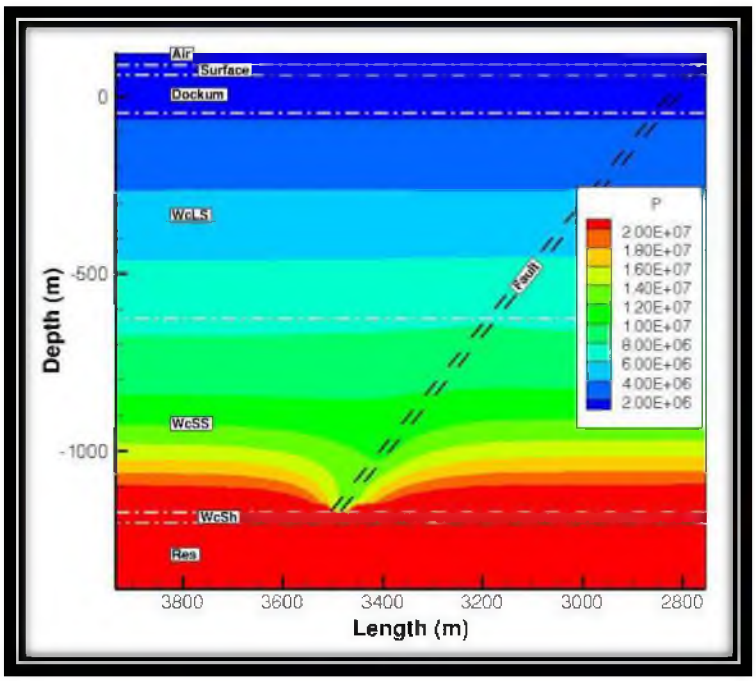

Case 3 (R1H2S1) Multiphase CO2 Fault-Penetrating-Seal Pressure in the Reservoir

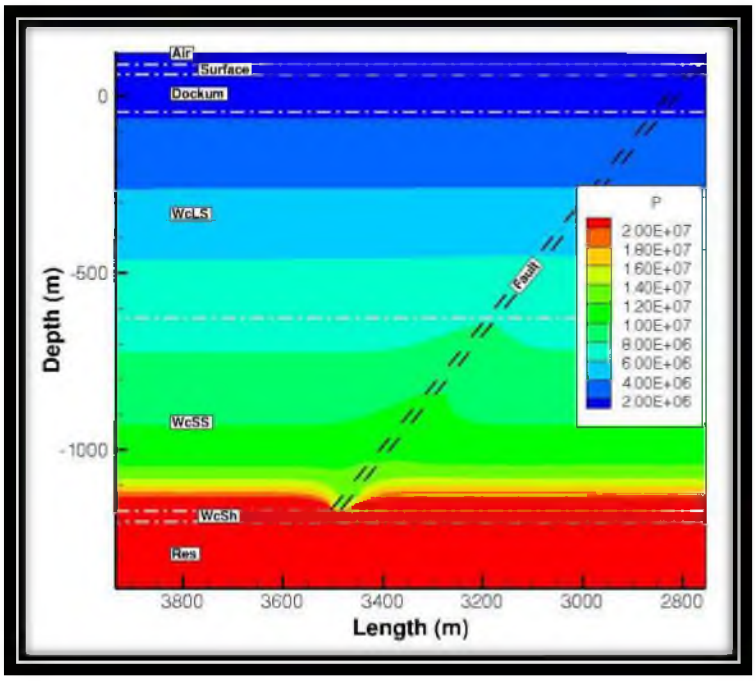

Case 4 (R1H2S2) Multiphase CO2 Fault-Penetrating-Seal Pressure in the Reservoir

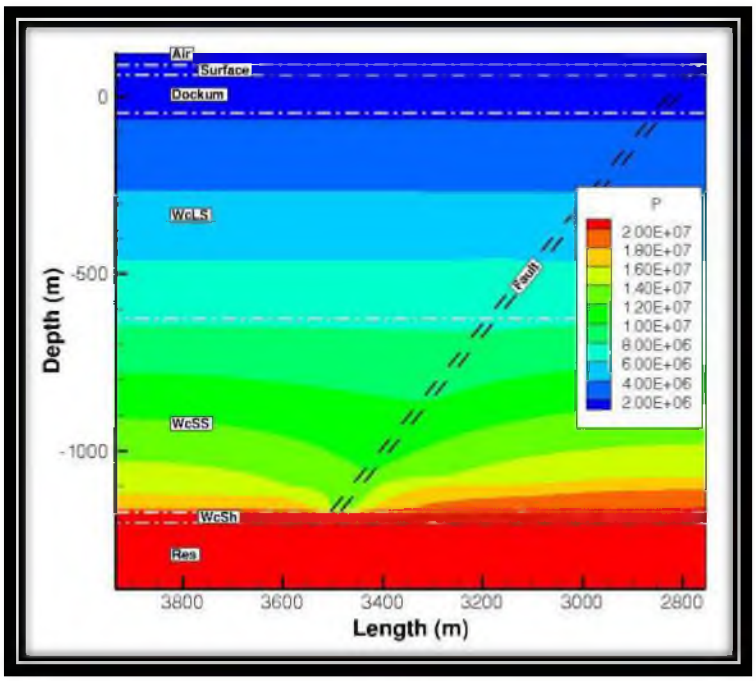

Case 5 (R2H1S1) Multiphase CO2 Fault-Penetrating-Seal Pressure in the Reservoir

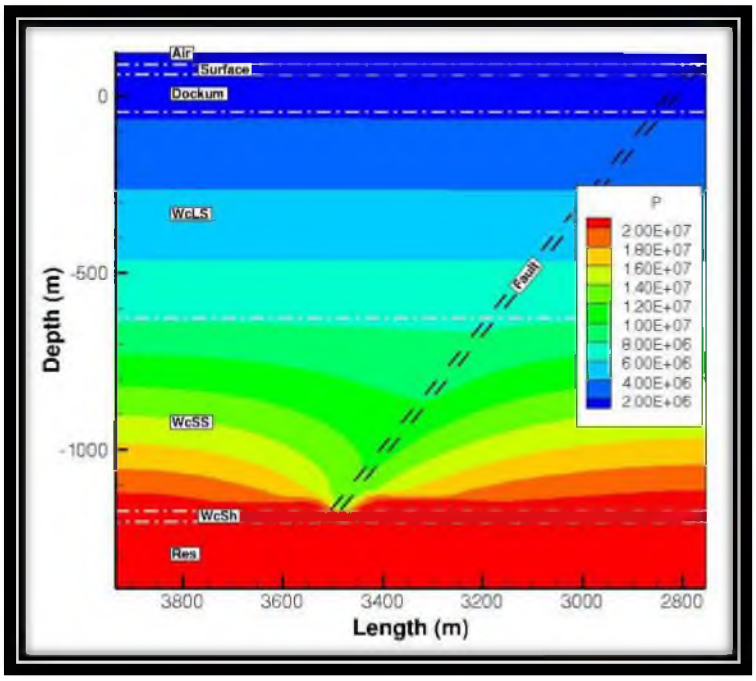

Case 6 (R2H1S2) Multiphase CO2 Fault-Penetrating-Seal Pressure in the Reservoir

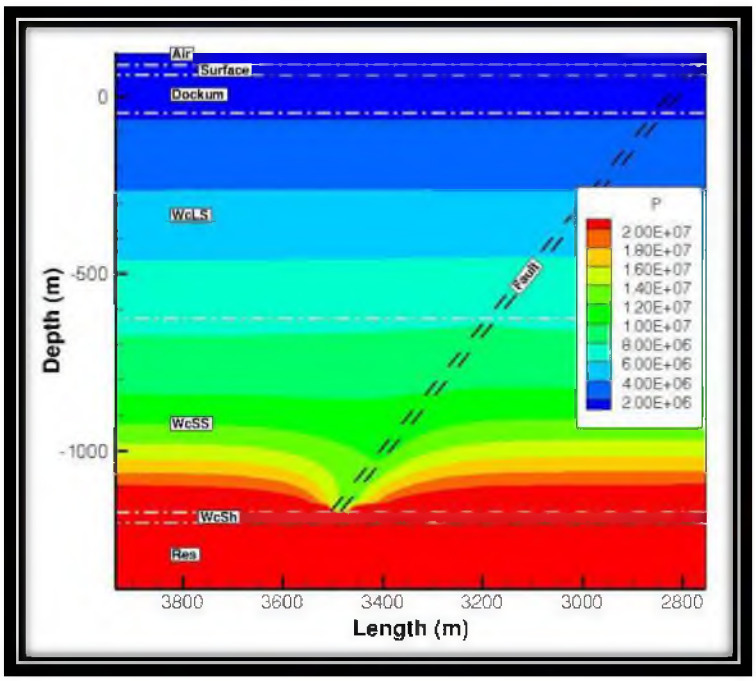

Case 7 (R2H2S1) Multiphase CO2 Fault-Penetrating-Seal Pressure in the Reservoir

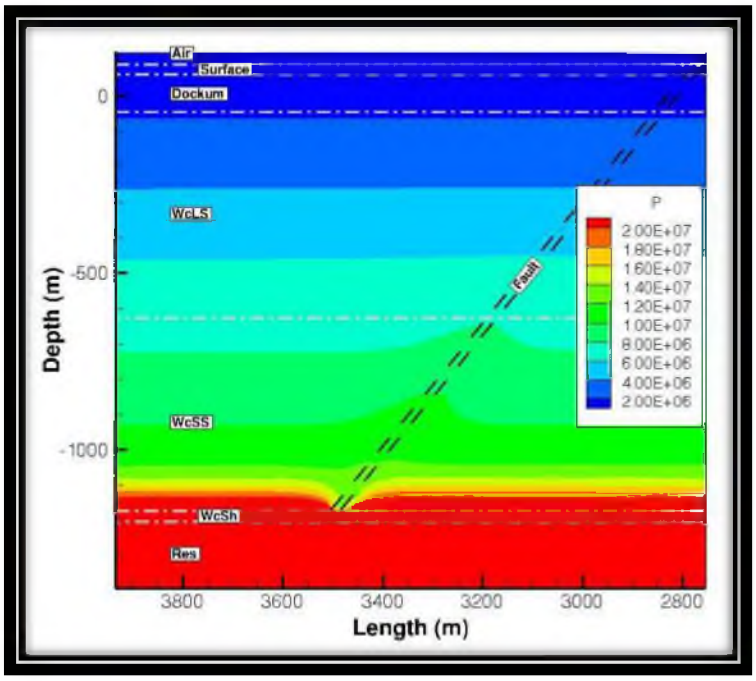

Case 8 (R2H2S2) Multiphase CO2 Fault-Penetrating-Seal Pressure in the Reservoir

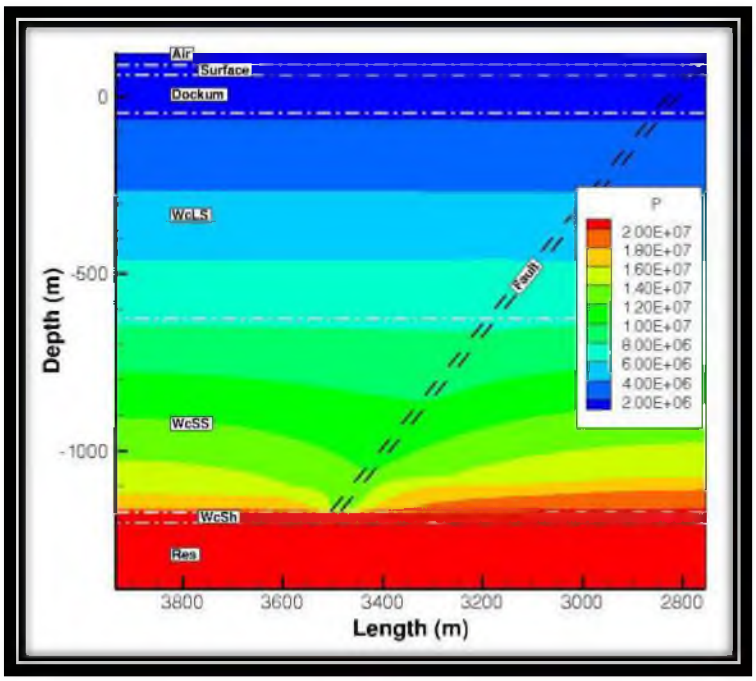

Case 9 (p1R1H1S1) Multiphase CO2 Fault-Penetrating-Seal Pressure in the Reservoir

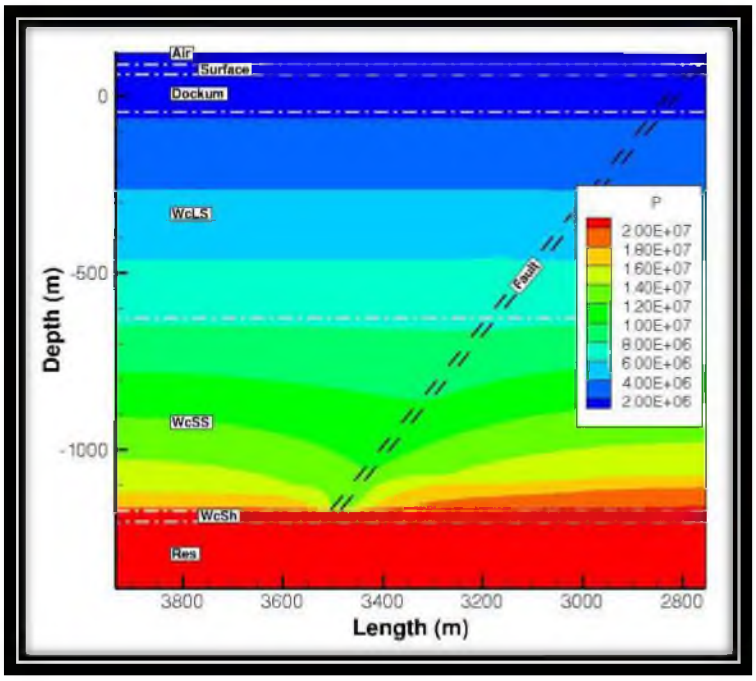

Case 10 (p2R1H1S1) Multiphase CO2 Fault-Penetrating-Seal Pressure in the Reservoir

APPENDIX K

MULTIPHASE CO2 FAULT-PENETRATING-SEAL IN THE RESERVOIR

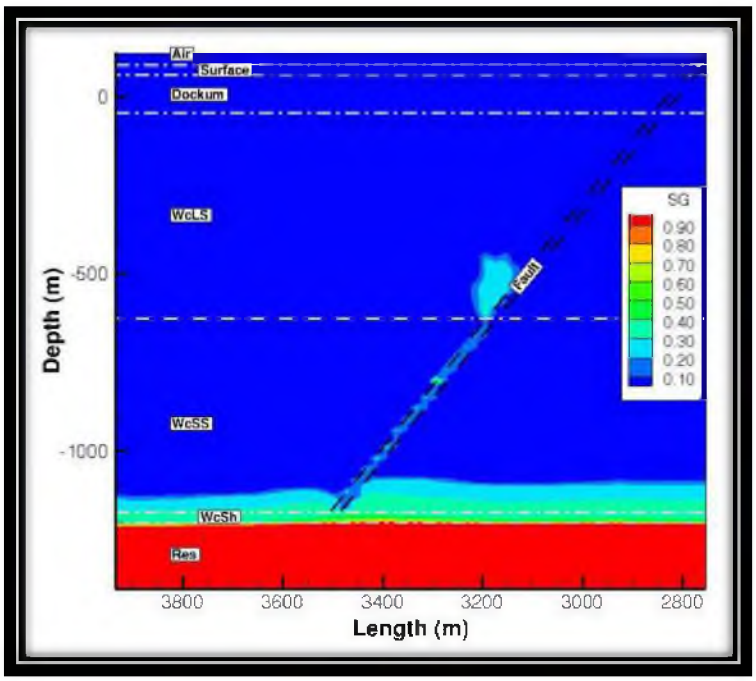

Case 1 (R1H1S1) Multiphase CO2 Fault-Penetrating-Seal in the Reservoir

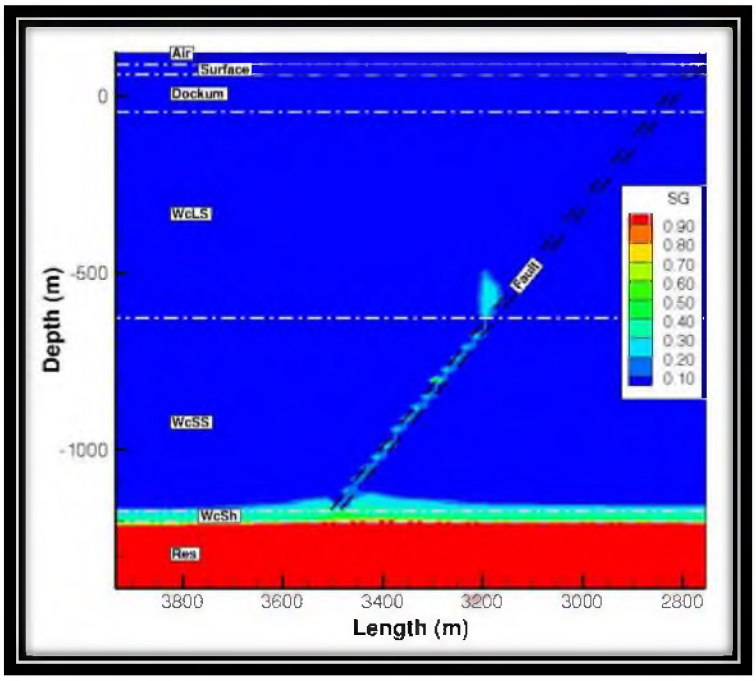

Case 2 (R1H1S2) Multiphase CO2 Fault-Penetrating-Seal in the Reservoir

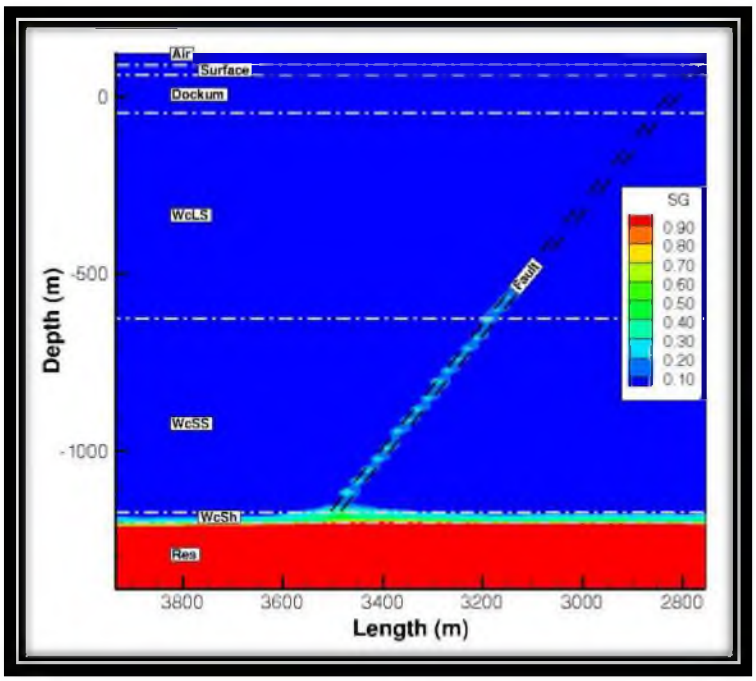

Case 3 (R1H2S1) Multiphase CO2 Fault-Penetrating-Seal in the Reservoir

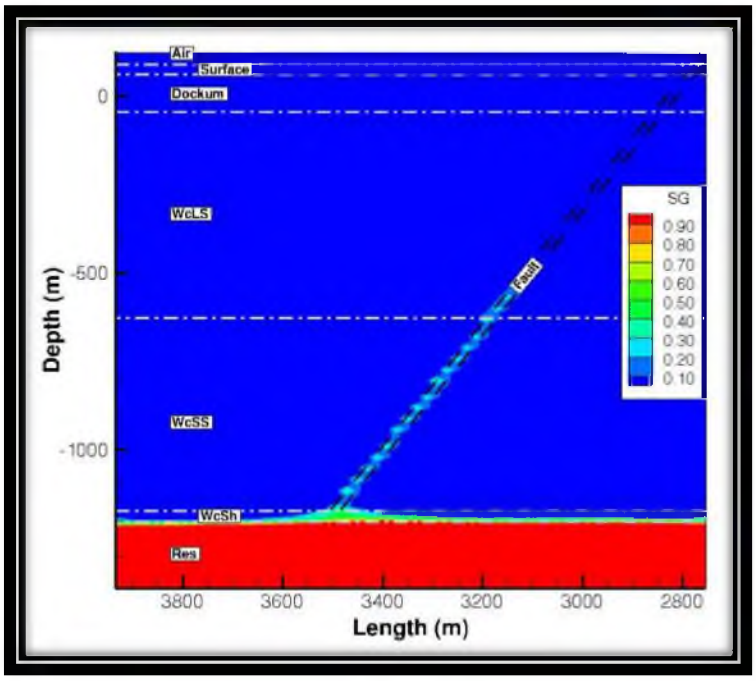

Case 4 (R1H2S2) Multiphase CO2 Fault-Penetrating-Seal in the Reservoir

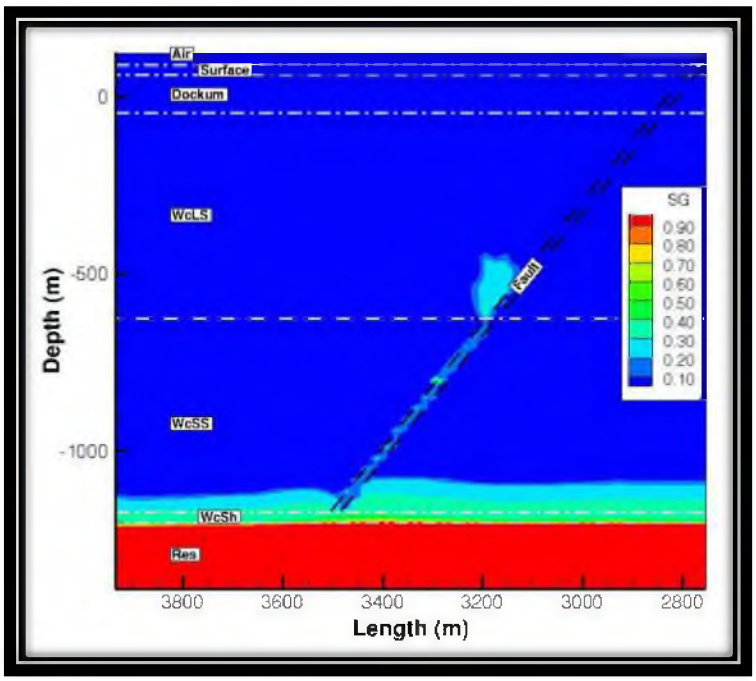

Case 5 (R2H1S1) Multiphase CO2 Fault-Penetrating-Seal in the Reservoir

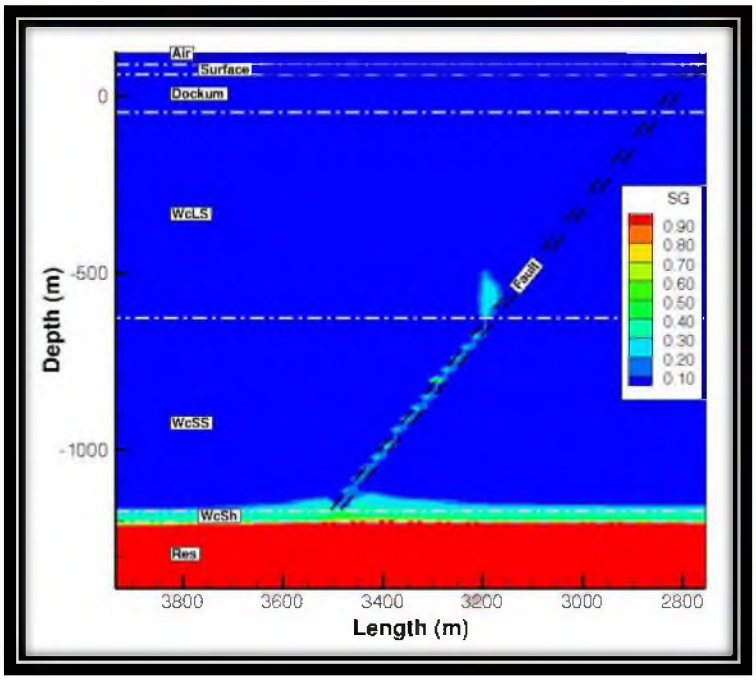

Case 6 (R2H1S2) Multiphase CO2 Fault-Penetrating-Seal in the Reservoir

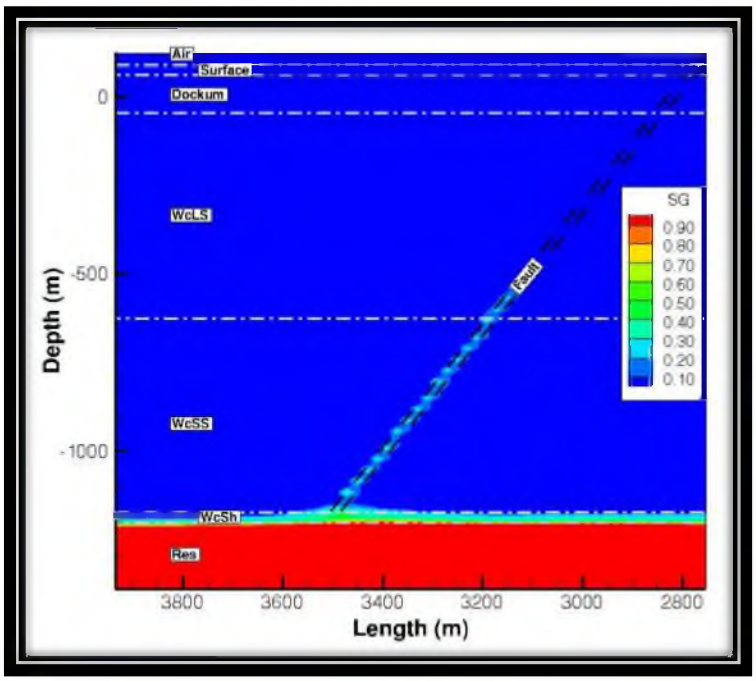

Case 7 (R2H2S1) Multiphase CO2 Fault-Penetrating-Seal in the Reservoir

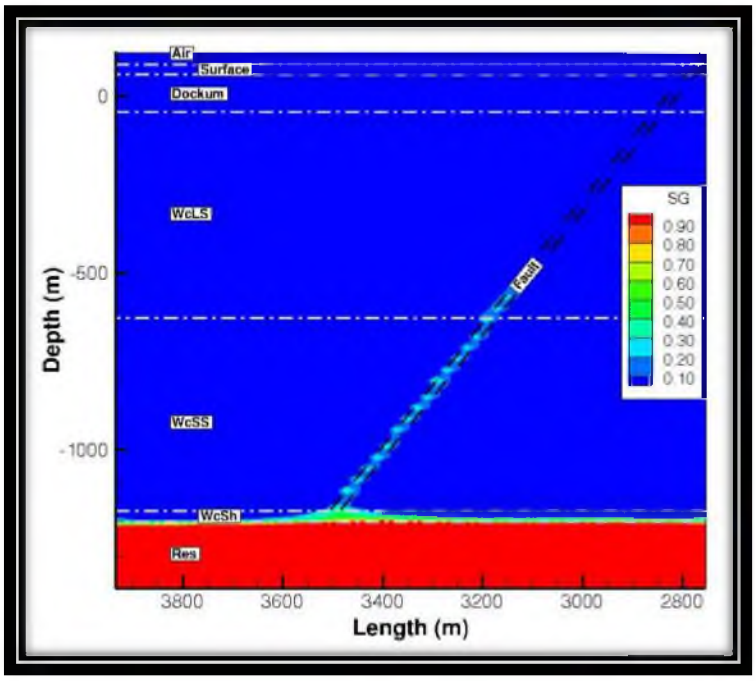

Case 8 (R2H2S2) Multiphase CO2 Fault-Penetrating-Seal in the Reservoir

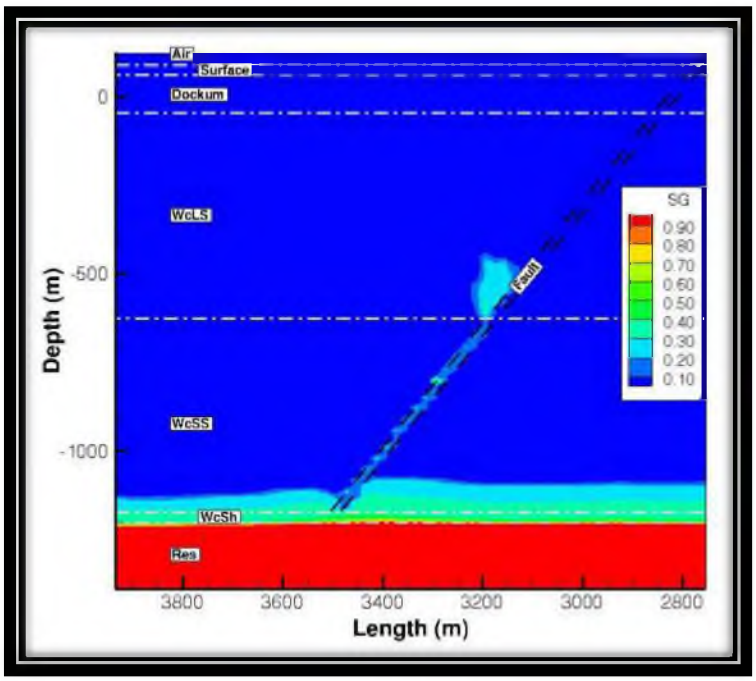

Case 9 (p1R1H1S1) Multiphase CO2 Fault-Penetrating-Seal in the Reservoir

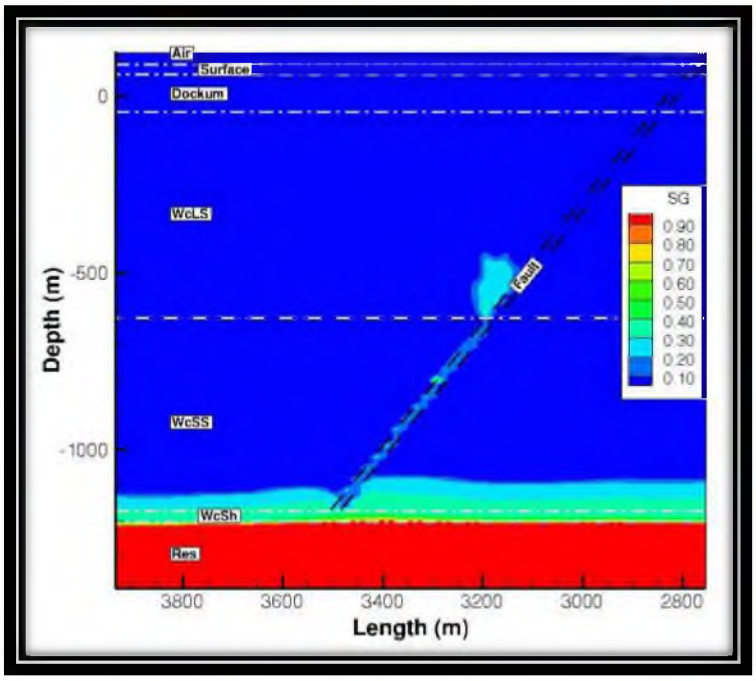

Case 10 (p2R1H1S1) Multiphase CO2 Fault-Penetrating-Seal in the Reservoir

APPENDIX L

MULTIPHASE CO2 FAULT-PENETRATING-SEAL

DISSOLVED PLUME

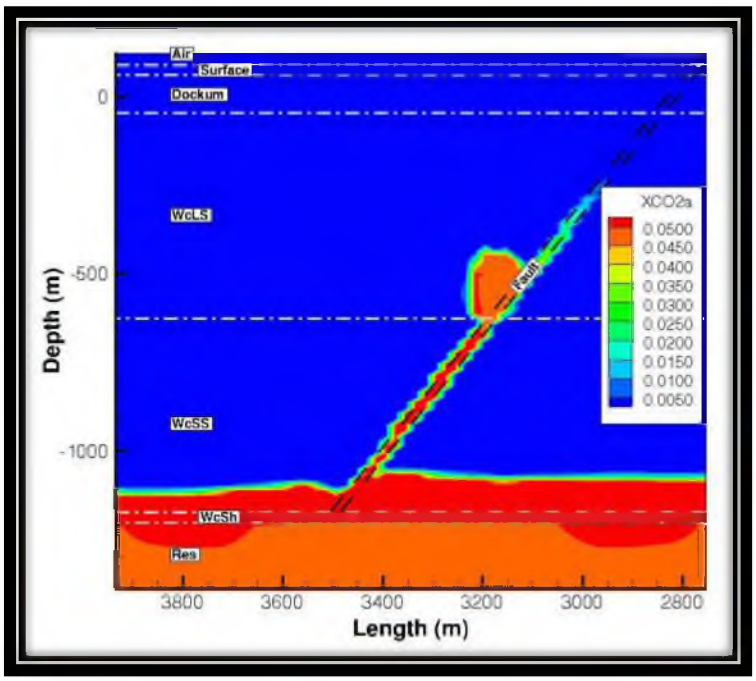

Case 1 (R1H1S1) Multiphase CO2 Fault-Penetrating-Seal Dissolved Plume

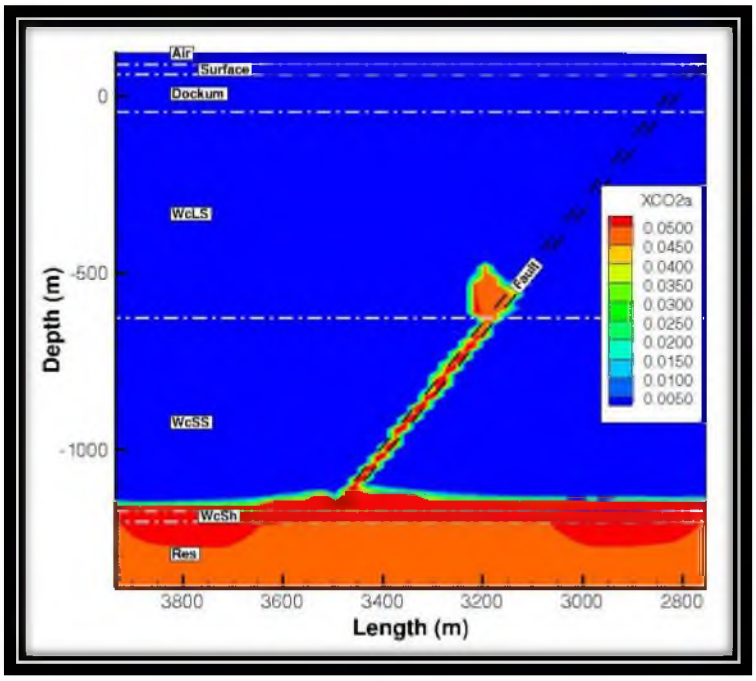

Case 2 (R1H1S2) Multiphase CO2 Fault-Penetrating-Seal Dissolved Plume

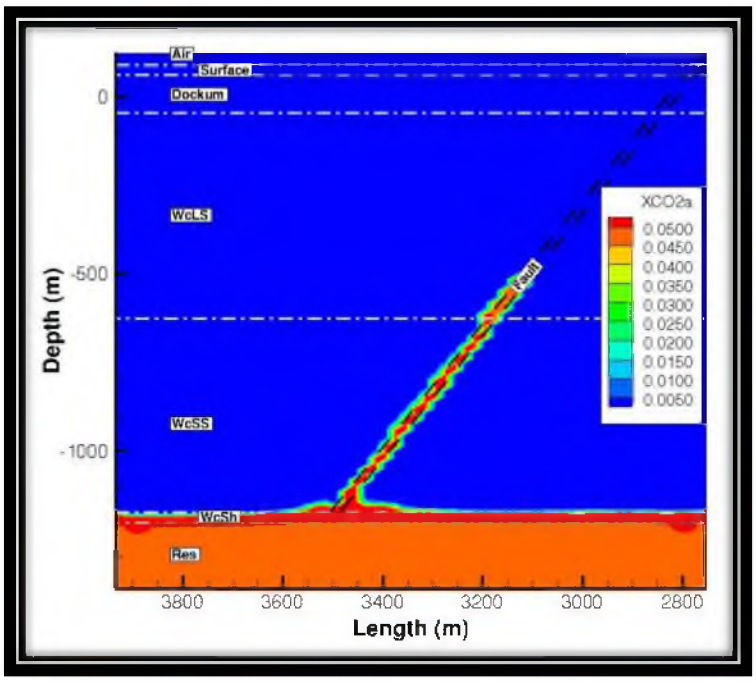

Case 3 (R1H2S1) Multiphase CO2 Fault-Penetrating-Seal Dissolved Plume

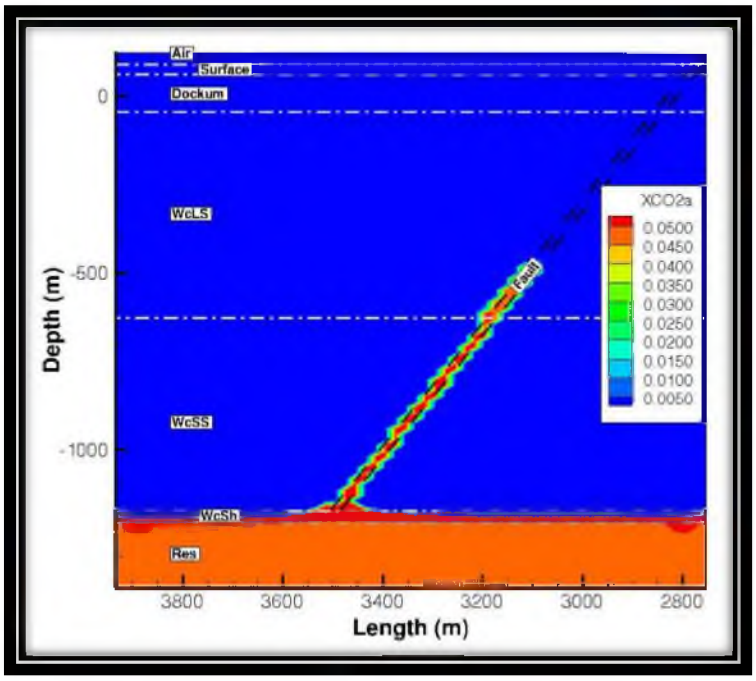

Case 4 (R1H2S2) Multiphase CO2 Fault-Penetrating-Seal Dissolved Plume

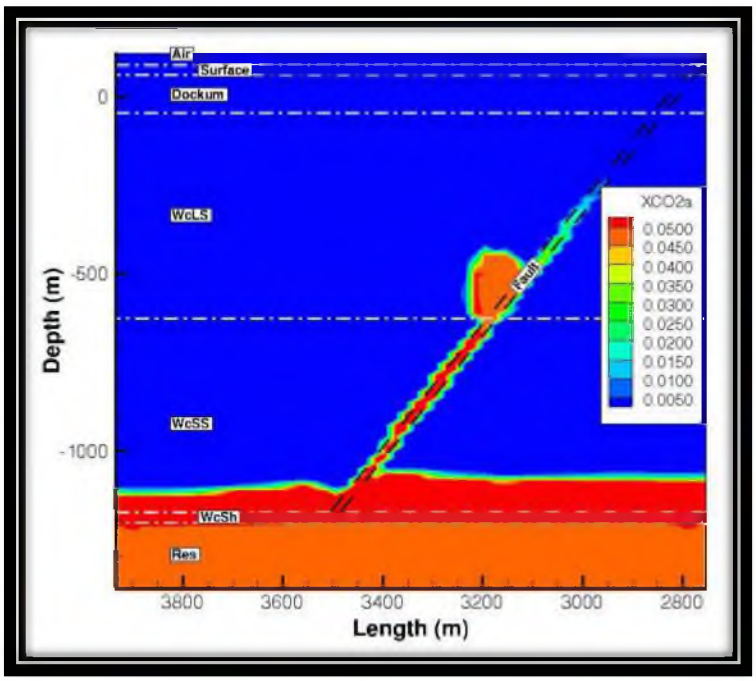

Case 5 (R2H1S1) Multiphase CO2 Fault-Penetrating-Seal Dissolved Plume

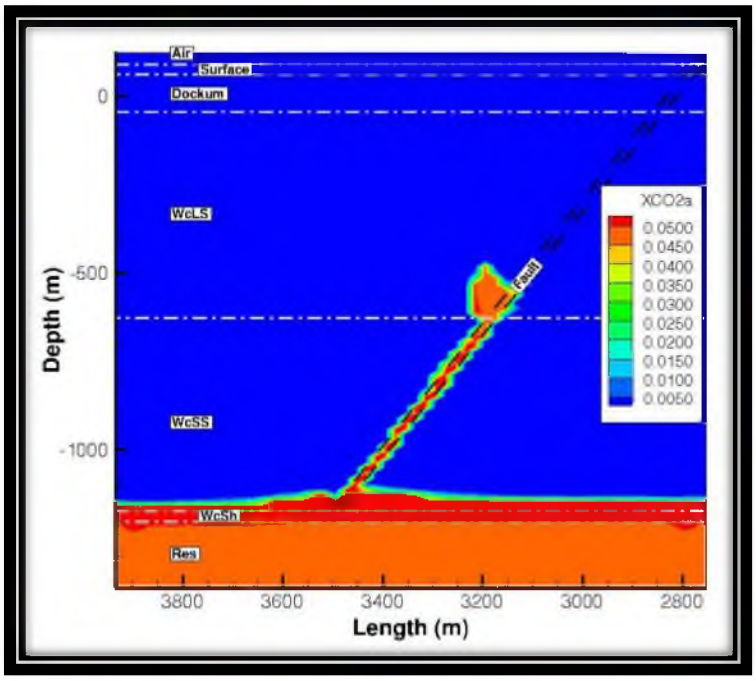

Case 6 (R2H1S2) Multiphase CO2 Fault-Penetrating-Seal Dissolved Plume

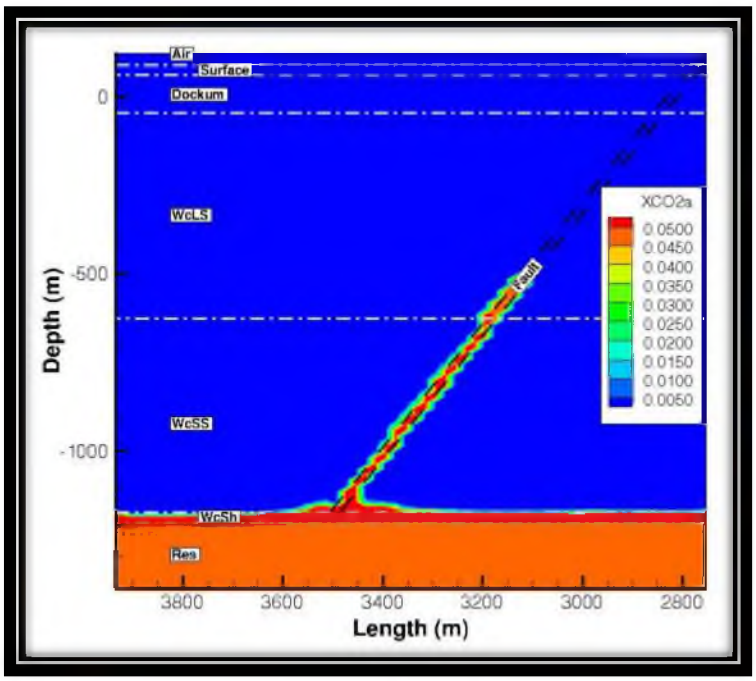

Case 7 (R2H2S1) Multiphase CO2 Fault-Penetrating-Seal Dissolved Plume

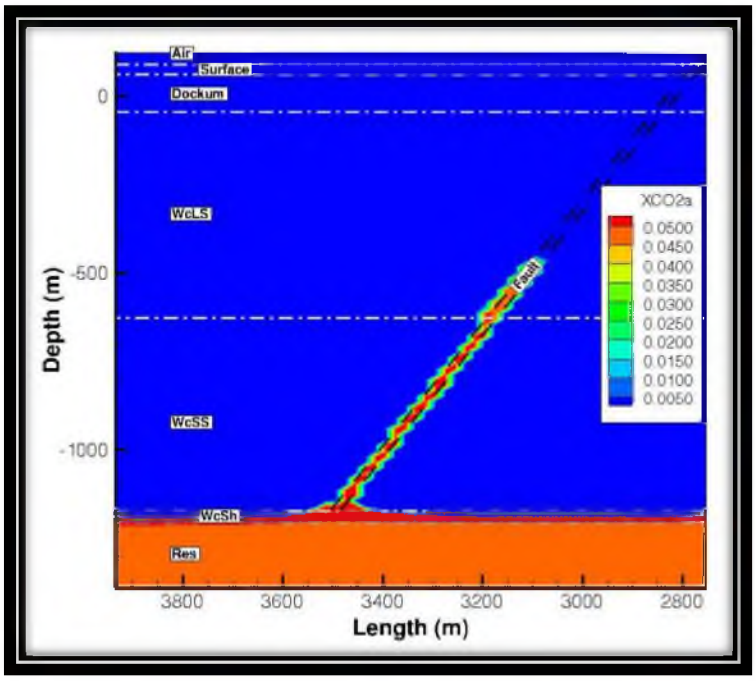

Case 8 (R2H2S2) Multiphase CO2 Fault-Penetrating-Seal Dissolved Plume

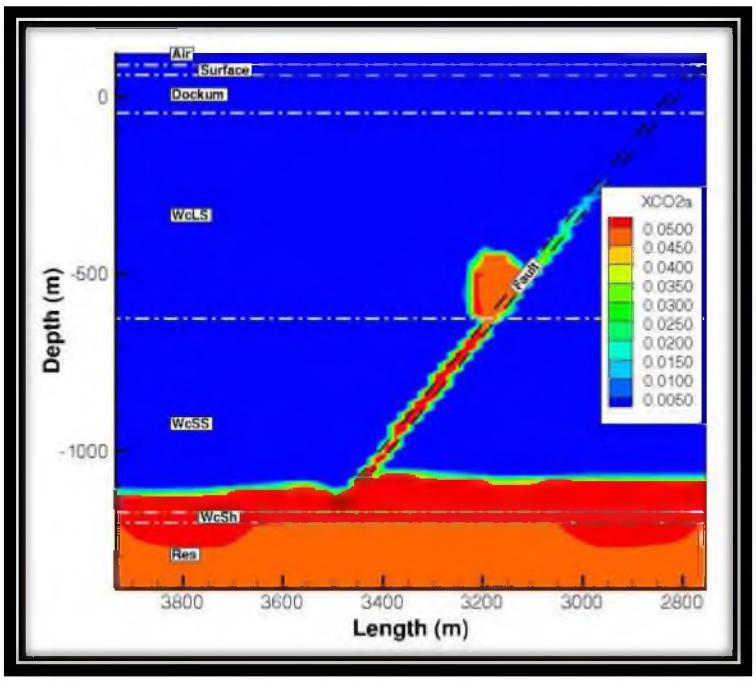

Case 9 (p1R1H1S1) Multiphase CO2 Fault-Penetrating-Seal Dissolved Plume

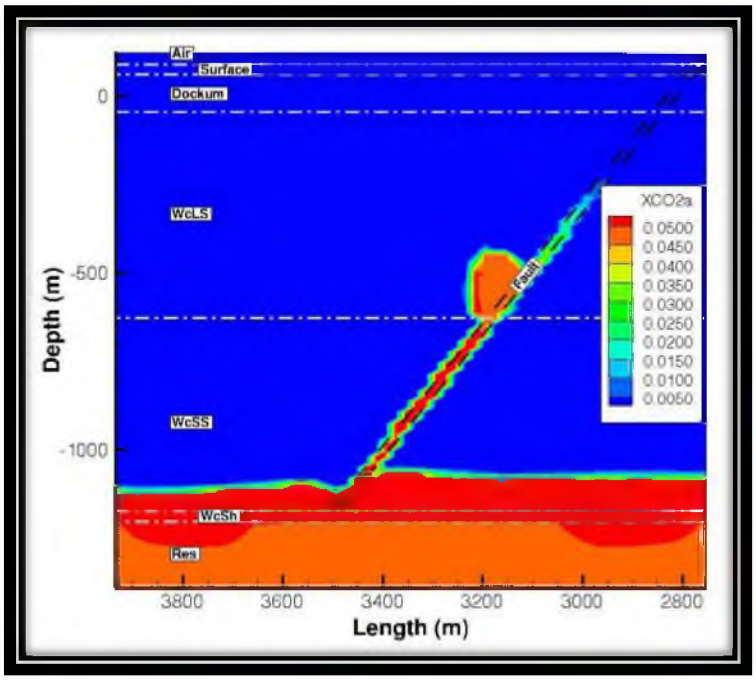

Case 10 (p2R1H1S1) Multiphase CO2 Fault-Penetrating-Seal Dissolved Plume

REFERENCE

Allis, R. G., Chidsey, T., Gwynn, W., Morgan, C., White, S., Adams, M., & Morre, J. (2001). *Natural CO2 reservoirs on the Colorado Plateau and South Rocky Mountains: Candidates for CO2 sequestration.* Technical Report.

Allis, R. G., Morre, J., & White, S. (2003). *Reactive multiphase behavior of CO2 in saline aquifers beneath the Colorado Plateau.* Quarterly Technical Report.

Al-Otaibi, S. S., & Al-Majed, A. A. (1998). Factors affecting pseudo relative permeability curves. *Journal of Petroleum Science Engineering, 21*, 249-261.

Al-Quraishi, A., & Khairy, M. (2005). Pore pressure verse confining pressure and their effect on oil-water relative permeability curves. *Journal of Petroleum Science and Engineering, 48*, 120-126.

Angeles, R., Torres-Verdin, C., Hadibeik, A., & Sepehmoon, K. (2010). Estimation of capillary pressure and relative permeability from formation-tester measurements using design of experiment and data-weighing inversion: Synthetic and field examples. *Journal of Petroleum Science and Engineering, 75*, 19-32.

Audigane, P., Gaus, I., Czernichowski-Lauriol, I., Pruess, K., & Xu, T. (2007). Two-dimensional reactive transport modeling of CO2 injection in a saline aquifer at the Sleipner site. *American Journal of Science, 307*, 974-1008.

Baalousha, H. (2008). Sensitivity, uncertainty, and reliability in groundwater modeling. *Groundwater Research and Issues*, 105-129.

Berkowitz, B. (2002). Characterizing flow and transport in fractured geological media: A review. *Advances in Water Resources, 25*, 861-884.

Birkholzer, J. T., Nicot, J. P., Oldenburg, C. M., Zhou, Q., Kraemer, S., & Bandilla, K. (2011). Brine flow up a well caused by pressure perturbation from geolgic carbon sequestration: Static and dynamic evaluations. *International Journal of Greenhouse Gas Control, 5*, 1025-1028.

Birkholzer, J. T., Zhou, Q., & Tsang, C. (2009). Large-scale impact of CO2 storage in deep saline a aquifers: A sensitivity study on pressure response in stratified systems. *International Journal of Greenhouse Gas Control, 3*, 181-194.

Burton, M., Kumar, N., & Bryant, S. L. (2009). CO2 injectivity into brine aquifers: Why relative permeability matters as much as absolute permeability. *Energy Procedia, 1*, 3091-3098.

Busch, A., & Muller, N. (2011). Determining CO2/brine relative permeability and capillary threshold pressures for reservoir rocks and caprocks: Recommendations for development of standard laboratory protocols. *Energy Procedia, 4*, 6053-6060.

Caine, J. S., Evans, J. P., & Forster, C. B. (1996). Fault zone architecture and permeability structure. *Geology, 24*, 1025-1028.

Cappa, F., & Rutqvist, J. (2010). Modeling of coupled deformation and permeability evolution during fault reactivation induced by deep underground injection of CO2. *International Journal of Greenhouse Gas Control, 5*, 336-346.

Choi, E. S., Cheema, T., & Islam, M. R. (1997). A new dual-porosity/dual-permeability model with non-Darcian flow through fractures. *Journal of Petroleum Science and Engineering, 17*, 331-344.

Dana, E., & Skocylas, F. (2002a). Experimental study of two-phase flow in three sandstones. I. Measuring relative permeabilites during two-phase steady-state experiments. *International Journal of Multiphase Flow, 28*, 1719-1736.

Dana, E., & Skoczylas, F. (2002b). Experimental study of two-phase flow in three sandstones. II. Capillary pressure curve measurement and relative permeability pore space capillary models. *International Journal of Multiphase Flow, 28*, 1965-1981.

Dockrill, B., & Shipton, Z. K. (2010). Structural controls on leakage from a natural CO2 geologic storage site: Central Utah, U.S.A. *Journal of Structural Geology, 32*, 1768-1782.

Doughty, C., & Pruess, K. (2004). Modeling supercritical carbon dioxide injection in heterogeneous porous media. *Vadose Zone, 3*, 837-847.

Dreuzy, J., Davy, P., & Olivier, B. (2001). Hydraulic properties of two-dimensional random fracture networks following a power law length distribution 2. Permeability of networks based on lognormal distribution of apertures. *Water Resources Research, 37*, 2079-2095.

Evans, J. P., Forster, C. B., & Goddard, J. V. (1997). Permeability of fault-related rocks, and implications for hydraulic structure of sault zones. *Journal of Structural Geology, 19*, 1393-1404.

Flett, M., Gurton, R., & Weir, G. (2007). Heterogeneous saline formations for carbon dioxide disposal: Impact of varying heterogeneity on containment and trapping. *Journal of Petroleum Science and Engineering, 57*, 106-118.

Frey, H. C., & Patil, S. R. (2002). *Identification and review of sensitivity analysis methods.* North Carolina State University, Civil Engineering Department, Raleigh, NC.

Gale, J. (2004). Geological storage of CO2: What do we know, where are the gaps and what more needs to be done. *Energy, 29*, 1329-1338.

Gasda, S. E., & Celia, M. A. (2005). Upscaling relative permeabilities in a structured porous medium. *Advances in Water Resources, 28*, 493-506.

Ge, S. (1997). A governing equation for fluid flow in rough fractures. *Water Resources Research, 33*, 53-61.

Geraud, Y., Diraison, M., & Orellana, N. (2006). Fault zone geometry of a mature active normal fault: A potential high permeability channel (Pirgaki fault, Corinth rift, Greece). *Tectonophysics, 426*, 61-76.

Gerke, H. H., & van Genuchten, M. T. (1993). A dual-porosity model for simulating the preferential movement of water and solutes in structured porous media. *Water Resources Research, 29*, 305-319.

Glass, R. J., Rajaram, H., Nicholl, M. J., & Detwiler, R. L. (2001). The interaction of two fluid phases in fractured media. *Current Opinion in Colloid & Interface Science, 6*, 223-235.

Han, W. S., & McPherson, B. (2010a). Optimizing geologic CO2 sequestration by injection in deep saline formations below oil reservoirs. *Energy Conversion and Management, 50*, 2570-2582.

Han, W. S., McPherson, B. J., Lichtner, P. C., & Wang, F. P. (2010b). Evaluation of trapping mechanisms in geologic CO2 sequestration: Case study of SACROC Northern platform, A 35-year CO2 injection site. *American Journal of Science, 310*, 282-324.

Hattingh, S. K., & Reddy, B. D. (2009). A finite element approach for modeling single-phase compressible flow in dual porosity. *Journal of Petroleum Science and Engineering, 69*, 1-24.

Haws, N. W., Rao, P. S., Simunek, J., & Poyer, I. C. (2005). Single-porosity and dual-porosity modeling of water flow and solute transport in subsurface-drained fields using effective field-scale parameters. *Journal of Hydrology, 313*, 257-273.

Helton, J. C. (1993). Uncertainty and sensitivity analysis techniques for use in performance assessment for radioactive waste disposal. *Reliability Engineering and System Safety, 42*, 327-367.

Holloway, S. (2005). Underground sequestration of carbon dioxide - A viable greenhouse gas mitigation option. *Energy, 30*, 2318-2333.

Ide, S. T., Jessen, K., & Orr Jr, F. M. (2007). Storage of CO2 in saline aquifers: Effects of gravity, viscous, and capillary forces on amount and timing of trapping. *International Journal of Greenhouse Gas Control, 1*, 481-491.

Iding, M., & Blunt, M. J. (2011). Enhanced solubility trapping of CO2 in fractured reservoirs. *Energy Procedia, 4*, 4961-4968.

IEA, IEA Greenhouse Gas R&D Programme (2001). *Putting Carbon Back in the Ground.* IEA Greenhouse Gas R&D Programme.

IPCC, Intergovernmental Panel on Climate Change (2005). *Carbon Dioxide Capture and Storage.* United Kingdom: Cambridge University Press.

Knauss, K. G., Johnson, J. W., & Steefel, C. I. (2005). Evaluation of the impact of CO2, co-contaminant gas, aqueous fluid and reservoir rock interactions on the geologic sequestration of CO2. *Chemical Geology, 217*, 339-350.

Kunstmann, H., & Kastens, M. (2006a). Determination of stochastic well head protection zones by direct propagation of uncertainties of particle tracks. *Journal of Hydrology, 323*, 215-229.

Kunstmann, H., & Kastens, M. (2006b). Direct propagation of probability density functions in hydrological equations. *Journal of Hydrology, 325*, 82-95.

Kunstmann, H., & Kinselbach, W. (2002). Conditional first-order second-moment method and its application to the quantification of uncertainty in groundwater modeling. *Water Resources Research, 38*, 1-14.

Li, K., & Horne, R. N. (2008). Numerical simulation without using experimental data of relative permeability. *Journal of Petroleun Science and Engineering, 61*, 67-74.

Masihi, M., Javanbakht, L., Bahaloo Horeh, F., & Rasaei, M. R. (2011). Experimental investigation and evaluation of three-phase relative permeability models. *Journal of Petroleum Science and Engineering, 79*, 45-53.

McPherson, B. J., & Sundquist, E. T. (2009). *Carbon Sequestration and Its Role in the Global Carbon Cycle* (Vol. Geophysical Monograph 183). American Geophysical Union.

Meckel, T. A., & Hovorka, S. D. (2009, November 2-4). Results from continuous downhole monitoring (PDG) at a field-scale CO2 demonstration project, Cranfield, MS. *Society of Petroleum Engineering International Conference*.

Morgan, C. D., & Chidsey, T. C. (1991). Gordon Creek, Farnham Dome, and Woodside fields, Carbon and Emery counties, Utah. *Utah Geological Association Publication 19*, pp. 301-309.

Nghiem, L., Yang, C., Shrivastava, V., Kohse, B., Hassam, M., & Card, C. (2009). Risk mitigation through the optimization of residual gas and solubility trapping for CO2 storage in saline aquifers. *Energy Procedia, 1*, 3015-3022.

Nguyen, V. H., Sheppard, A. P., Knackstedt, M. A., & Pinczewski, W. V. (2006). The effect of displacement rate on imbibitions relative permeability and residual saturation. *Journal of Petroleum Science and Engineering, 52*, 54-70.

Nilsen, T., & Aven, T. (2003). Models and model uncertainty in the context of risk analysis. *Reliability Engineering and System Safety, 79*, 309-317.

Oberkampf, W. L., DeLand, S. M., Rutherford, B. M., Diegert, K. V., & Alvin, K. F. (2002). Error and uncertainty in modeling and simulation. *Reliability Engineering and System Safety, 75*, 333-357.

Oberkampf, W. L., Helton, J. C., Joslyn, C. A., Wojtkiewicz, S. F., & Ferson, S. (2004). Challenge problems: Uncertainty in system response given uncertain parameters. *Reliability Engineering and System Safety, 85*, 11-19.

Orlic, B., ter Heege, J., & Wassing, B. (2011). Assessing the integrity of fault and top seals of CO2 storage sites. *Energy Procedia*, 4798-4805.

Orr, F. M. (2004). Storage of carbon dioxide in geologic formations. *Journal of Petroleum Technology, 56*, 90-97.

Pasala, S. M., Forster, C. B., Lim, S. J., & Deo, M. D. (2003, October 5-8). Simulating teh impact of faults on CO2 sequestration and enhanced oil recovery in sandstone aquifers. *Society of Petroleum Engineers Annual Technical Conference and Exhibition*.

Pate-Cornell, M. E. (1996). Uncertainties in risk analysis: Six levels of treatment. *Reliability Engineering and System Safety, 54*, 95-111.

Presho, M., Wo, S., & Ginting, V. (2011). Calibrated dual porosity, dual permeability modeling of fractured reservoirs. *Journal of Petroleum Science and Engineering, 77*, 326-337.

Price, P. N., & Oldenburg, C. M. (2009). The consequences of failure should be considered in siting geologic carbon sequestration projects. *International Journal of Greenhouse Gas Control, 3*, 658-663.

Pruess, K., Oldenburg, C., & Moridis, G. (1999). *TOUGH2 user's guide, version 2.0.* Berkeley, CA: University of California.

Rohmer, J., & Bouc, O. (2010). A response surface methodology to address uncertainties in cap rock failure assessment for CO2 geological storage in deep aquifers. *International Journal of Greenhouse Gas Control, 4*, 198-208.

Saghir, M. Z., & Islam, M. R. (1999). Double diffusive convection in dual-permeability, dual-porosity porous media. *International Journal of Heat and Mass Transfer, 42*, 437-454.

Samardzioska, T., & Popov, V. (2005). Numerical comparison of the equivalent continuum, non-homogeneous and dual porosity models for flow and transport in fractured porous media. *Advances in Water Resources, 28*, 235-255.

Schmit, D., & Burgmann, R. (2003). A response surface methodology to address uncertainties in cap rock failure assessment for CO2 geological storage in deep aquifers. *Journal of Geophysical Research, 108*, 1-13.

Schwartz, F. W., & Zhang, H. (2003). *Fundamentals of Ground Water.* John Wiley & Sons, Inc.

Shipton, Z. K., & Cowie, P. A. (2001). Damage zone and slip-surface evolution over μm to km scales in high-porosity Navajo sandstone, Utah. *Journal of Structural Geology, 23*, 1825-1844.

Sibson, R. (2000). Fluid involvement in normal faulting. *Journal of Geodynamics, 29*, 469-499.

Sidiq, H., Amin, R., Van der Steen, E., & Kennaird, T. (2011). Super critical CO2-methane relative permeability investigation. *Journal of Petroleum Science and Engineering, 78*, 654-663.

Soltanzadeh, H., & Hawkes, C. D. (2008). Semi-analytical models for stress change and fault reactivation induced be reservoir production and injection. *Journal of Petroleum Science and Engineering, 60*, 71-85.

Spiteri, E. J., & Juanes, R. (2006). Impact of relative permeability hysteresis on the numerical simulation of WAG injection. *Journal of Petroleum Science and Engineering, 50*, 115-139.

Stafford, P., Toran, L., & McKay, L. (1998). Influence of fracture truncation on dispersion: A dual permeability model. *Journal of Contaminant Hydrology, 30*, 79-100.

Streit, J. E., & Hillis, R. R. (2004). Estimating fault stability and sustainable fluid pressures for underground storage of CO2 in porous rock. *Energy, 29*, 1445-1456.

Suekane, T., Nobuso, T., Hirai, S., & Kiyota, M. (2008). Geological storage of carbon dioxide by residual gas and solubility trapping. *International Journal of Greenhouse Gas Control, 2*, 58-64.

Thararoop, P., Karpyn, Z. T., & Ertekin, T. (2012). Development of a multi-mechanistic, dual-porosity, dual-permeability, numerical flow model for coalbed methane reservoirs. *Journal of Nateral Gas Science and Engineering, 8*, 121-131.

Thomas, D., & Benson, S. (2005). Carbon dioxide capture for storage in deep geologic formations. *Results from the CO2 Capture Project, 2*, 1328.

Trivedi, J. J., & Babadagli, T. (2009). Experimental and numerical modeling of the mass transfer between rock matrix and fracture. *Chemical Engineering Journal, 146*, 194-204.

Tseng, P., Sciortino, A., & van Genuchten, M. (1995). A partitioned solution procedure for simulating water flow in a variably saturated dual-porosity medium. *Advances in Water Resources, 18*, 335-343.

Uleberg, K., & Kleppe, J. (1996). *Dual porosity, dual permeability formulation for fractured reservoir simulaiton.* Norwegian University of Science and Technology.

Vogel, T., Gerke, H. H., Zhang, R., & van Genuchten, M. T. (2000). Modeling flow and transport in a two-dimensional dual-permeability system with spatially variable hydraulic properties. *Journal of Hydrology, 238*, 78-89.

Wang, J., Zhu, X., Guo, H., Gong, X., & Hu, J. (2011). Synthesis and behavior evaluation of a relative permeability modifier. *Journal of Petroleum Science and Engineering, 80*, 69-74.

Wang, X., Zhou, Y., & Lou, W. (2010). A study on transient fluid flow of horizontal wells in dual-permeability media. *Journal of Hydrodynamics, 22*, 44-50.

Warren, J. E., & Root, P. J. (1963). The behavior of naturally fractued reservoirs. *Society of Petroleum Engineers, 3*, 245-255.

Wei, Z., & Zhang, D. (2010). Coupled fluid-flow and geomechanics for triple-porosity/dual-permeability modeling of coalbed methane recovery. *International Journal of Rock Mechanics & Mining Sciences, 47*, 1242-1253.

White, S. P., Allis, R. G., Moore, J., Chidsey, T., Morgan, C., Gwynn, W., & Adams, M. (2005). Simulation of reactive transport of injected CO2 on the Colorado Plateau, Utah, USA. *Chemical Geology, 217*, 387-405.

Winkler, R. L. (1996). Uncertainty in probabilistic risk assessment. *Reliability Engineering and System Safety, 54*, 127-132.

Wu, Y., & Pruess, K. (2000). Numerical simulation of non-isothermal multiphase tracer transport in heterogeneous fractured porous media. *Advances in Water Resources, 23*, 699-723.

Xia, L., Wenzhi, Z., Cancan, Z., Tongshan, W., & Chaoliu, L. (2012). Dual-porosity saturation model of low-porosity and low-permeability clasitc reservoirs. *Petroleum Exploration and Development, 39*, 88-98.

Xu, T., Apps, J. A., & Pruess, K. (2004). Numerical simulation of CO2 disposal by mineral trapping in deep aquifers. *Applied Geochemistry, 19*, 917-936.

Yang, J. (2011). Convergence and uncertainty analyses in Monte-Carlo based sensitivity analysis. *Environmental Modelling adn Software, 26*, 444-457.

Zhang, K., Woodbury, A. D., & Dunbar, W. S. (2000). Application of the Lanczos algorithm to the simulation of groundwater flow in dual-porosity media. *Advances in Water Resources, 23*, 579-589.

Zhang, W., Li, Y., Xu, T., Cheng, H., Zheng, Y., & Xiong, P. (2009). Long-term variations of CO2 trapped in different mechanisms in deep saline formations: A case study of the Songliao Basin, China. *International Journal of Greenhouse Gas Control, 3*, 161-180.

Zheng, C., & Bennet, G. (2002). *Applied contaminant transport modeling* (2nd ed.). A John Wiley & Sons, Inc.

Zhou, Q., Birkholzer, J. T., Mehnert, E., Lin, Y., & Zhang, K. (2010). *Modeling basin- and plume-scale process of CO2 storage for full-scale deployment.* Lawrence Berkeley National Laboratory.